FABRICATION AND CHARACTERIZATION OF MEMORY DEVICES BASED ON ORGANIC/POLYMER MATERIALS

SONG YAN

B.Sci (Xi'an Jiaotong University, P. R. China)

A THESIS SUBMITTED

FOR THE DEGREE OF DOCTOR OF PHILOSOPHY

DEPARTMENT OF

ELECTRICAL AND COMPUTER ENGINEERING

NATIONAL UNIVERSITY OF SINGAPORE

2007

ACKNOWLEDGEMENTS

I would like to express my gratitude to my advisors, Prof. Zhu Chunxiang and Prof. Kwong Dim-Lee, for valuable guidance in every aspect. I have learnt a lot from them. I would also like to thank Prof. Kang En-Tang and Prof. Daniel Siu-Hung Chan, for providing critical and helpful suggestions and feedback on the research results.

I also greatly appreciate my collaborators, Dr. Ling Qidan, Tan Yoke Ping, Lim Siew Lay, Eric Teo Yeow Hwee, Liu Gang, Alison Tong Shi Wun, and Zhang Chunfu for extensively discussion and the help in the experiment.

I was fortunate to be part of an active research group in Silicon Nano Device Laboratory at National University of Singapore. It provides me a great research environment not only with advanced facilities, but also with great members. I would like to thank the past and present members of Silicon Nano Device Lab, Gao Fei, Huang Jidong, Li Rui, Wang Xinpeng, Shen Chen, Fu Jia, Jiang Yu, Wang Jian, Yang Weifeng, Xie Ruilong, Tong Yi and many others. It was a great pleasure to work in such an enthusiastic group.

I would also like to express my gratitude towards my parents for their supports and understanding over the years.

TABLE OF CONTENTS

	Page
ACKNOWLEDGEMENTS	I
TABLE OF CONTENTS	II
ABSTRACT	VI
LIST OF TABLES	VIII
LIST OF FIGURES	IX
LIST OF SYMBOLS	XIII
CHAPTER 1. Introduction	1
1.1 MOSFET and Moore's Law	2
1.2 Current Memory Technologies	4
1.3 Prototypical Memory Technologies	10
1.4 Emerging Memory Technologies	13
1.5 Organic/Polymer Memory Fundamentals	16
1.5.1 Device Structures	16
1.5.2 Memory Architecture	17
1.5.3 Fabrication Methods	19
1.5.4 Basic I-V Characteristics	20
1.5.5 Performance Parameters	20
1.6 Current Status of Organic/Polymer Memory Device	20

1.6.1 Molecular Memories 21

1.6.1.1 Acene Derivatives 21

1.6.1.2 Charge Transfer Complexes 21

1.6.1.3 Organic Dyes 24

1.6.1.4 Trilayer Memories 26

1.6.2 Polymer Memories 27

1.6.2.1 Ferroelectric Polymers 27

1.6.2.2 Insulating Polymers 27

1.6.2.3 Semiconducting Polymers 28

1.6.2.4 Composite Materials 29

1.7 Motivation of Study 29

Reference 31

CHAPTER 2. Synthesis and WORM Memory Properties of a Conjugated Copolymer of Fluorene and Benzoate with Chelated Europium Complex 39

2.1 Introduction 39

2.2 Experiment 40

2.2.1 Synthesis of the Copolymer 40

2.2.2 Device Fabrication 43

2.3 Experimental Results 44

2.3.1 Characterization of PF8Eu 45

2.3.2 Device Performance 48

2.4 Discussion 52

2.5 Conclusion 57

Reference 59

CHAPTER 3. Non-Volatile Flash Memory Devices based on Copolymer Containing Carbazole Units and Europium Complex 62

3.1 Introduction 62

3.2 Experiment 63

3.2.1 Preparation and Characterization of the PKEu Copolymer 63

3.2.2 Device Fabrication and Characterization 64

3.3 Results and Discussions 65

3.4 Conclusion 77

Reference 78

CHAPTER 4. Material Properties and Electrical Performance of Mixed Polymer and Gold Nanoparticle based Flash Memory Device 81

4.1 Introduction 81

4.2 Experiment 83

4.3 Results and Discussions 86

4.3.1 Film Morphology 86

4.3.2 UV-Visible Absorption Spectra 88

4.3.3 Hole Mobility in Mixed Films 89

4.3.4 Device Performance of Device based on 12:1 Mixing Ratio 91

4.3.5 Device Performance under Different Mixing Ratio 96

4.3.6 Device Performance under Different Film Thickness 99

4.3.7 Device Performance under Different Top Metal Electrode 104
4.4 Conclusion 105
Reference 107

CHAPTER 5. Conclusions 109

5.1 Conclusions 109
5.2 Limitations 112
5.3 Suggestions for Future Work 113

APPENDIX: List of Publications 115

ABSTRACT

Organic materials have been aggressively explored for semiconductor device applications. As an emerging area in organic electronics, organic/polymer memories have become an active research topic in recent years. Organic/polymer memories based on bistable electrical switching are likely to be an alternative or supplementary technology to the conventional memory technology facing the problem in miniaturizing from micro- to nano-scale. This dissertation mainly presents the fabrications and characterizations of three different kinds of polymer material based memory device.

A conjugated copolymer containing fluorine and chelated europium complex (PF8Eu) was synthesized. Based on this copolymer material, we fabricated a metal-insulator-metal structured device. Under the current-voltage measurement, this device showed a write-once-read-many times (WORM) memory behavior. The memory device had a switching time of ～1 μs and an on/off current ratio as high as 10^6. No degradation in device performance was observed after 10^7 read cycles at a read voltage of 1 V under ambient conditions. The memory effect might come from the charge transfer between the fluorine moiety and europium complex.

After the write-once-read-many times device, a flash-typed memory device was fabricated successfully by using poly[NVK-*co*-Eu(VBA(TTA)$_2$phen)] or PKEu, a

copolymer containing carbazole units and europium complex moieties as the active layer between ITO and aluminum electrodes. The device could exhibit two distinctive bistable conductivity states by applying voltage pulses of different polarities. The device can remain in either state even after the power has been turned off. An on/off current ratio as high as 10^4 and a switching time of ~20 μs were achieved. More than a million read cycles were performed on the device under ambient conditions without any device encapsulation. A redox mechanism, governed by the donor-acceptor nature of the PKEu copolymer, was proposed to explain the memory effect of the device.

Beside the two kinds of europium complex contained copolymer materials, a device using polymer mixed with nanoparticles as the active layer between two metal electrodes was fabricated. The polymer we used here is poly(N-vinylcarbazole) (PVK), which is a good electron donor. The nanoparticle we used here is gold nanoparticle (GNP), which is a good electron acceptor. The device with PVK:GNPs mixing weight ratio of 12:1 could transit between low conductivity and high conductivity easily by applying an electrical field. Between the low conductivity state and high conductivity state, an on/off current ratio as high as 10^5 at room temperature was achieved. The memory effect was attributed to electric-field-induced charge transfer complex formed between PVK and the gold nanoparticles. Following that, the influence of different PVK:GNPs mixing ratio, different active layer thickness and different top metal electrode to the device performance were also studied.

LIST OF TABLES

Page

Table 1.1: Comparison of memory technologies. 15

Table 4.1: Root-mean-square surface roughness of different films. 88

Table 4.2: Zero-field hole mobility μ_0 in different PVK:GNPs films sandwiched between ITO and Au. 91

Table 5.1: Comparison of electrical characteristics among 3 kinds of device. 112

LIST OF FIGURES

Page

Figure 1.1: A typical MOSFET structure in the modern IC circuits. The current between the source (S) and the drain (D) through the channel is controlled by the gate (G). When a voltage is applied to the gate, carriers can flow from the source to the drain and form the ON current (I_{on}). 2

Figure 1.2: CPU transistor counts from 1970s to present, showing the device scaling according to Moore's Law; © Intel corp. 4

Figure 1.3: Schematic structure of a conventional floating gate flash memory cell. 7

Figure 1.4: Schematic structure of a nanocrystal flash memory cell. 9

Figure 1.5: Schematic illustrating the mechanism of a FeRAM. 11

Figure 1.6: Schematic diagram showing the programming operation mode of a MRAM memory. 12

Figure 1.7: Schematic cross-section of a PCM cell. The active region is adjacent to the GST-heater interface. 13

Figure 1.8: Basic cell structure of an electrical memory device. 16

Figure 1.9: Cross point memory array with memory cells separated by a resistive layer. 17

Figure 1.10: Principal arrangement of 3D stacked organic memory. 19

Figure 2.1: Synthetic route for the conjugated copolymer containing fluorene and europium complex in the main chain. 41

Figure 2.2: Schematic structure of the Al/PF8Eu/ITO memory device. 43

Figure 2.3: (a) ^{1}H NMR (300MHz) and (b) ^{13}C NMR (75MHZ) spectra of the PF8Eu copolymer in d_6-THF. 44

Figure 2.4: Positive ion ToF-SIMS spectra of the PF8Eu film spin-cast from THF solution on ITO glass. 46

Figure 2.5: TEM images of (a) the PF8Eu film spin-cast from the toluene solution and (b) a polyfluorene film doped with the Eu complex to the same concentration as that of PF8Eu. 47

Figure 2.6: (a) Typical *J*-*V* characteristics of the Al/PF8Eu/ITO device (PF8Eu thickness=50 nm). Voltage was swept from 0 V to 6 V. (b) the ON- to OFF-current ratio as a function of applied voltage for the same sweep. 49

Figure 2.7: Typical *J*-*V* characteristics of the Al/PF8Eu/ITO device switched to the ON-state by using quasi-static (closed diamonds) and pulsed (open circles) switching. 50

Figure 2.8: Effect of read pulses on the OFF- and ON-states. Inset: characteristics of the pulse used for the tests. 51

Figure 2.9: Stability of the Al/PF8Eu/ITO device in either ON- or OFF-state under a constant stress of 1 V. 52

Figure 2.10: Cyclic voltammetry (CyV) of a thin film of PF8Eu on a platinum disk electrode in acetonitrile with tetrabutylammoniumhexafluorophosphate ($n\text{-}Bu_4NPF_6$) as the supporting electrolyte, Ag/AgCl as the reference electrode and a platinum wire as the counter electrode. 53

Figure 2.11: Absorption spectra of the PF8 moiety (solid curve) and Eu complex (dotted curve) in THF. The absorption edges (indicated by arrows) correspond to the energy band gaps. 54

Figure 2.12: Energy band diagrams with reference to different functional groups in the PF8Eu copolymer. 54

Figure 2.13: Experimental and fitted *J*-*V* curves of the Al/PF8Eu/ITO device: (a) OFF-state with the Schottky emission model and (b) ON-state with the trap-limited space-charge-limited model. 56

Figure 3.1: Molecular structure of the copolymer PKEu with the composition of x:y=0.987:0.013. 65

Figure 3.2: Schematic diagram of the memory device consisting of a thin film (~50 nm) of PKEu sandwiched between an ITO substrate and an aluminium top electrode. 66

Figure 3.3: TEM image of (a) the PKEu film spin coated from the toluene solution; and (b) the PVK film doped with europium complex to a comparable Eu content of 1% (w/w) to PKEu. 67

Figure 3.4: *J-V* characteristics of the Al/PKEu/ITO device based on a spin-cast film of PKEu (~50 nm) for two sweep directions. Arrows indicate the sweep directions of the applied voltage. 68

Figure 3.5: CyV sweep (from (i) to (iv)) of a thin film of PKEu on a platinum disk electrode in acetonitrile with 0.1 M of n-Bu_4NPF_6 as the supporting electrolyte. The inset is the CyV, sweep in the same electrolyte, of a PKEu film sandwiched between ITO and Al electrodes, with ITO as the working cathode. 69

Figure 3.6: The oxidation, reduction and charge migration processes in the copolymer during memory device operation (write/erase). 71

Figure 3.7: Electrode processes: (a) the oxidation (p-doping) and (b) reduction (n-doping) processes of the carbazole groups and Eu complex moieties in copolymer PKEu. 73

Figure 3.8: Effect of read cycles on the ON state and OFF state. 75

Figure 3.9: Ratio of the ON- to OFF-state current as a function of applied voltage. 75

Figure 3.10: (a) Transient response of current density *vs*. time, showing a short switching time from ON to OFF state; (b) the corresponding circuit for measurement. 76

Figure 4.1: Molecular structure of PVK (left) and schematic structure of gold nanoparticle (right). 83

Figure 4.2: (a) Transmission electron micrograph picture of gold nanoparticles and (b) histogram of GNPs. 84

Figure 4.3: Schematic diagram of the sandwich structure device. 85

Figure 4.4: AFM images of (a) TaN film (150 nm); (b) pure PVK film (200 nm); (c) 20:1 PVK:GNPs (200 nm); (d) 12:1 PVK:GNPs film (200 nm); (e) 6:1PVK:GNPs film (200 nm); (f) 3:1 PVK:GNPs film (200 nm). The scan size in the AFM images is 5 μm x 5 μm with the height given in nanometer. 87

Figure 4.5: (a) UV-visible absorbance spectra of GNPs, PVK and PVK:GNPs in THF solutions ($1x10^{-5}$mol/L); (b) UV-visible absorbance spectra of GNPs, PVK, and PVK:GNPs films on quartz (the curves are normalized for a better view). 89

Figure 4.6: Current density vs. voltage characteristics of 3:1 PVK:GNPs (triangles), 20:1 PVK:GNPs (squares), and 99:1 PVK:GNPs (circles) films sandwiched between ITO and Au electrodes. The filled symbols are experimental data, while the open symbols are fitting data based on space charge limited current theory. 90

Figure 4.7: Typical *J-V* characteristics of the Al/12:1 PVK:GNPs (130 nm)/TaN device. 93

Figure 4.8: The ON- to OFF-current ratio as a function of applied voltage. 93

Figure 4.9: *J-V* characteristics of the Al/PVK/TaN device. Inset: Schematic diagram of the Al/PVK/TaN device. 94

Figure 4.10: The stability characteristics of the Al/PVK:GNPs/TaN devices in either ON or OFF state under a 1 V constant voltage stress. 95

Figure 4.11: The *J-T* characteristics of the Al/PVK:GNPs/TaN device in either ON or OFF state under a 1 V read voltage. 95

Figure 4.12: *J-V* characteristics of the Al/PVK:GNPs (130 nm)/TaN devices with different PVK:GNPs weight ratio. Area I: 99:1 PVK:GNPs and 20:1 PVK:GNPs based devices; area II: 12:1 PVK:GNPs based device; area III: 6:1 PVK:GNPs and 3:1 PVK:GNPs based devices. 97

Figure 4.13: *J-V* characteristics of the Al/12:1 PVK:GNPs/TaN devices based on different polymer thickness (a) 1.3 μm; (b) 130 nm; (c) 50 nm; (d) 25 nm. 101&102

Figure 4.14: *J-V* characteristics of the 12:1 PVK:GNPs based devices with same active layer film thickness and different top metal electrodes (a) Cu; (b) Au. 103

LIST OF SYMBOLS

A^*	effective Richardson constant
d	thickness
H_t	total density of traps
I	current
I_{on}	on current
I_{off}	off current
J	current density
k	Boltzmann constant
K	stability constant
l	empirical parameter
N_v	density of states
q	elementary charge
T	temperature
V	voltage
ε	relative dielectric constant
ε_0	vacuum dielectric constant
ε_i	insulator permittivity
μ	mobility
μ_0	zero-field mobility

θ	shallow trapping factor
ϕ_B	barrier height

Chapter 1

Introduction

Nowadays, with the development of semiconductor and communication technologies, mobile phones, computers, PDAs, digital cameras, and other mobile devices have been used in our daily life and given us much convenience. With these devices, we can easily access the latest news and communicate with our friends who are in other places in the world. Among all of the devices, there are important parts which are used to store data, named the memory parts. There are several different kinds of memory devices based on their functions, such as write-once-read-many times (WORM) memory, flash-typed memory, dynamic random access memory (DRAM), static random access memory (SRAM), etc. Of all these kinds of memory devices, the traditional technology used to is the silicon-based complementary metal oxide semiconductor (CMOS) technology. According to Moore’s law, CMOS device will scale down to half its size every two years [1]. Based on current CMOS device structure, the gate dielectric layer is only 1 to 2 nm, which are only several atom layers. Thus, this CMOS technology will reach its physical limitation in the near future. Therefore, memory technology and new materials are urgently demanded for future development. It is a simple matter to suggest that the ultimate integrated circuits will be constructed at the molecular level. Organic materials are promising for

future molecular size device applications. Their attractive features include miniaturized dimensions and the possibility for molecular design through chemical synthesis [2]. In particular, polymer materials have attracted considerable attention because of their good scalability, mechanical strength, flexibility, and most important of all, ease of processing [3]. Before discussing the advantages of organic devices, the following section will give a preview of conventional memory technology and its boundaries.

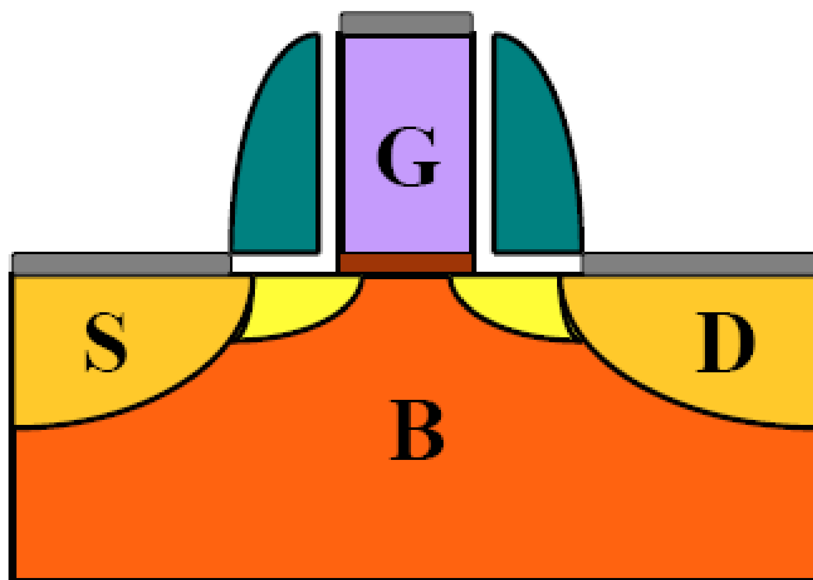

Figure 1.1 A typical MOSFET structure in the modern IC circuits. The current between the source (S) and the drain (D) through the channel is controlled by the gate (G). When a voltage is applied to the gate, carriers can flow from the source to the drain and form the ON current (I_{on}).

1.1 MOSFET and Moore's Law

Since the invention of the first integrated circuit (IC) in 1958, the semiconductor industry has undergone unprecedented growth through the latter half of 20th century. Today, the silicon-based IC products are all based on the metal-oxide-semiconductor field effect transistor (MOSFET), the basic element in IC chips. Fig 1.1 shows the schematic of MOSFET. MOSFET is a switch in digital circuits, which is controlled by its gate (G) terminal. Carriers (electrons or holes) flow from source (S) to drain (G) in the semiconductor channel forming current when it is ON (I_{on}), and the leakage current should be small when it is OFF (I_{off}). A larger output current (I_{on}) will result in faster charging of the capacitive load, and a consequent higher switching speed. Driven by the demand for IC chips with higher speed, greater functionality, and lower cost, the physical dimensions of MOSFET have been scaled down continuously over the past 40 years. In 1965, Gordon Moore of Intel predicted the trend of MOSFET scaling, which is popularly known as Moore's Law: the number of transistors on a chip doubles about every two years [1], as shown in Fig 1.2 [4]. This trend has been made possible by the advancing of semiconductor process technology from 8 μm in 1972 to the current 65 nm technology. According to the prediction of the latest 2006 update International Technology Roadmap for Semiconductor (ITRS), the physical gate length for high performance logic applications will shrink down to 6 nm in the year of 2020 [5].

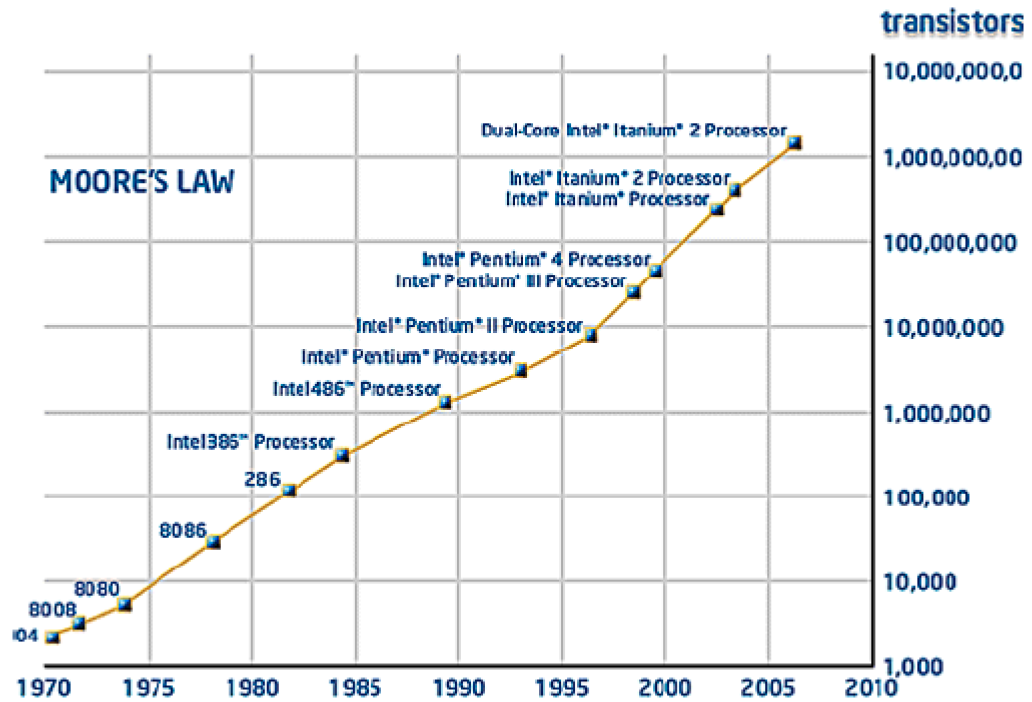

Figure 1.2 CPU transistor counts from 1970s to present, showing the device scaling according to Moore's Law; © Intel corp. [4].

1.2 Current Memory Technologies

The simplest form of a memory cell is a simple switch which can assume the state of "0" and "1", and memorize the state. Memories can be based on mechanical, magnetic, optical, biological and electronic technologies. Electrical memory is used extensively in computers and portable equipments since it is fast in response and compact in size. Electrical memory can electrically read/write directly when connected to the central processing unit. This feature distinguishes electrical memory from other forms of storage (CD, DVD, floppy disk, and hard disk), for the latter units need a driver to convert optical, magnetic or other signal to electrical signal for computer system to recognize. In contemporary usage, "memory" usually refers to a form of solid state storage known as random access memory (RAM) and sometimes

other forms of fast but temporary storage. Similarly, “storage” is more commonly referred to mass storage-optical discs (such as CD and DVD), forms of magnetic storage (such as hard disks), and other types of storage which are slower than RAM, but of a more permanent nature.

Memory can be divided into two primary categories according to its volatility: volatile and non-volatile memories. Volatile memory loses the stored data as soon as the system is turned off. It requires a constant power supply to retain the stored information. Non-volatile memory can retain the stored information even when the electrical power supply has been turned off. Memory can also be divided into two primary categories according to its rewriting ability: read-only memory (ROM) and random-access memory (RAM). ROM is a type of non-volatile memory that is capable of holding data and being read from repeatedly. However, it is not feasible to modify its data. Even for some ROMs that can be reprogrammed, they are still categorized as ROMs since the reprogramming process is relatively infrequent. Occasionally, ROMs that can be written only once physically, but be read from many times are called write-once read-many times (WORM) memories. RAM is often used interchangeably with “rewritable memory”. In this sense, RAM is the “opposite” of ROM, although it is more realistically a sequential access memory.

The current memory technologies have evolved around semiconductor-based processing technologies. The memories are implemented on semiconductor-based ICs, and thus the so-called semiconductor memory. Semiconductor memory encodes “0” and “1” signals from the amount of charges stored in capacitors or transistors. The

current mainstream memory technologies include dynamic random-access memory (DRAM), static random-access memory (SRAM), and flash memory (NAND and NOR).

DRAM is a random access memory that stores each bit of data in a separate capacitor. As the real-world capacitors are not ideal and have tendency to leak electrons, the information eventually fades unless the capacitor charge is refreshed periodically. Since DRAM loses its data when the power supply is removed, it is in the class of volatile memory devices.

For SRAM, the term “static” indicates that the memory retains its stored information as long as power remains applied, unlike DRAM that needs to be periodically refreshed. However, SRAM is also a volatile memory and the data are preserved only while power is continuously applied.

Flash memory stores information in an array of floating gate transistors (Fig 1.3), called “cells”, each of which traditionally stores one bit of information. Flash memory is a type of non-volatile memory, which means that it does not require power to retain the information stored in the chip. In addition, flash memory can be electrically erased and reprogrammed. NOR flash memory, characterized by faster random access but larger cell size, is used mainly for code storage, where the program or the operating system is stored and executed by the microprocessor or microcontroller in place. NAND flash memory, characterized by a smaller cell size and higher storage density, but with slow sequential access, is used mainly for mass storage, where data files are sequentially recorded and read [6].

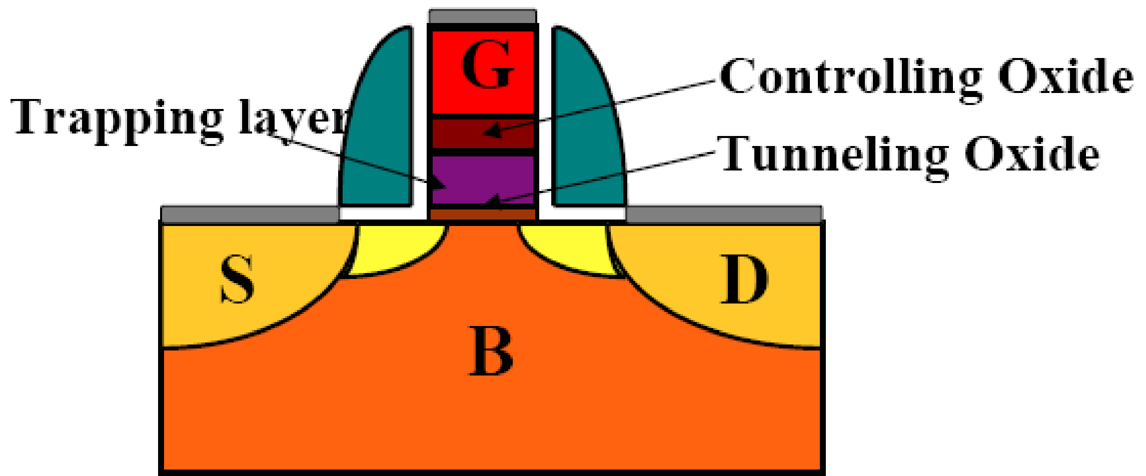

Figure 1.3 Schematic structure of a conventional floating gate flash memory cell.

Current mainstream memory technology based on semiconductors can only be sustained for several years due to the miniaturization problem [7]. Some recent technological developments have been considered for overcoming this limitation and to further scale down the conventional memory architecture. Both multi-level cell (MLC) and mirror bit technologies can double the memory density without significantly increasing the chip size. They can probably survive the memory processing technologies, without significantly changing at least the 65 nm technology node, using various self alignment techniques and advanced lithography [8]. Immediately beyond are two evolutionary memory technologies: trapping site storage and nanocrystal storage assisted by vertical processing techniques. These new technologies will permit scaling without changing the external character of the memory for a generation or so [8].

Multi-level cell (MLC) has the ability to store more than one bit per memory cell. For instance, 2 bits/flash cell can be realized by storing graduated charges that can be sensed by a comparator capable of distinguishing among four voltage levels. These voltage levels are assigned binary levels 00, 01, 10 and 11, setting two cell-bit values. MLC requires much better sensing amplifiers and more of them. The increase in area is compensated by doubling the bit storage [9].

Mirror bit memory stores two distinct bit charges per cell. It does this by providing two different access paths to the read or write cell-bit storage dielectric. This method allows the cell to address two different bit storage points. Obviously, the mirror bit is not expandable to 4 bit unless it utilizes the MLC technique as well [9].

Trapping site storage replaces the floating gates dielectric storage medium with a nitride trapping material sandwiched between two silicon-dioxide layers (ONO), and stores charge in trapping sites. These characteristics make it an evolutionary step from conventional floating gate flash storage. It is sufficiently similar in operation and support circuitry to the latter to make the phase-over relatively transparent to the market [8]. There are several variations of nitride storage cells, generally referred to as nitride ROM (NROM) and semiconductor-oxide-nitride-oxide-semiconductor (SONOS or MONOS). They differ in the erase mechanism and in the thickness of the gate layers. NROM uses a relatively thick bottom oxide to retain data. Hot-hole erase is used since the bottom oxide layer is too thick for tunneling [10]. SONOS (MONOS) tends to use the same programming and erase mechanisms commonly used by the floating gate flash memories and can also be used for embedded flash applications.

Making a nitride storage gate, either NROM or SONOS, requires fewer mask steps during the manufacturing process. Trapping site storage has the advantages of low power dissipation, low programming voltages and potential for multi-level storage [11].

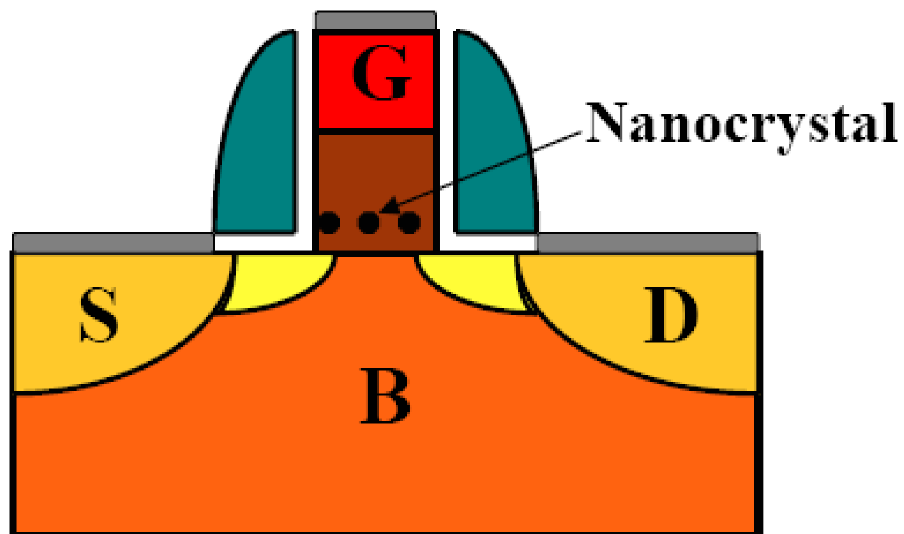

Figure 1.4 Schematic structure of a nanocrystal flash memory cell.

Nanocrystal storage uses a silicon nanocrystal as the floating gate, and is also called nano-floating gate memory (NFGM). Instead of injecting charges in the floating gate, charges are trapped in the silicon nanocrystals that act as nano-floating gates (Fig 1.4) [12]. By using electrically isolated charge-storage silicon dots, charge leakage through localized oxide defects is greatly reduced. A major benefit of the nano-floating gate approach is the improved reliability. Non-uniform distribution and size of the nanocrystals can be an issue leading to lack of reproducibility of device characteristics [13]. One recently reported method for improving uniformity in

nanocrystal size and distribution involves using self assembly of polymer blocks to define the nanocrystal size and location [14].

1.3 Prototypical Memory Technologies

To go beyond the current memory technology, alternative technologies that exploit new materials and concepts to allow better scaling, and to enhance the memory performance have been developed. Unlike the current memory technologies with the memory effects associated with a special cell structure, the new technologies are based on electrical bistability of materials arising from changes in certain intrinsic properties, such as magnetism, polarity, phase, conformation, in response to the applied electric field. The technologies based on organic materials are still at the conceptual and experimental levels, while some of those based on inorganic materials are almost matured and are identified as prototypical memory technologies by the ITRS in 2005 [15]. These prototypical technologies include ferroelectric random-access memory (FeRAM), magnetoresistive random access memory (MRAM) and phase-change memory (PCM) or ovonic unified memory (OUM).

FeRAM stores data as a remnant polarization in a ferroelectric material [16]. Two classes of ferroelectric materials are currently used for FeRAM memories: perovskite structures and layered structures. Actually, the most widely used perovskite material for ferroelectric memories is a Pb-Zr-Ti oxide, $Pb(Zr, Ti)O_3$, also called PZT, which is referred to as SBT [16]. When an electric field is applied to a ferroelectric crystal, the central atom will move in the direction of the field. As the atom moves within the

crystal, it passes through an energy barrier, causing a charge spike. Internal circuits sense the charge spike and set the memory. If the electric field is removed from the crystal, the central atom stays in position, preserving the state of the memory (Fig 1.5) [9]. Therefore, the FeRAM memory needs no periodic refresh and when power fails, it still retains its data [17]. FeRAM provides a relatively fast random access read and a fast write with relatively low power consumption. FeRAM, however, is read destructive and has limited capability for memory rewrite [9].

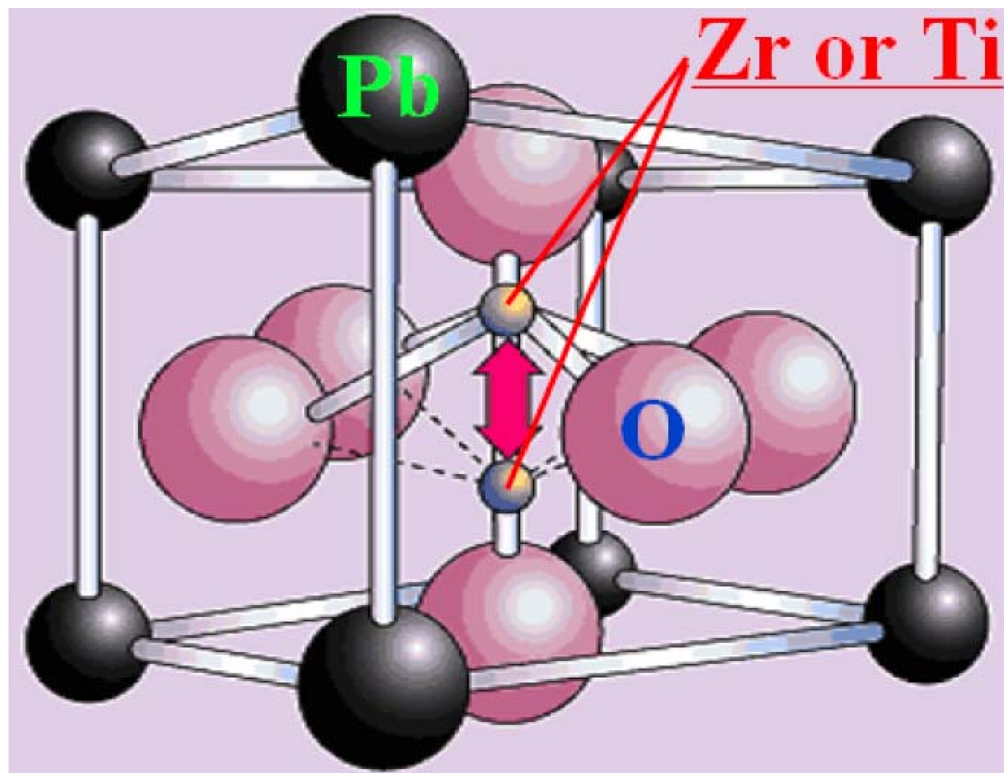

Figure 1.5 Schematic illustrating the mechanism of a FeRAM [9].

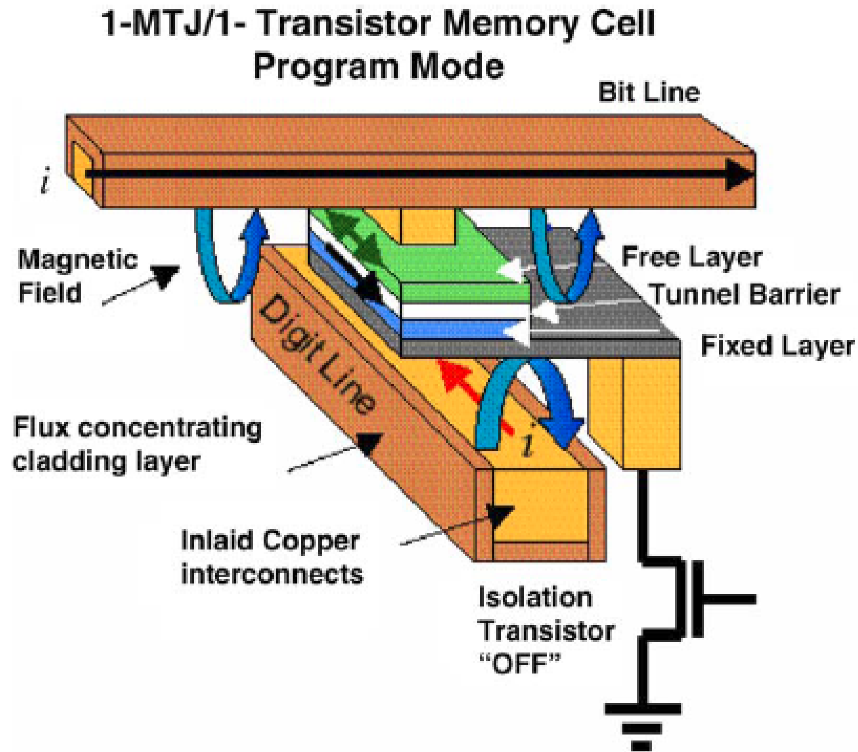

Figure 1.6 Schematic diagram showing the programming operation mode of a MRAM memory [12].

MRAM stores data using the orientation of two magnetic layers separated by a thin dielectric layer (e.g., Al_2O_3) [18]. The magnetic materials can be $Co_{90}Fe_{10}$ (ferromagnet), $Mn_{55}Fe_{45}$ (antiferromagnet), and others [19]. When the magnetic layers are oriented in the same direction and a voltage is applied across them, current tunnels through the dielectric layer. When the layers are oriented in opposite directions, a smaller percentage of current tunnels through. The percentage change in current is called the magnetoresistance and can be sensed in magnetic tunnel junction, or MTJ (Fig 1.6) [12]. MRAM is a non-volatile memory and is read non-destructive with unlimited read and write endurance. However, material incompatibility in integration the magnetic material into a silicon process for reliable production may present a problem [9].

PCM (or OUM) uses the unique behavior of chalcogenide glass, which can be switched between two states, crystalline or amorphous, with the application of heat [20]. The storage medium, chalcogenide glass, for example, $Ge_2Sb_2Te_5$ (GST), is made from Group VI elements in the periodic table [21]. The bit state is changed by heating a small amount of the chalcogenide material with an electrical current. When the material melts, it loses all the crystalline structure and becomes a resistor. When the material returns to the crystalline state, it becomes a conductor again (Fig 1.7). Thus, PCM is a rewritable and non-volatile memory with nondestructive reads. The cell can run at low voltages with relatively low power dissipation [21].

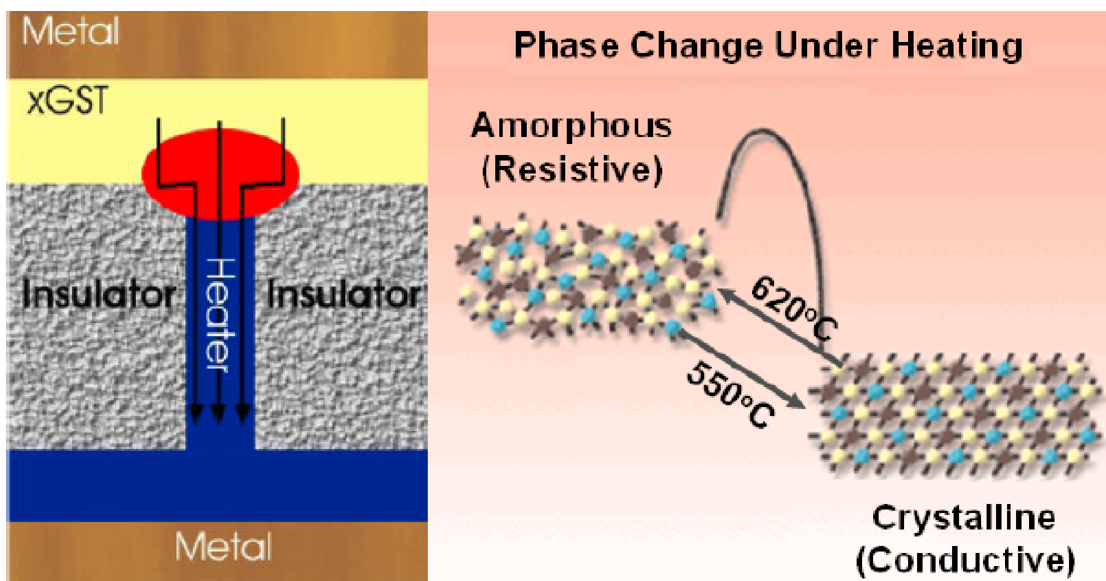

Figure 1.7 Schematic cross-section of a PCM cell. The active region is adjacent to the GST-heater interface [21].

1.4 Emerging Memory Technologies

Among the several emerging memory technologies on the horizon are the organic molecular/polymer memories [15]. Organic memory is a broad term encompassing

different proposals for using individual or small collections of molecules as building blocks of memory cells. Rather than encoding “0” and “1” as the amount of charge stored in a cell in silicon devices, organic memory stores data, for instance, based on the high- and low- conductivity response to an applied voltage. Organic materials are promising candidates for future nano-scale and molecular-scale device applications. Their attractive features include miniaturized dimensions and the possibility for molecular design through chemical synthesis. Indeed, assemblies of nanostructures with engineered properties and specific functions can be tailored via organic synthesis [2]. Advantages of molecular/polymer memories include simplicity in device structure, good scalability, low cost potential, low power operation, multiple state property, three-dimensional (3D) stacking capability and large capacity for data storage [22]-[29]. In particular, polymer materials possess unique properties, such as good mechanical strength, flexibility, and most important of all, ease of processing. As an alternative to the more elaborated processes of vacuum evaporation and deposition of inorganic and organic molecular materials, manufacturers can eventually use an ink-jet printer or spin-coater, for examples, to deposit polymers on a variety of substrates (plastics, wafers, glass or metal foils) [22].

A comparison of reported chip sizes and performances for the various memory technologies discussed above is shown in Table 1.1 [15].

Table 1.1.Comparison of memory technologies (data from ITRS 2005 [15]).

	Baseline Technologies					Prototypical Technologies			Emerging Technologies	
	DRAM		SRAM	Flash		FeRAM	MRAM	PCM	Molecular	Polymer
	Standalone	Embedded		NOR	NAND					
Storage mechanism	Charge on a capacitor		Interlocked state of logic gates	Charge on floating gate		Remanent polarization on a Fe capacitor	Magnetization of Fe contacts	Reversibly phase changing	Unknown	Unknown
Cell elements	1T1C		6T	1T		1T1C	1T1R	1T1R	1T1R or 1R	1T1R or 1R
Feature size F (nm)	80	130	90	130	130	130	180	90	5-10	5-10
Cell area	7.5 F^2	12 F^2	140 F^2	10 F^2	5 F^2	34 F^2	25 F^2	7.2 F^2	5 F^2	8/5 F^2
Read time	<15 ns	1 ns	0.4 ns	14 ns	70 ns	80 ns	<25 ns	60 ns	<10 ns	<10 ns
Write time	<15 ns	1 ns	0.4 ns	1 µs	1 ms	15 ns	<25 ns	50 ns	<40 ns	Unknown
Erase time	<15 ns	1 ns	0.4 ns	10ms	0.1 ms	15 ns	<25 ns	120 ns	<40 ns	Unknown
Retention time	64 ms	64 ms		>10y	>10y	>10y	>10y	>10y	Unknown	Unknown
Write cycles	>3E16	>3E16	>3E16	>1E5	>1E5	1E13	>1E15	1E12	>3E16	>3E16
Write voltage	2.5 V	2.5 V	1.2 V	12 V	15 V	0.9-3.3 V	1.8 V	3 V	2 V	Unknown
Read voltage	2.5 V	2.5 V	1.2 V	2.5 V	2.5 V	0.9-3.3 V	1.8 V	3 V	0.3 V	0.7 V
Write energy (J/bit)	1E-16	1E-16	7E-16	8E-15	8E-15	2E-14	1E-10	1E-10	2E-14	Unknown
Notes	a) 1T1C=1 transistor and 1 capacitor, 1R=1 transistor, etc; b) Best projected values for molecular/polymer memory technologies.									

1.5 Organic/Polymer Memory Fundamentals

1.5.1 Device Structures

The memory cell usually has a sandwich structure of organic molecular or polymer thin film between two electrodes on a substrate (plastic, wafer, glass or metal foil) (Fig 1.8). The configuration of electrodes can be symmetric or asymmetric, with Al, Au, Cu, *p*- or *n*-doped Si and indium-tin oxide (ITO) as the most widely used electrode materials. This kind of metal-insulator-metal (MIM) device is referred as a single-layer (active layer) memory device. Triple-layer memory device, consisting of an organic/metal-nanocluster/organic structure interposed between two electrodes, has also been widely used. In some cases, the memory devices may also contain one or more buffer layers.

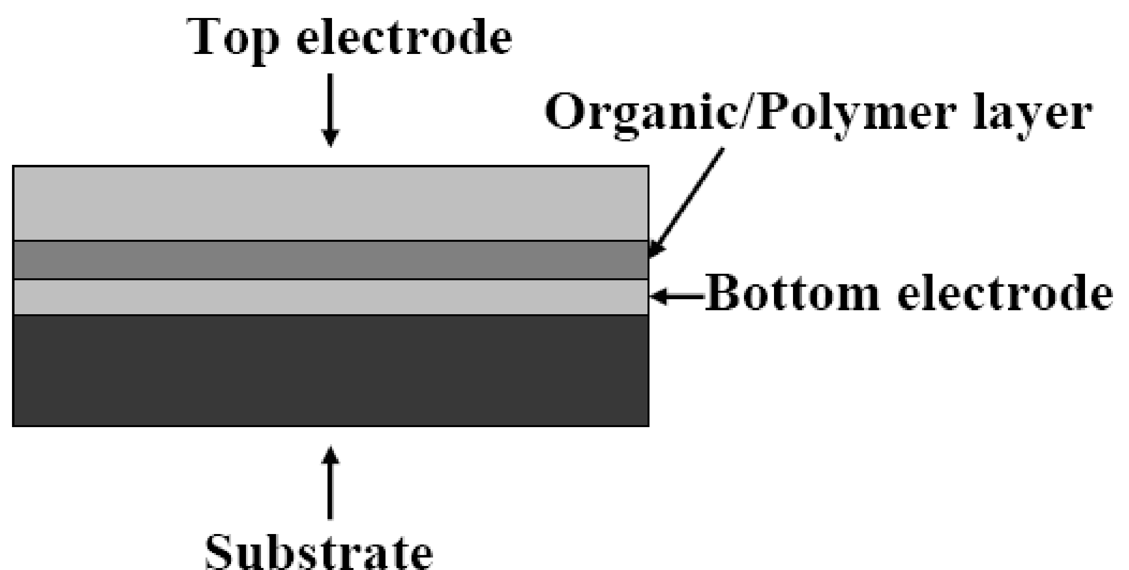

Figure 1.8 Basic cell structure of an electrical memory device.

1.5.2 Memory Architectures

Transistor-selected memories Molecular/polymer memory cells can be integrated to arrays and driven by the conventional thin-film transistor (TFT) technology. A cell with a transistor (1T1R) can be faster and more readily integrate with traditional electronics. However, transistor-selected memories are not able to meet the high density and low-cost requirements, since the cell size at best can be similar to the NOR Flash.

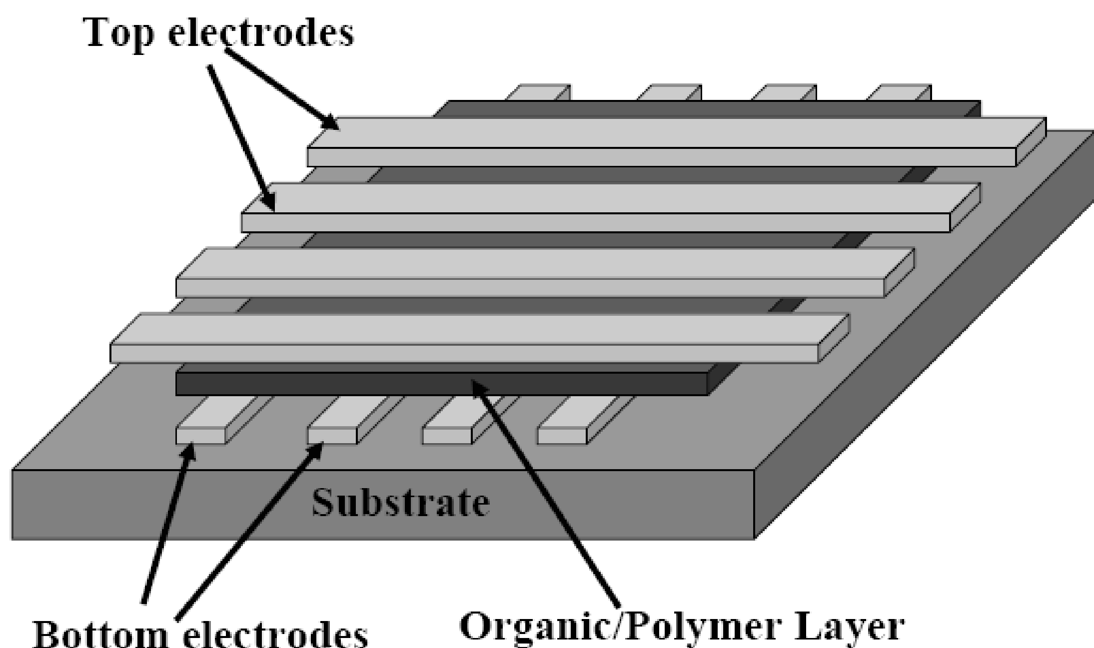

Figure 1.9 Crosspoint memory array with memory cells separated by a resistive layer.

Passive array or crosspoint memories Crosspoint arrays with cells separated by a resistive layer (1R) can have potentially smaller cell size and can define wire arrays with a pitch on the nanometer length scale (Fig 1.9). However, the parasitic leakage currents in a passive array can affect the reading and programming processes [30].

The easiest and more compact solution is the integration of one diode in series with the cell, at least for the resistive type of memories, and the use of intermediate voltages on non-selected cells [6].

SPM probe storages Scanning probe microscope (SPM), such as the scanning tunneling microscope (STM) or the atomic force microscope (AFM), appears to be a powerful tool to shrink the size of a memory system. In this system, the ultra-sharp probe electrode replaces the top electrode in a MIM structure and a memory with huge capacity can be realized. The probe storage relies on a "seek-and-scan" mechanism, actuated typically through a MEMS motor [6]. The main advantage of the probe storage is in its independence of lithography. However, the drive requirement of the probe storage makes it unsuitable for embedded systems, thus limits its application in mass data storage rather than an electrical memory.

Three-dimension (3D) memories Molecular/polymer memories are two-terminal devices. Thus, the memory layers can be stacked on top of each other, separated by an insulator. The principal configuration of a 3D stacked organic hybrid memory is shown in Fig 1.10 [31]. The Si chip includes all the CMOS circuits necessary to operate the array. They can be placed under the array, resulting in very high cell efficiency. Electrodes may also be shared among different memory layers, further reducing the processing steps for the memory array. 3D stacking can drastically increase the memory density.

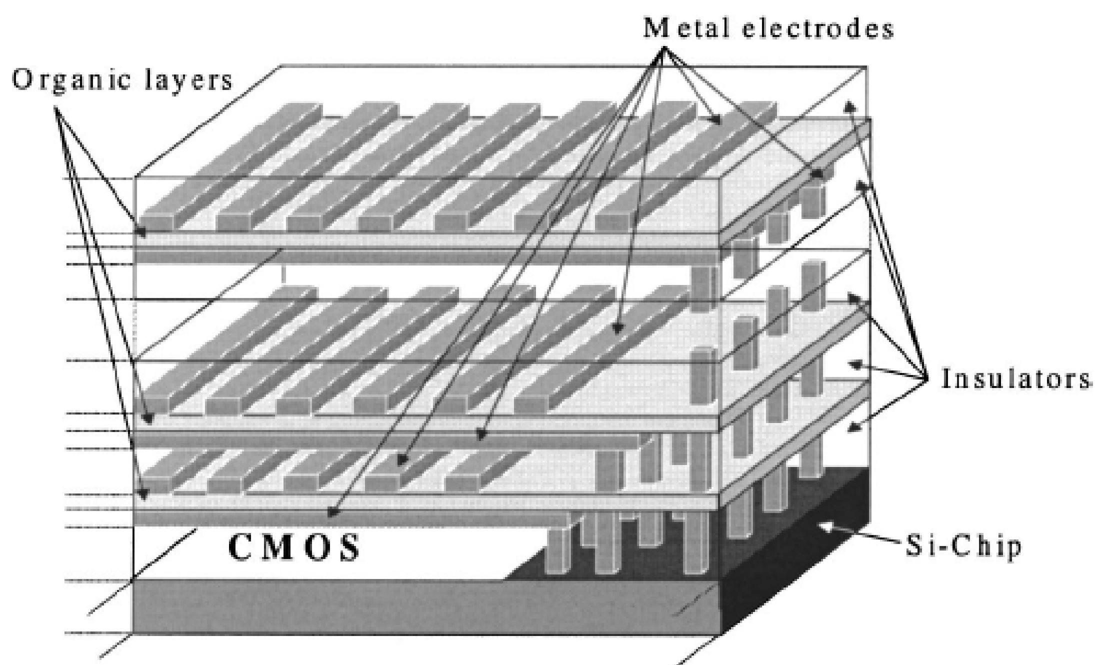

Figure 1.10 Principal arrangement of 3D stacked organic memory [31].

1.5.3 Fabrication Methods

Silicon device fabrication is a top-down approach: etching away at a silicon crystal to form micrometer-sized devices and circuitry. By contrast, molecular construction is a bottom-up technology that uses atoms to build nanometer-sized molecules. The latter could further self-assemble into a desired computational circuitry. This bottom-up approach gives rise to the prospect of manufacturing electronic circuits in rapid, cost-effective, flow-through processes. Currently, molecular/polymer films can be prepared by vacuum or thermal evaporation, spin-coating, ink-jet printing, self-assembly (SAM), Langmuir-Blodgett (LB) film formation, electrostatic self-assembly (ESA), template-directed assembly, surface grafting, and other techniques depending on material property.

1.5.4 Basic I-V Characteristics

Application of a sufficient high electric field to an organic material can eventually lead to deviation from linearity in the resultant current. Such deviation is referred to as the non-ohmic conductivity. The related effects of concern include (a) threshold switching, (b) memory switching, (c) electrical hysteresis, (d) rectifying (diode), and (e) negative differential resistance (NDR). Among them, (b) and (c) have electrical bistability in a voltage or current range. Thus they, including few cases of (d), can be utilized for data storage.

1.5.5 Performance Parameters

Some basic parameters are important to the performance of an organic memory device. These parameters include, (a) ON/OFF current ratio; (b) switching (writing and erasing) time; (c) retention ability; (d) write-read-erase-read (WRER) cycle; (e) stability under voltage stress; (f) stability under read pulses; and (g) long-term stability.

1.6 Current Status of Organic/Polymer Memory Device

On 1960s, some scientists found if they inserted some organic materials into two metal electrodes, the devices would show some memory effect. This is the beginning of organic/polymer memory research. During the past several decades, many materials were found that they would show memory effect under certain structure. In this section, organic/polymer materials for memories will be reviewed in summary.

1.6.1 Molecular Memories

1.6.1.1 Acene Derivative

The memory switching effects of several acene derivatives including naphthalene [32], anthracene [32, 33], tetracene [32, 34-36], pentacene [37], perylene [32, 35], *p*-quaterphenyl [36], *p*-quinquephenyl [38] and some of their derivatives, such as *N*, *N*'-di(naphthalene-1-yl)-*N*, *N*'-diphenyl-benzidine (NPB) [39] and 9, 10-bis-{9,9-di-[4-(phenyl-*p*-tolyl-amino)-phenyl]-9*H*-fluoren-2-*yl*}-anthracene (DAFA) [40], have been reported.

The memory switching was firstly observed in thin (600 nm) tetracene films sandwiched between aluminum and gold electrodes in 1969 [34]. Initially the tetracene film has a very high-resistance of about 10^{10} Ω. As the voltage is increased, the current increases rapidly in proportion to V^n, with $n>2$. As long as the voltage does not exceed a certain critical value this current-voltage characteristic is quite reversible under repeated cycling of the voltage. When the critical voltage is exceeded, the electrical resistance of the film decreases abruptly to a resistance of the order of 10^5 Ω [34].

1.6.1.2 Charge Transfer Complexes

A charge transfer complex (CT complex) is defined as an electron donor-electron acceptor complex, characterized by electronic transition to an excited state in which there is a partial transfer of electronic charge from the donor to the acceptor moiety [41]. The threshold switching and electrical memory phenomena of CT complex were

first reported in 1979 on a copper (electron donor) and 7,7,8,8-tetracyanoquinodimethane (TCNQ, acts as an electron acceptor) complex (Cu-TCNQ) [42]. Subsequently, a wide variety of organometallic and all-organic CT complexes have been explored for use in non-volatile organic memories [43].

A. Organometallic CT Complexes

The first CT complex memory was observed in a lamellar structure with a film of microcrystalline Cu-TCNQ sandwiched between Cu and Al electrodes. The switching effect is insensitive to moisture and is observed over a large temperature range. The current-voltage characteristics reveal an abrupt decrease in impedance from 2 MΩ to less than 200 Ω at field strength of $4x10^3$ V/cm [42]. The transition from a high- to low-impedance state occurs with delay and switching times of approximately 15 and 10 ns, respectively. When the applied voltage was removed, the device either acted as a threshold switch returning to the OFF state, or under the conditions of higher-power dissipation, a memory switch remaining in the ON state [42]. When operating as a memory switch, it is possible to drive the unit back to the high-impedance state by the application of a short pulse of current of either polarity. In addition, the high-resistance state can also be re-established by allowing the cell to remain for extended periods of time without an external electric field [42].

Stimulated by this discovery, many other organometallic CT complexes with different metals and organic acceptors have been prepared and explored for memory effects over the past few decades. These complexes include mainly:

(a) TCNQ with different metal donors: Cu [44], Ag [45], Li [46], K [47], Rb [48], Fe, Na, Ca, Mg, Mn, In, Cd and Pb [49].

(b) Ag or Cu with different acceptors: TCNQF4 [50], TCNE [51], TNAP [51], BDCB [52], BDCP [53], TDCN [54], SCN [55], and DDME [56].

(TCNQF4=2,3,5,6-tetrafluorotetracyanoquinodimethane, TCNE=tetracyanoethylene, TNAP=11,11,12,12-tetracyano-2,6-napthoquinodimethane, BDCB=1,4-bis(2,2-dicyanovinyl) benzene, BDCP=2,6-bis(2,2-dicyanovinyl)pyridine, TDCN=toluylene 2,4-dicarbamidonitrite, SCN=2,2'-(1,5,7,11-tetrathiaspiro[5.5]undecane-3,9-diylidene)dimalononitrile, DDME=1,1-dicyano-2,2-(4-dimethylaminophenyl)ethylene.)

B. All-Organic CT Complexes

When both the electron donor and acceptor are organic, the formed charge transfer complex is an all-organic CT complex. These molecular donor-acceptor compounds have been extensively studied as prospective organic electronics materials [57]. After the memory effects were demonstrated in metal-TCNQ salts, it was suggested that organic-TCNQ complexes might also exhibit electrical bistable states. In 1989, an improved tetrakis(methyltelluro)tetrathiafulvalene ($TTeC_1TTF$) with TCNQ as a mixed-stack CT crystal exhibited the switching effect at low temperature (200 K) [58]. Later, electrical switching was also observed in MTPA-$TCNQ_2$ (MTPA=methyltriphenylarsonium) crystals at room temperature (300 K) under pressure (up to 8 GPa) [59]. The characteristic switching is associated with the intrinsic negative resistance effect of the organic CT crystals [60]. This phenomenon

is therefore thought to reveal important features inherent to organic materials with electron-lattice instability. A series of all-organic CT complexes, including C_{60}-BDCP [61], C_{60}-TCNQ [62], C_{60}-DDME [63], MC-TCNQ [64], BBDN-TCNQ [64], DC-BDCB [65], DC-BDCP [66], DAB-NBMN [67], *p*-DA-NBMN [68], and TTF-NBMN [69], were prepared by alternative, mixed or dual deposition in a vacuum chamber. All films of these organic CT complexes exhibit electrical bistable states under room temperature and a short transition time from high to low resistance [55, 64].

(MC=melamine cyanurate, BBDN=bis[2-butene-2,3-dithiolato(2-)-s,s']-nickel; DC=decacyclene, NBMN=2-(3-nitrobenzylidene)malononitrile, DAB=diamino benzene, and *p*-DA=1,4-phenylenediamine.)

1.6.1.3 Organic Dyes

Organic dyes, such as cyanine dyes, phthalocyanines (Pc) and azo-metal complexes, are widely used in optical data storage [70]. Some of the organic dyes have also been explored for electrical memory effects since 1970 [71].

A. Phthalocyanine Derivatives

Phthalocyanines have been extensively investigated as a class of weakly semiconducting organic dye materials. Their thermal stability makes them suitable for thin film deposition by thermal sublimation and for applications in data storage, molecular switching, gas sensing, photovoltaic and others [72]. Metal-free

phthalocyanine (Pc) is known to exist in several polymorphic forms and the crystal modification strongly influences the electrical properties. Through employing the metal/metal-free Pc/metal sandwich structures with suitable organic layer thickness, bistable memory switching at a threshold voltage of about 40 V will be observed on this device [73]. Similar phenomena can also be observed from some other phthalocyanine derivatives, such as lead phthalocyanine (PbPc) [74], nickel phthalocyanine (NiPc) [75], copper phthalocyanine (CuPc) [76], and zinc phthalocyanine (ZnPc) [77].

B. Porphyrin Complexes

Porphyrins are natural pigments containing a fundamental skeleton of four pyrrole nuclei united through the α-positions by four methane groups to form a macrocyclic structure [78]. Molecular switching device utilizing LB monolayer films containing 5,10,15,20-tetrakis-octadecyloxymethylphenyl-porphyrin-Zn(II) (Zn-Por) as a redox-active component has been reported [79]. The devices (metal/Zn-Por LB monolayer/metal) exhibit outstanding switching diode and tunneling diode behavior at room temperature. These electrical properties of the devices may be applicable as active components in memory and/or logic circuits in the future.

C. Xanthene Derivatives

Xanthene is the basis of a class of dyes, including Rose Bengal (RB), fluorescein, Eosins and rhodamines. Among them, RB has electron acceptor groups all over the

surface of the molecule but without any donor group. Conductance switching was observed in either spin-coated or ESA RB films sandwiched between ITO and Al [80]. The single layer device based on spin-coated RB film has a large ON/OFF current ratio (10^5). However, the ON/OFF current ratio for the device based on ESA film is only 50-100 [80].

1.6.1.4 Trilayer Memories

This type of memory devices has a unique 3-layer structure consisting of organic/metal/organic layers sandwiched between two outer metal electrodes [81]. The device has two distinctive states of conductivity (OFF and ON) that can be achieved by applying voltage pulses with different polarities. The memory device is non-volatile and rewritable [81]. The model trilayer device, Al/AIDCN/Al/AIDCN/Al, had an ON/OFF ratio of more than 10^6 and a million write and erase cycles had been performed on this device (AIDCN=2-amino-4,5-imidazoledicarbonitrile) [81]. It was believed that the embedded metal layer played an important role in establishing the sudden increase in injection current and in the retention of high-conductivity state after the bias was removed [81]. Similar switching and memory behavior to that of the model trilayer device have also been observed when the embedded Al layer was replaced by the less reactive metals, such as Cu, Ag, and relatively inert Au. However, when it was replaced by a thin layer of lithium fluoride (LiF), an electrically insulating material, no electrical bistability was observed [82].

1.6.2 Polymer Memories

1.6.2.1 Ferroelectric Polymers

The most promising polymer materials for use in non-volatile memories are the class of ferroelectric polymers, with the vinylidene-fluoride polymers, such as poly(vinylidene-fluoride) (PVDF) and its copolymers with trifluoroethylene (TrFE) or tetrafluoroethylene (TeFE). The operation mechanism of a polymer ferroelectric memory (PFRAM) is similar to that of a FeRAM. The molecular units in the polymer chains of PVDF have net dipole moments pointing from the electronegative fluorine to the electropositive hydrogen. These chains can crystallize in parallel rows and, in the ferroelectric state, the dipoles of all chains are aligned along a two fold crystalline axis, resulting in a macroscopic polarization. Switching is accomplished by applying a large electric field opposing the polarization. The main advantages of ferroelectric polymers relative to ferroelectric perovskites are the low production costs, 3D stacking for high density storage, ease and flexibility of fabrication in a variety of thin-film forms, chemical stability, and resistance to degradation caused by strain or defects [83, 84].

1.6.2.2 Insulating Polymers

Bistable switching and memory behavior from devices based on Saran® wrap, a thermoplastic resin derived from vinylidene chloride were observed in 1970 [71]. Following that, a wide variety of insulating polymers have been reported to show threshold and memory switching effects. These polymers include polystyrene (PS)

[71], polyethylene (PE) [85], polymethylmethacrylate (PMMA) [86], polyethylmethacrylate (PEMA) [86], etc. A wide variety of electrodes, such as Au, Al, Cu, Pt, Ag, Mo have been successfully in memory devices. The memory switching in these device is mostly due to the formation of filamentary conduction paths [71, 85, 86]. The formed filaments sometimes could be observed under an optical or scanning electron microscope [71, 86]. The observed current-voltage characteristics can be explained by postulating the existence of a number of filaments with various resistances and threshold voltage [87]. Electrical switching in these polymer devices is then a consequence of the forming, rupture and reforming of these filaments [88].

1.6.2.3 Semiconducting Polymers

Since the initial discovery in 1977 that polyacetylene $(CH)_x$, now commonly known as the prototype conducting polymer, can be *p*- or *n*-doped either chemically or electrochemically to the metallic state, development in the field of conducting polymers has continued at a rapid pace [89]. A wide range of electroactive polymers have been discovered and become of great scientific and technological importance, since they have commercial or potential applications in many areas. One of the applications is memory application. In 1985, a LB multi-layer film of polydiacetylene (PDA) has been considered for memory application [90]. Following that, a wide variety of semiconducting polymers have been reported to show threshold and memory switching effects. These polymers include polythiophene (PTh) derivatives such as poly(4-dicyanomethylene-4*H*-cyclopenta[2,1-b:3,4-b']dithiophene) (PCPDT)

[91], poly[3-(6-methoxyhexyl)thiopene] (P6OMe) [92], poly(ethylene dioxythiophene) (PEDT): polystyrene sulfonic acid (PSS) or (PEDOT) [93], and poly(*p*-phenylenevinylene) (PPV) such as PPV [94] and poly[2-methoxy-5-(2'-ethylhexyloxy)-1,4-phenylenevinylene] (MEH-PPV) [95].

1.6.2.4 Composite Materials

Polymers have also been blended with organic compounds, such as CT complexes, organic dyes, organic metal particles and carbon-rich compounds to form composite materials and to facilitate solution process in memory fabrications. Examples of such kinds of materials include PS: C_{60} composite [96], PVP:C_{60} composite [97], P3HT: carbon nanotube (CNT) composite [98], PS: 8-hydroxyquinoline (8HQ) : gold nanoparticle (GNP) [99], etc.

1.7 Motivation of Study

As discussed above, to go beyond the current silicon-based memory technology, alternative technologies that exploit new materials and concepts to allow better scaling, and to enhance the memory performance need to be developed. Among the several emerging memory technologies (FeRAM, MRAM, PCM, and organic/polymer memory), organic/polymer memories have a lot of advantages such as simplicity in device structure, good scalability, low-cost potential, possibility for molecular design through chemical synthesis. All of these advantages suggest that organic/polymer memory should be a good candidate for future memory technology.

Although memory effect has been observed from a lot of organic/polymer materials based device since 1960s, none of the devices based on these materials can fulfill all the requirements for memory application. It is commonly known that, the current organic and polymer materials are not as stable as silicon, especially under at high temperature environment. Compared with the well developed silicon-based traditional semiconductor industry, organic electronics is quite a novel field. Thus, we cannot expect that the performance of the organic device to compete with the silicon device at the current stage. Improvement on this organic device performance needs further research work. This leads to the main aim of the study which was to investigate the possible organic and polymer materials that can be used in memory device and to develop a sandwiched metal-insulator-metal (MIM) device structure for memory application. Results of the present study may enhance our understanding of the application of organic and polymer materials to the organic memory device and it may also contribute to further investigations on the material selection for organic memory device.

Reference

[1] G.E. Moore, Digest of the 1975 International Electron Devices Meeting, IEEE, New York, pp.11 (1975).

[2] F.M. Raymo, Adv. Mater. **14**, 401 (2002).

[3] S.R. Forrest, Nature. **428**, 911 (2004).

[4] From Intel corp.; http://www.intel.com/technology/mooreslaw/index.htm

[5] International Technology Roadmap of Semiconductors (ITRS), Semiconductor Industry Association (SIA), SanJose, CA 95110. Available: http://www.itrs.net/Links/2006Update/2006UpdateFinal.htm

[6] R.Bez, Microelectron. Eng. **80**, 249 (2005).

[7] K.Galatsis, K.Wang, Y. Botros, Y. Yang, Y. H. Xie, J. F. Stoddard, r. B. Kaner, C. Ozkan, J. L. liu, M. Ozkan, C. W. Zhou, and K. W. Kim, IEEE Circuits Devices **22**, 12 (2006).

[8] B. Prince, in Non-Volatile Memory Technology Symposium (NVMTS), IEEE Computer Society, Dallas, TX, USA, pp.55 (2005).

[9] R. Weiss, Electron. Design. **49**, 56 (2001).

[10] L. Larcher, P. Pavan, and B. Eitan, IEEE Trans. Electron Devices. **51**, 1593 (2004).

[11] M. H. White, Y. Wang, S. J. Wrazien, and Y. Zhao, Int. J. High Speed Electron. Sys. **16**, 479 (2006).

[12] R. Bez and A. Pirovano, Mater. Sci. Semicond. Proc. **7**, 349 (2004).

[13] D. Tsoukalas, P. Dimitrakis, S. Kolliopoulou, and P. Normand, Mater. Sci. Eng. B

124, 93 (2005).

[14] K. W. Guarini, C. T. Black, Y. Zhang, I. V. Babich, E. M. Sikorski, and L. M. Gignac, Digest of the 1975 International Electron Devices Meeting, IEEE, Washington, DC, USA, pp. 22 (2003).

[15] International Technology Roadmap of Semiconductors (ITRS), Semiconductor Industry Association (SIA), SanJose, CA 95110. Available: http://www.itrs.net/Links/2005ITRS/Home2005.htm

[16] N.Setter, D. Damjanovic, L. Eng, G. Fox, S. Gevorgian, S. Hong, A. Kingon, H. Kohlstedt, N. Y. Park, G. B. Stephenson, I. Stolitchnov, A. K. Taganstev, D. V. Taylor, T. Yamada, and S. Streiffer, J. Appl. Phys. **100**, 051606 (2006).

[17] J. F. Scott, J. Phys. Condens. Matter **18**, 361 (2006).

[18] B. J. De, R. W. Van, J. Das, V. Motsnyi, Z. Liu, L. Lagae, H. Boeve, K. Dessein, and G. Borghs, Semicon. Sci. Tech. **17**, 342 (2002).

[19] R. L. Comstock, J. Mater. Sci. Mater. Electron. **13**, 509 (2002).

[20] S. Hudgens and B. Johnson, MRS Bull. **29**, 829 (2004).

[21] A. L. Lacaita, Solid State Electron. **59**, 24 (2006).

[22] A. Stikeman, Technol. Rev. **105**, 31 (2002).

[23] Y. Yang, J. Ouyang, L. P. Ma, R. J. Tseng, and C. W. Chu, Adv. Funct. Mater. **16**, 1001 (2006).

[24] L. Fu, L. c. Cao, Y. Q. Liu, and D. B. Zhu, Adv. Colloid Interfac. **111**, 133 (2004).

[25] C. Li, W. D. Fan, B. Lei, D. H. Zhang, S. Han, T. Tang, X. L. Liu, Z. Q. Liu, S. Asano, M. Meyyappan, J. Han, and C. W. Zhou, Appl. Phys. Lett. **84**, 1949

(2004).

[26] E. Guizzo, IEEE Spectrum. **41**, 17 (2004).

[27] Y. Yang, L. P. Ma, and J. H. Wu, MRS Bull. **29**, 833 (2004).

[28] R. F. Service, Science. **293**, 1746 (2001).

[29] J. C. Scott, Science. **304**, 62 (2004).

[30] Z. Y. Hua and G. R. Chen, Vacuum. **43**, 1019 (1992).

[31] C. U. Pinnow and T. Mikolajick, J. Electrochem. Soc. **151**, K13 (2004).

[32] S. G. Garrett, R. Pethig, and V. Soni, J. Chem. Soc. Faraday Trans. II. **70**, 1732 (1974).

[33] A. R. Elsharkawi and K. C. Kao, J. Phys. Chem. Solids. **38**, 95 (1977).

[34] A. Szymanski, D. C. Larson, and M. M. Labes, Appl. Phys. Lett. **14**, 88 (1969).

[35] J. Kevorkian, M. M. Labes, D. C. Larson, and D. C. Wu, Disc. Faraday Soc. **51**, 139 (1971).

[36] H. Kasica, W. Wlodarski, H. Kurczewska, and A. Syzmanski, Thin Solid Films. **30**, 325 (1975).

[37] D. Tondelier, K. Lmimouni, D. Vuillaume, C. Fery, and G. Haas, Appl. Phys. Lett. **85**, 5763 (2004).

[38] J. Swiatek, Thin Solid Films. **61**, 321 (1979).

[39] J. S. Chen and D. G. Ma, Appl. Phys. Lett. **87**, 23505 (2005).

[40] J. S. Chen, L. L. Xu, J. Lin, Y. H. Geng, L. X. Wang, and D. G. Ma, Appl. Phys. Lett. **89**, 083514 (2006).

[41] A. Wilkinson, *Compendium of Chemical Terminology: IUPAC Recommendations*,

2nd ed. Blackwell Science, Boston (1997).

[42] R. S. Potember, T. O. Poehler, and D. O. Cowan, Appl. Phys. Lett. **34**, 405 (1979).

[43] K. Wang, H. Zhang, D. Wang, and Z. Xue, Vac. Sci. Tech. **16**, 277 (1996).

[44] C. Sato, S. Wakamatsu, K. Tadokoro, and K. Ishii, J. Appl. Phys. **68**, 6535 (1990).

[45] Q. Zhang, L. Z. Kong, Q. J. Zhang, W. J. Wang, and Z. Y. Hua, Solid State Commun. **130**, 799 (2004).

[46] J. P. Gong and Y. Osada, Appl. Phys. Lett. **61**, 2787 (1992).

[47] Q. J. Cai, G. R. Chen, X. L. Mo, Z. Y. Fan, H. H. Gu, Y. Yao, J. Yang, Z. Y. Hua, and H. H. Xu, Vac. Sci. Tech. **21**, 364 (2001).

[48] N. Watanabe, Y. Iwasa, and T. Koda, Phys. Rev. B. **44**, 11111 (1991).

[49] H. L. Duan, D. O. Cowan, and J. Kruger, Synth. Met. **42**, 1657 (1991).

[50] R. S. Potember, T. O. Poehler, A. Rappa, D. O. Cowan, and A. N. Bloch, Synth. Met. **4**, 371 (1982).

[51] R. S. Potember, T. O. Poehler, D. P. Cowan, and A. N. Bloch, ACS Division of Organic Coatings and Plastics Chemistry, Preprints. **43**, 380 (1980).

[52] K. Z. Wang, Z. Q. Xue, M. Ouyang, H. X. Zhang, and C. H. Huang, Solid State Commun. **96**, 481 (1995).

[53] Z. Q. Xue, M. Ouyang, K. Z. Wang, H. X. Zhang, and C. H. Huang, Thin Solid Films. **288**, 296 (1996).

[54] H. J. Gao, Z. Q. Xue, Q. D. Wu, and S. J. Pang, J. Vac. Sci. Technol. B. **13**, 1242 (1995).

[55] Z. Y. Hua, W. Xu, G. R. Chen, X. J. Yan, X. L. Mo, and Q. Zhang, Synth. Met. **137**, 1531 (2003).

[56] K. Z. Wang, Z. Q. Xue, M. Ouyang, D. W. Wang, H. X. Zhang, and C. H. Huang, Chem. Phys. Lett. **243**, 217 (1995).

[57] S. Horiuchi, T. Hashgawa, and Y. Tokura, J. Phys. Soc. Jpn. **75**, 051016-1 (2006).

[58] Y. Iwasa, T. Koda, Y. Tokura, S. Koshihara, N. Iwasawa, and G. Saito, Appl. Phys. Lett. **55**, 2111 (1989).

[59] T. Ravindran and S. V. Subramanyam, Appl. Phys. Lett. **62**, 1251 (1993).

[60] Y. Tokura, H. Okamoto, T. Koda, T. Mitani, and G. Saito, Phys. Rev. B. **38**, 2215 (1988).

[61] M. Ouyang, K. Z. Wang, H. X. Zhang, Z. Q. Xue, C. H. Huang, and D. Qiang, Appl. Phys. Lett. **68**, 2441 (1996).

[62] H. J. Gao, Z. Q. Xue, K. Z. Wang, Q. D. Wu, and S. Pang, Appl. Phys. Lett. **68**, 2192 (1996).

[63] M. Ouyang, Z. Q. Xue, K. Z. Wang, Q. D. Wu, and D. Qiang, J. Vac. Sci. Technol. B. **15**, 1304 (1997).

[64] W. Xu, G. R. Chen, R. J. Li, and Z. Y. Hua, Appl. Phys. Lett. **67**, 2241 (1995).

[65] K. Z. Wang, Z. Q. Xue, M. Ouyang, H. X. Zhang, and C. H. Huang, J. Mater. Sci. Lett. **15**, 977 (1996).

[66] M. Ouyang, S. M. Hou, H. F. Chen, and K. Z. Wang, Phys. Lett. A. **235**, 413 (1997).

[67] H. J. Gao, L. P. Ma, H. X. Zhang, H. Y. Chen, Z. Q. Xue, and S. J. Pang, J. Vac.

Sci. Technol. B. **15**, 1581 (1997).

[68] H. J. Gao, K. Sohlberg.Z. Q. Xue, H. Y. Chen, S. M. Hou, L. P. Ma, X. W. Fang, S. J. Pang, and S. J. Pennycook, Phys. Rev. Lett. **84**, 1780 (2000).

[69] J. C. Li, Z. Q. Xue, W. M. Liu, S. M. Hou, X. L. Li, and X. Y. Zhao, Phys. Lett. A. **266**, 441 (2000).

[70] H. Mustroph, M.Stollenwerk, and V. Bressau, Angew. Chem. Int. Ed. **45**, 2016 (2006).

[71] P. O. Sliva, G. Dir, and C. Griffiths, J. Non-Cryst. Solids. **2**, 316 (1970).

[72] C. C. Leznoff and A. B. P. Lever, *Phthalocyanines, Properties and Applications*, Vol. 1-4, Wiley-VCH, New York (1997).

[73] M. Fustoss-Wegner and K. Ritvay-Emandity, **KFKI-75-17**, 5 (1975).

[74] T. Frauenheim, C. Hamann, and M. Mueller, Phys. Status Solidi A. **86**, 735 (1984).

[75] H. S. Majumdar, A. Bandyopadhyay, and A. J. Pal, Org. Electron. **4**, 39 (2003).

[76] C. H. Tu, Y. S. Lai, and D. L. Kwong, Appl .Phys. Lett. **89**, 62105 (2006).

[77] L. P. Ma, Q. F. Xu, and Y. Yang, Appl. Phys. Lett. **84**, 4908 (2004).

[78] R. Guilard, *The Porphyrin Handbook*, Academic Press, New York (1999).

[79] J. R. Koo, H. S. Lee, Y. Ha, Y. H. Choi, and Y. K. Kim, Thin Solid Films. **438**, 123 (2003).

[80] A. Bandyopadhyay and A. J. Pal, Appl. Phys. Lett. **82**, 1215 (2003).

[81] L. P. Ma, J. Liu, and Y. Yang, Appl. Phys. Lett. **80**, 2997 (2002).

[82] L. P. Ma, J. Liu, S. Pyo, Q. F. Xu, and Y. Yang, Mol. Cryst. Liq. Cryst. **378**, 185

(2002).

[83] S. Ducharme, T. J. Reece, C. M. Othon, and R. K. Rannow, IEEE Trans. Device Mater. Re. **5**, 720 (2005).

[84] A. J. Lovinger, in *Developments in Crystalline Polymers* edited I. D. C. Basset, Applied Sciences, London, UK, pp.195 (1981).

[85] J. Gazso, Thin Solid Films. **21**, 43 (1974).

[86] H. K. Henisch and W. R. Smith, Appl. Phys. Lett. **24**, 589 (1974).

[87] G. Dearnaley, D. V. Morgan, and A. M. Stoneham, J. Non-Cryst. Solids. **4**, 593 (1970).

[88] L. F. Pender and R. J. Fleming, J. Appl. Phys. **46**, 3426 (1975).

[89] A. G. MacDiarmind, Angew. Chem. Int. Ed. **40**, 2581 (2001).

[90] E. G. Wilson, Mol. Cryst. Liq. Cryst. **121**, 271 (1985).

[91] D. M. Taylor and C. A. Mills, J. Appl. Phys. **90**, 306 (2001).

[92] H. S. Majumdar, A. Bandyopadhyay, A. Bolognesi, and A. J. Pal, J. Appl. Pys. **91**, 2433 (2002).

[93] T. Johansson, L. A. A. Pettersson, and O. Inganas, Synth. Met. **129**, 269 (2002).

[94] S. K. Majee, H. S. Majumdar, A. Bolognesi, and A. J. Pal, Synth. Met. **156**, 828 (2006).

[95] M. Lauters, B. McCarthy, D. Sarid, and G. E. Jabbour, Appl. Phys. Lett. **89**, 13507 (2006).

[96] H. S. Majumdar, J. K. Baral, R. Osterbacka, O. Ikkala, and H. Stubb, Org. Electron. **6**, 188 (2005).

[97] S. Paul, A. Kanwal, and M. Chhowalla, Nanotechnology. **17**, 145 (2006).

[98] B. Pradhan, S. K. Batabyal, and A. J. Pal, J. Phys. Chem. B. **110**, 8274 (2006).

[99] J. Ouyang, C. W. Chu, C. R. Szmanda, L. P. Ma, and Y. Yang, Nat. Mater. **3**, 918 (2004).

Chapter 2

Synthesis and WORM Memory Properties of a Conjugated Copolymer of Fluorene and Benzoate with Chelated Europium Complex

2.1 Introduction

From the previous chapter we know that there is a growing interest on organic electronics, motivated by their potential low cost, light weight, good processability, and molecularly tailored electrical properties [1]. And a great deal of attention has been focused on organic and molecular memory devices [2]-[16]. A variety of promising approaches based on conformational changes [2], formation of conducting filaments [3, 4], formation of charge transfer complexes [5-7], redox process [8, 9], and charge-trapping [10-12] have been demonstrated. A number of polymer-based systems, such as poly(ethylenedioxythiophene):poly(styrene sulphonic acid) (PEDOT)/Si p-i-n diode [13], poly[3-(6-methoxyhexyl)thiophene] [14], polyfluorene embedded with Ag layers [15], polyaniline nanofibers with gold nanoparticles [16], and polystyrene as matrices for gold nanoparticles [10-12], have been studied for memory applications. Direct design and synthesis of processable polymers, which can provide the required electronic properties within a single macromolecule, for memory applications is an alternative approach.

In this chapter, we will describe the study on the synthesis and characterization of a conjugated copolymer of 9,9'-diethylhexylfluorene and europium complex-chelated benzoate (PF8Eu). The fluorene moieties are the backbone of the copolymer and serve as electron donors. The europium complex is an electron acceptor group and can be used to hold charges [17]. In addition to the high electron affinity (EA) property of the rare earth complex, the europium complexes in the chelated form also allow high quality films to be cast or processed directly from solutions of the copolymer without phase segregation. Nonvolatile memory effects were demonstrated in a metal/PF8Eu/metal sandwich structure. The current-voltage characteristics of the device indicate that it is potentially useful as a write-once read-many-times (WORM) memory. The stability and performance of the device as a WORM memory were also evaluated.

2.2 EXPERIMENT

2.2.1 Synthesis of the Copolymer

The synthetic route for the conjugated copolymer (PF8Eu) containing 9,9'-diethylhexylfluorene and europium complex-chelated benzoate units in the main chain is shown in Fig. 2.1. It involved three steps: 1) a copolymer of 2,7-bis(trimethylene boronate)-9,9-diethylhexylfluorene and methyl 3,5-dibromobenzoate (**P1**) was synthesized through a palladium-catalyzed Suzuki coupling reaction [18], 2) the copolymer was then hydrolyzed to provide the active carboxylic ligands in the main chains [19] (**P2**), and 3) the polymeric ligands,

together with dibenzoylmethane (DBM) and 1,10-phenanthroline (phen), chelated the highly reactive europium triisoproxide [20] to form the desirable copolymer complex

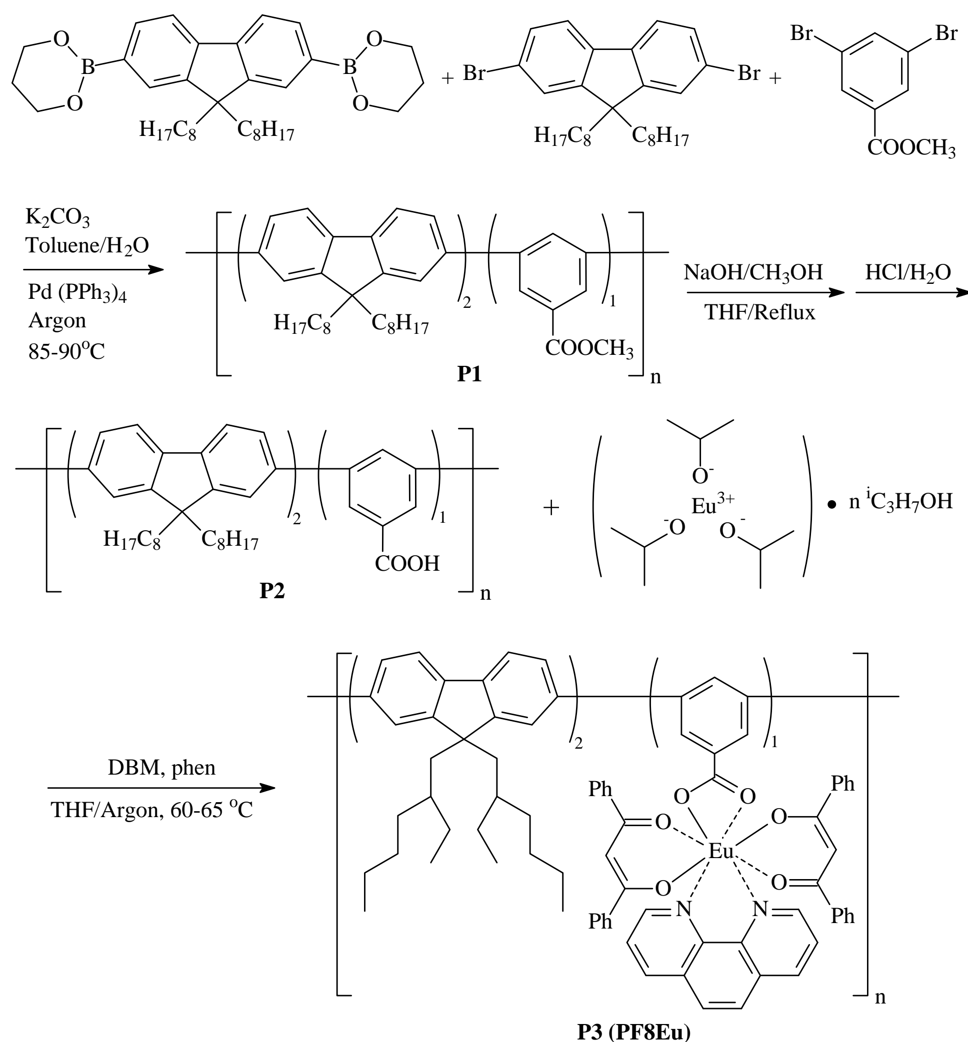

Figure 2.1 Synthetic route for the conjugated copolymer containing fluorene and europium complex in the main chain.

(**P3,** named as PF8Eu). PF8Eu is readily soluble in toluene, chloroform and THF, and can be cast into transparent films with good mechanical flexibility. The europium triisoproxide [20], palladium catalyst [21], and monomers [22] were prepared according to procedures described in the literature.

In the FT-IR spectrum of **P1**, the C=O stretching absorption band appeared at 1727 cm^{-1}. After hydrolysis (**P2**), this characteristic C=O band has split into two peaks, one located at 1670 cm^{-1}, near that of the C=O band in 3,5-dibromobenzoic acid, and another at 1736 cm^{-1}, near that of the corresponding monomer, methyl 3,5-dibromobenzoate. Thus, the ester groups of the copolymer were hydrolyzed completely, consistent with the reversible nature of ester hydrolysis. The typically broad absorption band of the –OH group appeared at around 3100 cm^{-1}. After incorporation of the europium complex, the C=O stretching vibration of the carboxylic group at 1670 cm^{-1} had disappeared in the FT-IR spectrum of **P3**, while the antisymmetric and symmetric stretching vibrations of the carboxylate group at about 1579 and 1411 cm^{-1} had appeared [23]. The results suggested that a coordination bond had formed between the Eu(III) ion complex and the carboxylic group of the copolymer. Furthermore, the broad absorption band of the –OH group had disappeared, suggesting that almost all of the carboxylic groups of the copolymer were chelated to the europium ions. The C=O and C=C stretching vibrations of the coordinated DBM occurred at about 1607 and 1540 cm^{-1}, respectively [24]. The infrared absorption bands of other functional groups, such as the alkyl chains, the phenyl groups and the 1,10-phenanthroline, were also detected.

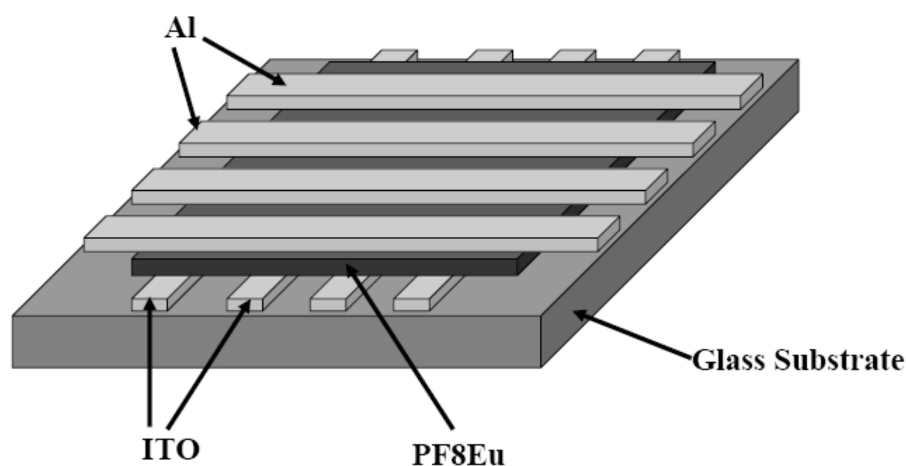

Figure 2.2 Schematic structure of the Al/PF8Eu/ITO memory device.

2.2.2 Device Fabrication

As shown in Fig. 2.2, the memory device comprised of a PF8Eu film sandwiched between an indium-tin-oxide (ITO) bottom electrode and an Al top electrode. The ITO coated glass (ITO thickness: 150 nm) substrate was patterned with 2 mm wide lines and cleaned with deionized water, acetone and isopropanol, in that order, in an ultrasonic bath for 20 min. The ITO was defined as the cathode and grounded in all electrical measurements. A toluene solution of PF8Eu (8 mg/ml) was sequentially spin-coated on the ITO substrate. The film was baked at $60^{o}C$ for 9 h in a vacuum chamber at 10^{-5} Torr to remove the solvent. Finally, Al with a line width of 0.2 mm and thickness of about 200 nm was vacuum-deposited at a pressure of $\sim 10^{-7}$ Torr through a shadow mask to form the top Al electrode. The shadow mask was used to pattern and define the top electrode area. The top and bottom electrodes were aligned perpendicular to each other, so as to define an active device area of 2 mm $\times$ 0.2 mm. The thickness of the polymer film was about 50 nm, as measured by a step profiler.

Electrical measurements were carried out in a dark chamber using a HP 4156A semiconductor parameter analyzer, an Agilent 4284A precision LCR meter, and an Agilent 41501B SMU and pulse generator. All electrical measurements were conducted under ambient condition without any encapsulation.

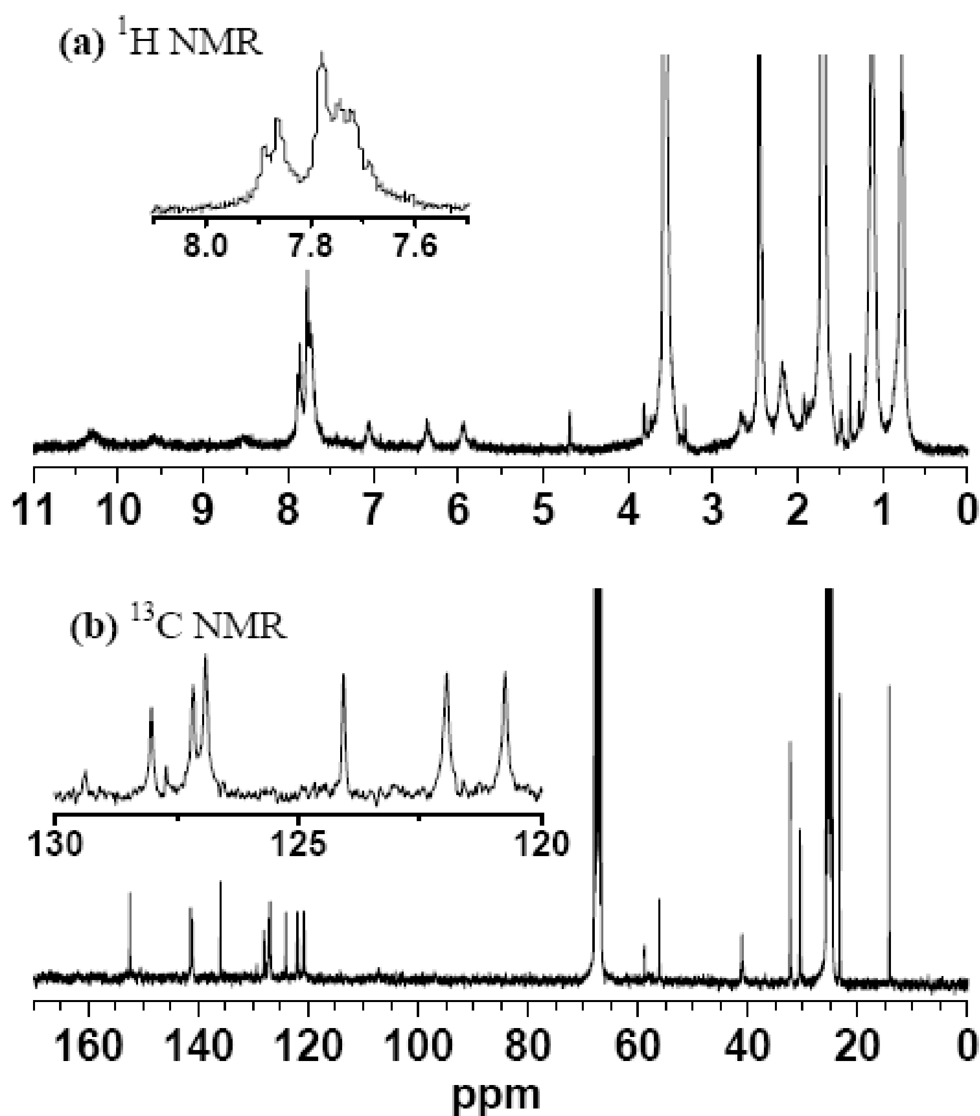

Figure 2.3 (a) ^{1}H NMR (300MHz) and **(b)** ^{13}C NMR (75MHZ) spectra of the PF8Eu copolymer in d_6-THF.

2.3 Experimental Results

2.3.1 Characterization of PF8Eu

In the ^{1}H NMR spectrum of **P3** or PF8Eu (Fig. 2.3(a)), the two main groups of peaks associated with the chemical shifts at 7.71-7.88 and 0.76-2.46 ppm can be attributed to the aromatic and the alkyl protons, respectively. There are three weak chemical shifts in the low magnetic field region (10.31, 9.59, and 8.52 ppm). These three broad peaks are attributable to the protons near the coordinated atoms in the ligands. It is difficult to assign the peaks individually. Due to the fact that the Eu(III) ion is paramagnetic, the ^{1}H NMR peaks of the protons around the O and N atoms may shift substantially to a lower field and become relatively broad. As a result of coordination with the Eu(III) ions, the electron cloud delocalizes throughout the whole complex, and gives rise to an increase in electron density of the ligands. Thus, the chemical shifts of the other protons in the ligands appear at higher fields (7.04, 6.36, and 5.92 ppm). A well-resolved ^{13}C NMR spectrum of PF8Eu is shown in Fig. 2.3(b). In the regions of chemical shifts for the aromatic (120.7-152.4 ppm) and aliphatic (14.27-56.08 ppm) carbon atoms, the spectrum is similar to that of the copolymer before chelation (**P2**). This result indicates that the effect of the europium complex on the carbon atoms, which are not bonded directly to the coordinated oxygen atoms, is negligible. The NMR results, thus, further confirm the formation of the copolymer complex.

Time-of-flight secondary ion mass spectrometry (ToF-SIMS) is useful for the determination of molecular structures in polymers [25]. Fig. 2.4 shows the positive ion ToF-SIMS spectra of PF8Eu. Fragments containing the europium complex are

found in the high mass region (m/z =525-780). In the mid-mass region (m/z =180-375), fragments of the polymers backbone (fluorene and phenylene) and the ligands (DBM and phen) are found. The europium ion appears at m/z around 152. The spectrum in the mass region of 0-120 contains fragments from the alkyl side chains.

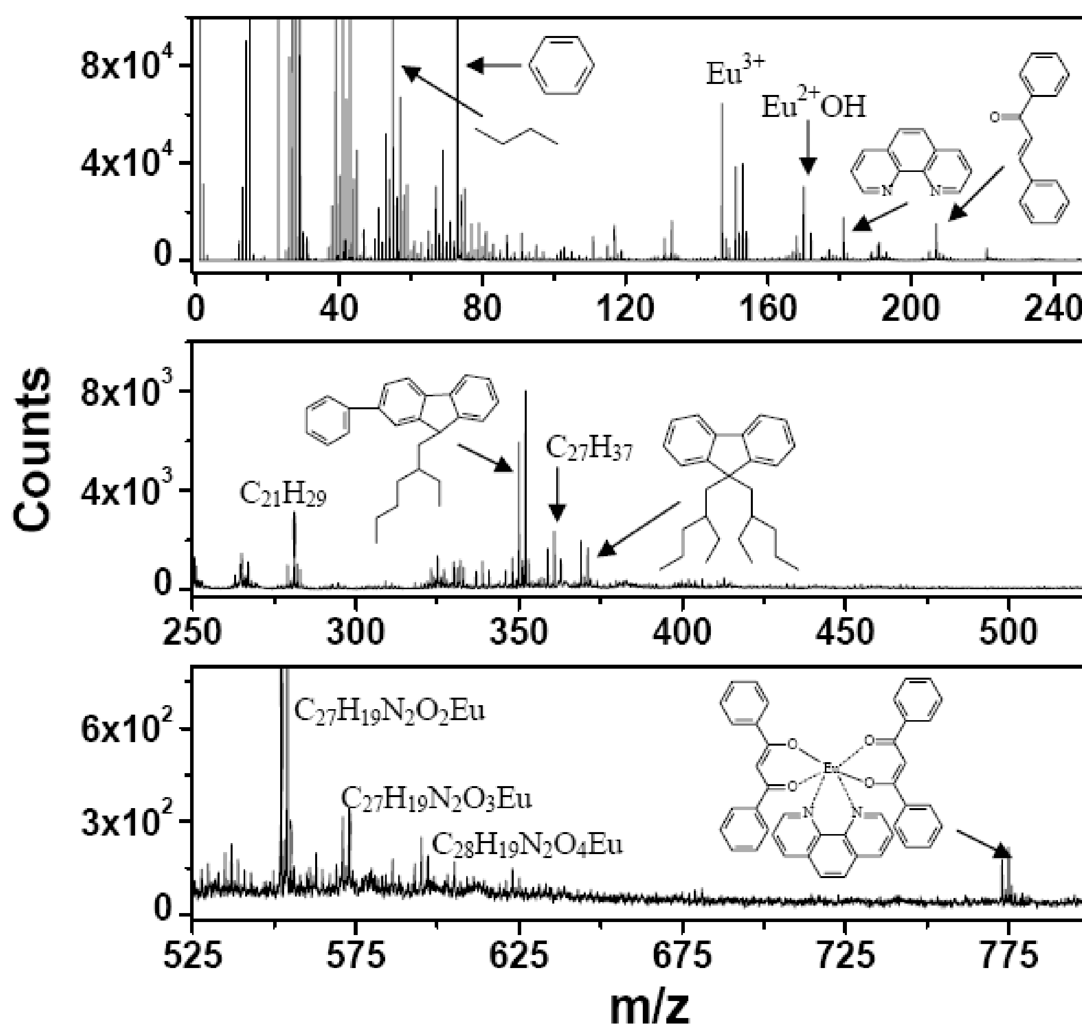

Figure 2.4 Positive ion ToF-SIMS spectra of the PF8Eu film spin-cast from THF solution on ITO glass.

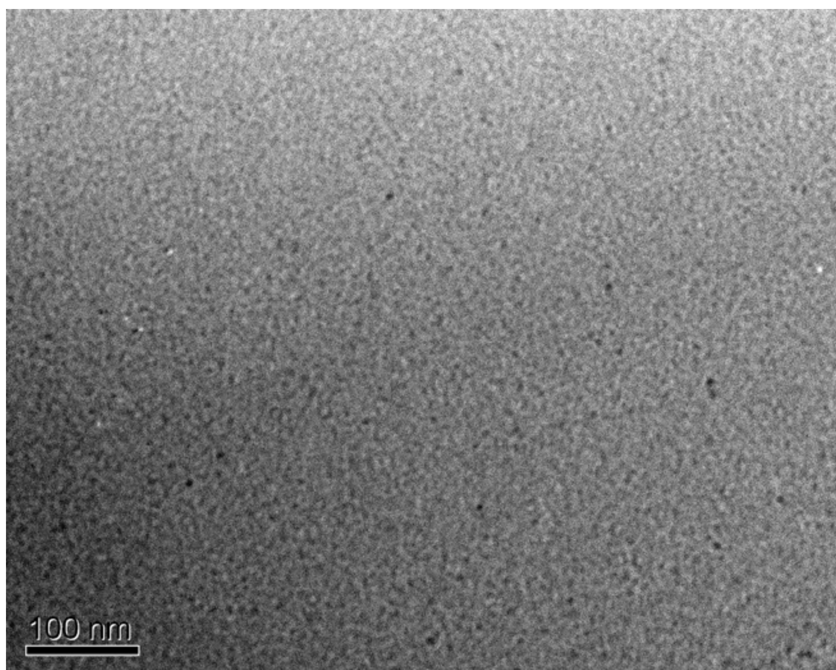

(a)

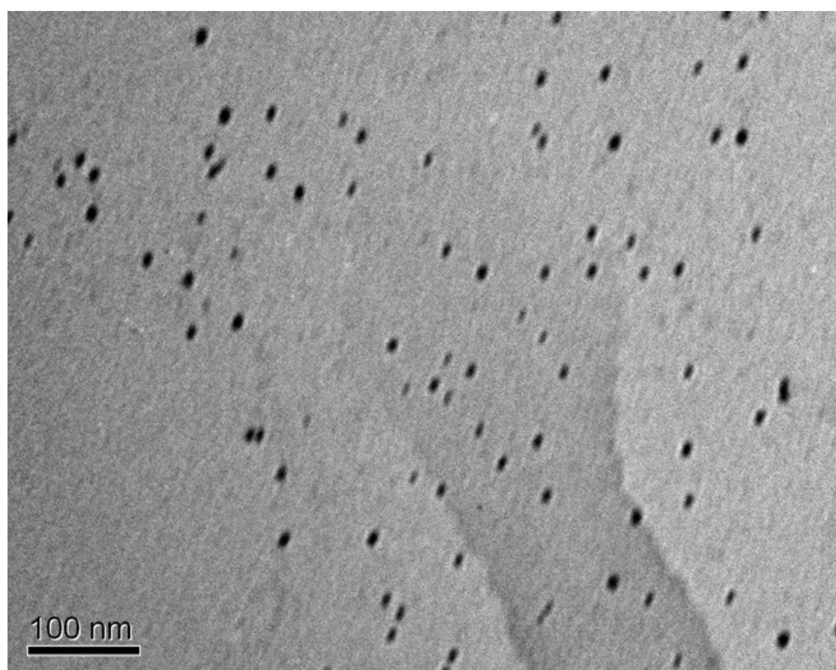

(b)

Figure 2.5 TEM images of **(a)** the PF8Eu film spin-cast from the toluene solution and **(b)** a polyfluorene film doped with the Eu complex to the same concentration as that of PF8Eu.

2.3.2 Device Performance

With a long chain molecular structure and chelated europium complexes, the copolymer can be readily cast into uniform and homogeneous films, which are essential to device fabrication and performance. As revealed by the transmission electron microscope (TEM) image of Fig. 2.5(a), the film cast from copolymer PF8Eu is completely homogeneous. Fig. 2.5(b) shows the TEM image of the composite film of polyfluorene doped with the europium complex and having an Eu content comparable to that of PF8Eu. Segregated particles of sizes in the range of 7-15 nm are observed in the TEM image of the composite film. The particles were probably ionic molecular aggregates of the europium complex that had phase separated in the composite film. This phenomenon can occur extensively in polymer films containing europium complexes and in doped polymer systems [26, 27].

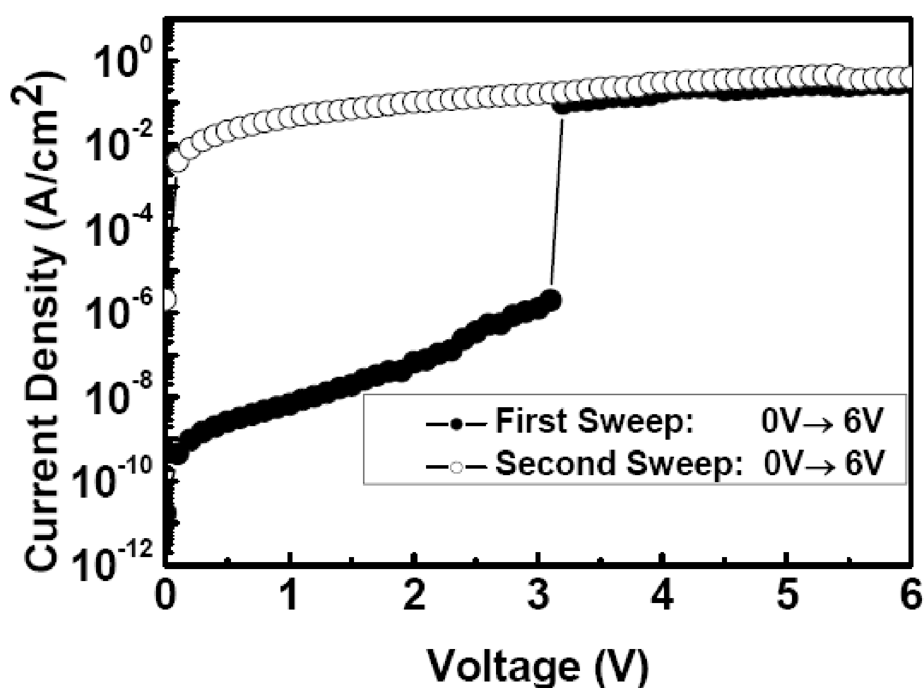

(a)

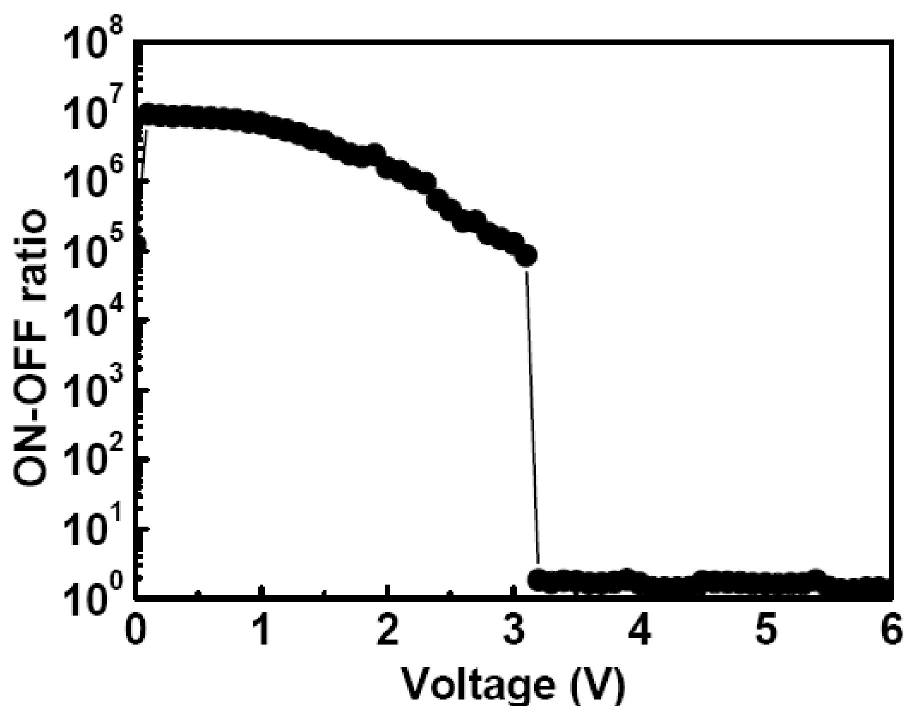

(b)

Figure 2.6 (a) Typical *J-V* characteristics of the Al/PF8Eu/ITO device (PF8Eu thickness=50 nm). Voltage was swept from 0 V to 6 V. **(b)** the ON- to OFF-current ratio as a function of applied voltage for the same sweep.

The memory effect of the device is observed in the *J-V* (current density - voltage) characteristics of the Al/PF8Eu/ITO sandwich device. Fig. 2.6(a) shows a typical *J-V* characteristic of the device. The data were taken with a voltage sweep from 0 V to 6 V at a rate of 0.1 V per step and integration time of 640 μs per step. It distinctively displays two conductivity states. Initially, though the current increases slowly with the applied voltage, the current remains low (9×10^{-9} A/cm^2 at 1 V). This is referred to as the low conductivity state (OFF-state). When the applied voltage is increased further to ~3 V, a sharp increase in current is observed, indicating the device transition from the low conductivity state (OFF-state) to a high conductivity state (ON-state). This transition from the OFF-state to the ON-state serves as the "writing" process for the

memory device. For the programmed device, the device shows a high current for the voltage applied. The current density at 1 V is about 4×10^{-2} A/cm^2. The device remains in this ON-state even after turning off the power and cannot be returned to the low conductivity state by applying a negative bias. For a memory device, the ON/OFF current ratio is a key performance indicator. Fig. 2.6(b) shows the ratio of the ON- to the OFF-state current as a function of applied voltage for the same sweep. An ON/OFF current ratio as high as 10^6 has been achieved. This feature promises a low misreading rate through the precise control over the ON- and OFF-states.

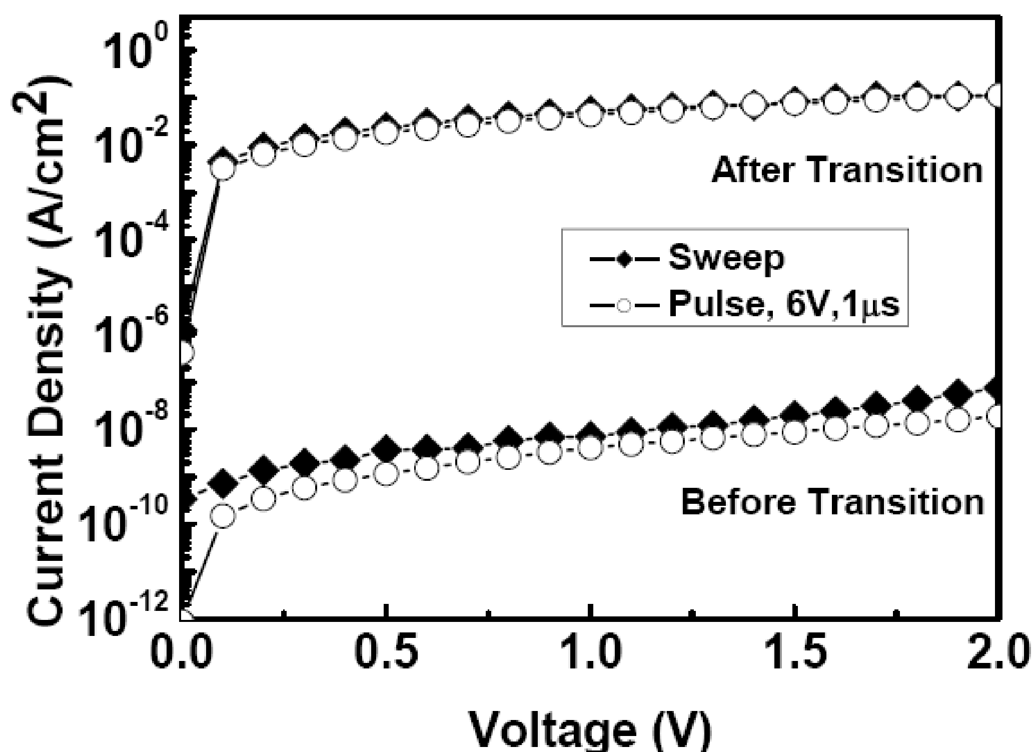

Figure 2.7 Typical *J-V* characteristics of the Al/PF8Eu/ITO device switched to the ON-state by using quasi-static (closed diamonds) and pulsed (open circles) switching.

Fig. 2.7 compares the *J-V* characteristics of the device programmed using a

quasi-static voltage sweep to those of the device programmed using a single voltage pulse of 6 V with a pulse width of 1 μs. Both devices exhibit identical characteristics before and after switching. This result indicates that a single voltage pulse has an equivalent action on switching the device as that of a quasi-static voltage sweep. The conductivity in both cases increases by a factor of ~ 10^6.

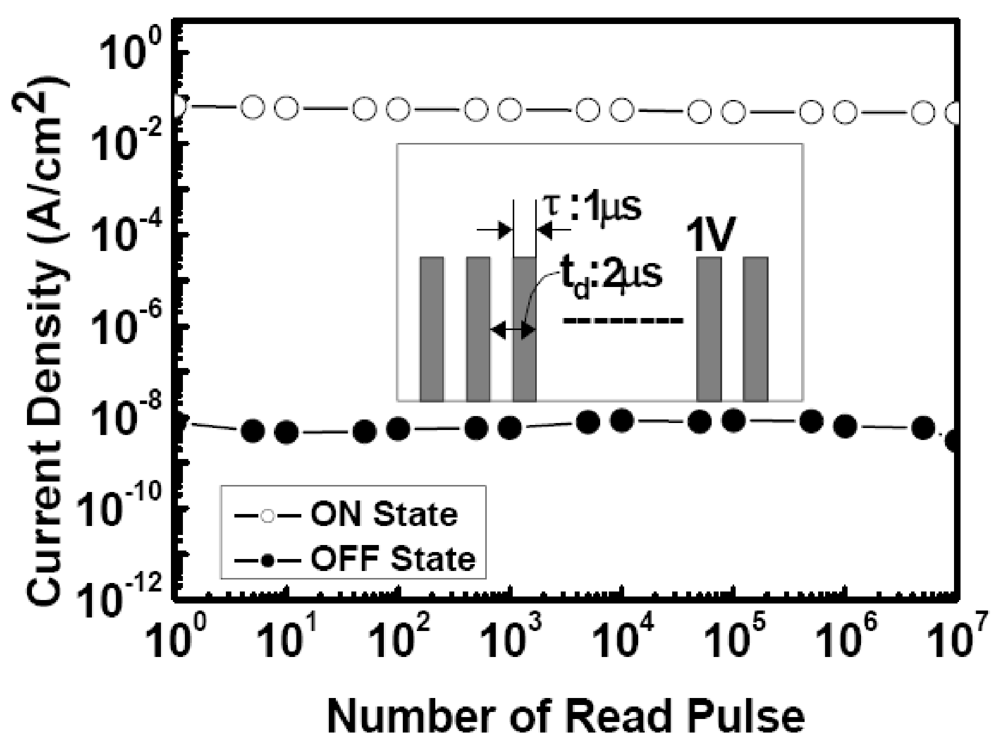

Figure 2.8 Effect of read pulses on the OFF- and ON-states. Inset: characteristics of the pulse used for the tests.

For a memory device, stability is always an important issue. Fig. 2.8 shows the continuous read pulses on the ON- and OFF-states. A continuous 1 V pulse with width of 1 μs (inset, Fig. 2.8) was used as the read voltage. No significant degradation was observed for both the ON- and OFF-states up to ten million read cycles, indicating that both states are insensitive to read cycles. In addition to the continuous read pulses,

the stability of the device under stress was evaluated under the continuous bias condition. A constant 1 V voltage stress was applied to the device in both ON- and OFF-states, and the current was recorded every minute. As shown in Fig. 2.9, after 10 h of constant stress test, degradation of both states was negligible and an ON/OFF current ratio of 10^6 could still be maintained.

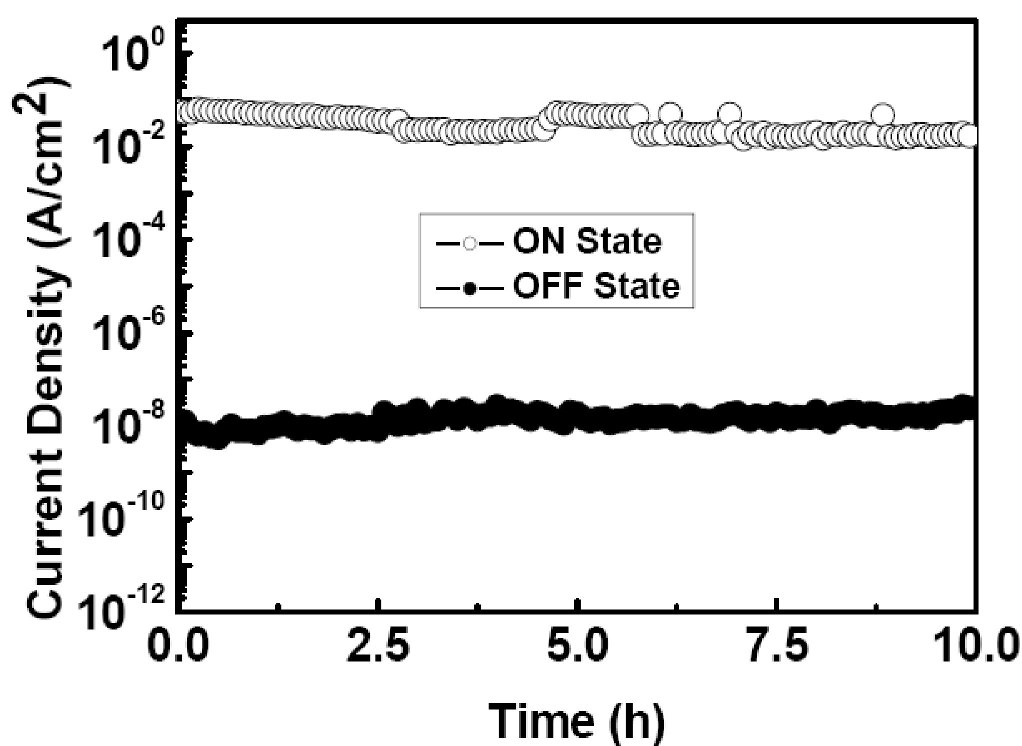

Figure 2.9 Stability of the Al/PF8Eu/ITO device in either ON- or OFF-state under a constant stress of 1 V.

2.4 Discussion

For PF8Eu, the highest occupied molecular orbital (HOMO) and the lowest unoccupied molecular orbital (LUMO) are -5.39 and -3.47 eV, respectively, as determined from the onset redox potentials in cyclic voltammetry [28] (Fig. 2.10). In the cyclic voltammetry (CyV) of PF8Eu, the reduction peak is contributed by the

europium complex (Eu DBM) and the oxidation peak by the fluorene moiety (PF8). Thus, the LUMO of PF8Eu is associated with the europium complex and the HOMO of PF8Eu is associated with the fluorene moiety. The band gaps of the fluorene moiety and europium complex are 2.98 and 3.05 eV, respectively, as determined from the UV-visible absorption edges [29] of the fluorene moiety and the europium complex (Fig. 2.11). Thus, the LUMO of the fluorene moiety in PF8Eu is at -2.41 eV and the HOMO of the europium complex in PF8Eu is at -6.52 eV. The energy levels of PF8Eu are shown in Fig. 2.12.

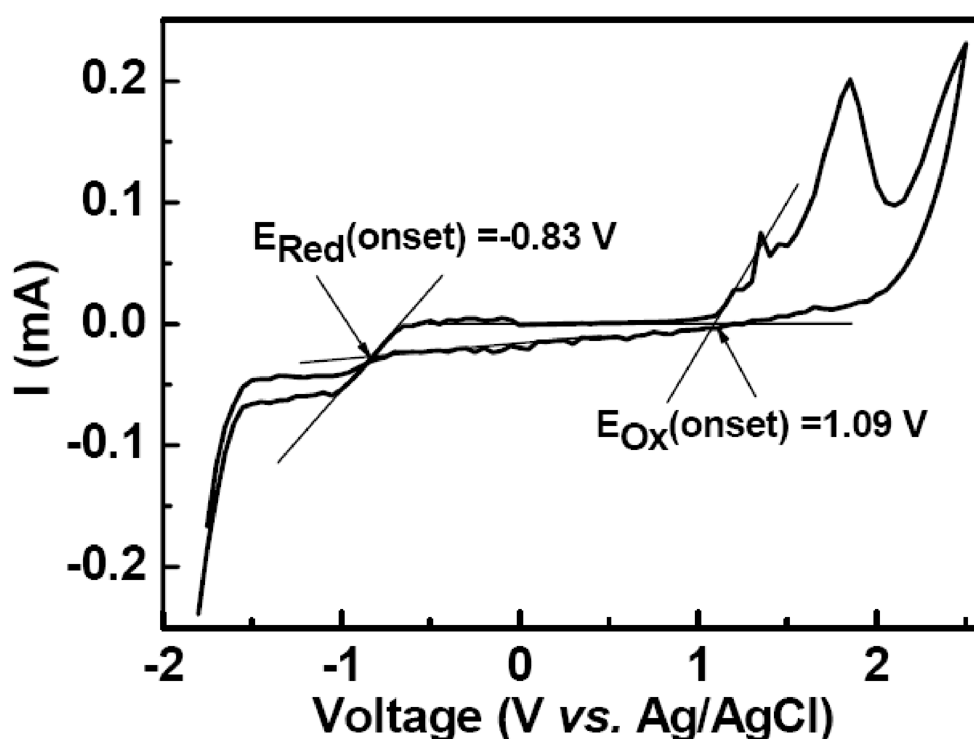

Figure 2.10 Cyclic voltammetry (CyV) of a thin film of PF8Eu on a platinum disk electrode in acetonitrile with tetrabutylammoniumhexafluorophosphate (n-Bu_4NPF_6) as the supporting electrolyte, Ag/AgCl as the reference electrode and a platinum wire as the counter electrode.

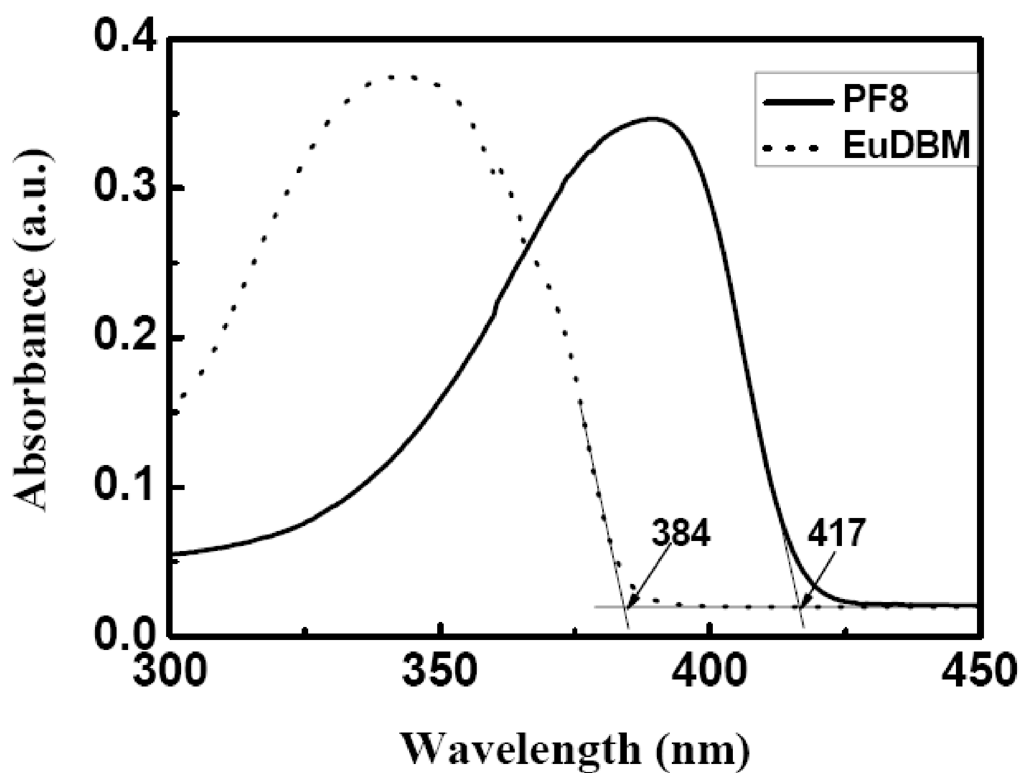

Figure 2.11 Absorption spectra of the PF8 moiety (solid curve) and Eu complex (dotted curve) in THF. The absorption edges (indicated by arrows) correspond to the energy band gaps.

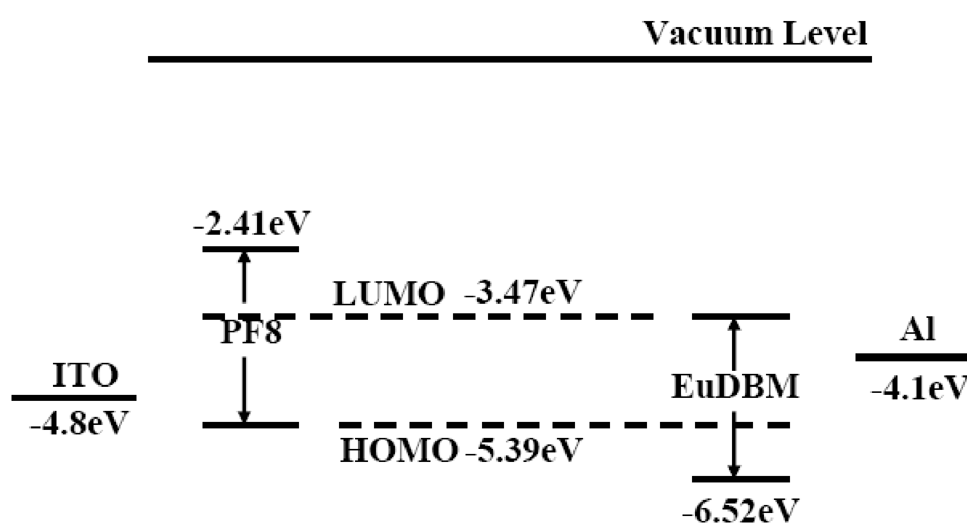

Figure 2.12 Energy band diagrams with reference to different functional groups in the PF8Eu copolymer.

In PF8Eu, the fluorene moieties form the backbone and serve as the path for charge carriers transport. From the energy level diagram of Fig. 2.12, electron injection into the polymer is difficult since there is a large barrier between the ITO and PF8Eu. Under this condition, the conductivity of the polymer is quite low. In the europium complex, lanthanide ions have a $[Xe]4f^n5s^25p^6$ electronic configuration, in which the electrons in the 4f level are shielded by the filled $5s^2$ and $5p^6$ orbital, resulting in a weak crystal field and directional effect. The lanthanide complexes distinguish themselves from the transition metal complexes by a high (up to 12, due to larger ionic radii) and variable coordination number (3-12, due to weaker crystal fields) [24]. The coordination number of the europium complex in PF8Eu is 8. Thus, it is an electron-deficient complex and can act as an electron acceptor. When the applied electrical field reached the threshold value, electrons can migrate from the fluorene moiety to the europium complex. Thus, the fluorene moiety becomes positively charged (radical cation), and the europium complex negatively charged (radical anion). The distortion due to the presence of a charge tends to change the electronic states in the vicinity of the charge such that the HOMO energy level shifts upward and the LUMO energy level shifts downward [30, 31]. This change will cause a decrease in the barrier between the ITO and the LUMO of the fluorene moiety in PF8Eu. Thus, the conductivity of PF8Eu increases significantly. Due to the high EA of the Eu complex (3.97 eV, as calculated from the CyV results [32]), the radical anions can coexist with the surrounding radical cations of the fluorene moieties. The stability constant (K) of the radical anions can be estimated from the onset potentials

of the first and second reduction peaks in the CyV curve of Fig. 2.10 [33]: $\lg K = \frac{E^2_{\mathrm{Re}d} - E^1_{\mathrm{Re}d}}{0.059} = 13.6$, indicating that the radical anions are quite stable. For the fluorene radical cations, a sufficient degree of spin delocalization of the conjugated fluorene segments in PF8Eu will stabilize the radical cations. Thus, the 'doped state' of PF8Eu is stable and the high conductive state can be maintained. It has also been reported that a stable structure of long chain fluorene moieties can be achieved under positive bias [34].

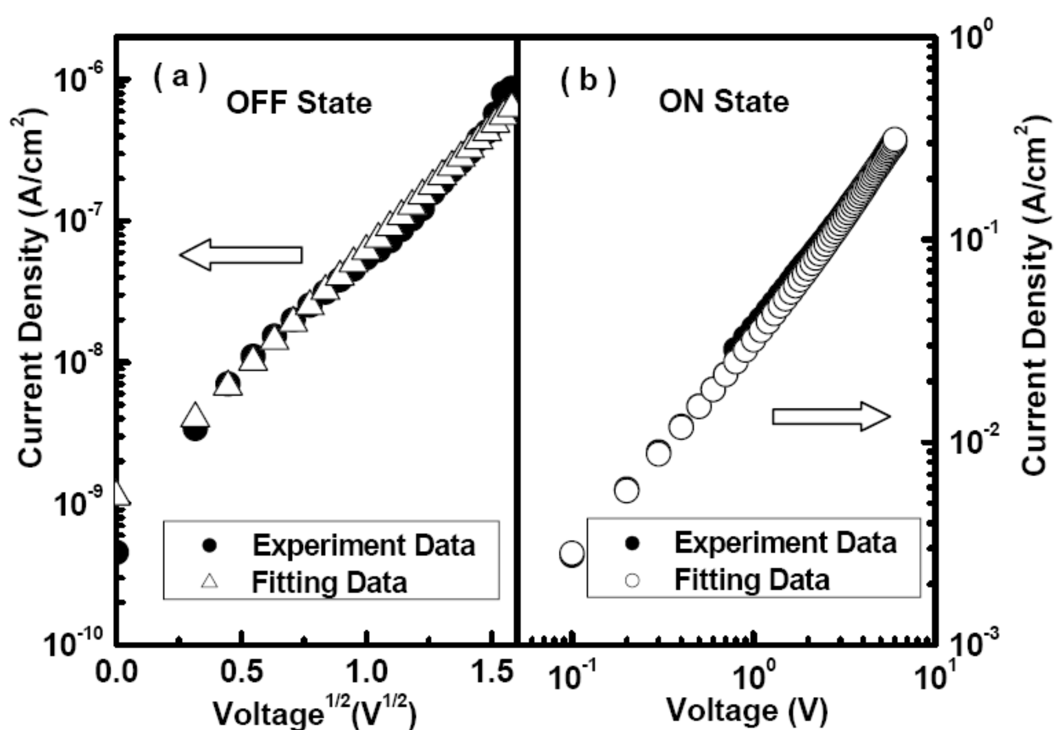

Figure 2.13 Experimental and fitted *J-V* curves of the Al/PF8Eu/ITO device: **(a)** OFF-state with the Schottky emission model and **(b)** ON-state with the trap-limited space-charge-limited model.

To further understand the device transition from the OFF-state to the ON-state, the *J-V* curves in both states were fitted with appropriate current transport models. For

the OFF-state, the *J-V* curve can be fitted by the Schottky emission model [35]:

$$J = A^* T^2 \exp[\frac{-q(\phi_B - \sqrt{qV/4\pi\varepsilon_i d})}{kT}]$$

where, A* is the effective Richardson constant, ϕ_B is the barrier height, ε_i is the insulator permittivity, and d is the insulator thickness. As shown in Fig. 2.13(a), a linear relation between log J and $V^{1/2}$ is obtained. From the curve, the dielectric constant of PF8Eu is deduced to be about 3. Thus, the current of the device in the OFF-state is dominated by the Schottky emission. However, for the ON-state, the *J-V* curve can be fitted predominantly by a trap-limited space-charge-limited model [36]:

$$J \sim N_v \mu e[\frac{\varepsilon\varepsilon_i l \sin(\pi/l)}{qH_t(\pi/l)(1+l)}]^l (\frac{2l+1}{l+1})^{l+1} \frac{V^{l+1}}{d^{l+1}}$$

where N_v is the density of states within kT of the valence band edge, H_t is the total density of traps, μ is the mobility of carriers and l is an empirical parameter. The fitted curve indicates that $J \propto V^{1.2}$, as shown in Fig. 2.13(b). This observation suggests that after an electrical transition, the current through the device has changed from the Schottky emission current to the trap-limited space-charge-limited current. The electrical transition is consistent with the reduction in barriers when the device is programmed to the ON-state.

2.5 Conclusion

A conjugated copolymer, PF8Eu, containing fluorene moieties as the electron donors and europium complexes as the electron acceptors, was synthesized. The copolymer film, when sandwiched between an ITO and an Al electrode, exhibited

WORM-like memory behavior. The device exhibited two conductivity states with an ON/OFF current ratio as high as 10^6. By using a 1 V with 1 μs-width read pulse, both the ON- and OFF-states were stable after 10^7 read pulse testes. Both the ON- and OFF-states also showed good stability under 1 V constant stress test, with no appreciable degradation after 10 h of stress. In the low conductivity state, the device was dominated by a charge injection controlled current. In the high conductivity state, the device switched to a space-charge-limited current. The present polymer device thus exhibits good potential for WORM memory applications.

Reference

[1] S. R. Forrest, Nature. **428**, 911 (2004).

[2] H. J. Gao, K. Sohlberg, Z. Q. Xue, H. Y. Chen, S. M. Hou, L. P. Ma, X. W. Fang, S. J. Pang, and S. J. Pennycook, Phys. Rev. Lett. **84**, 1780 (2000).

[3] H. K. Henish, and W. R. Smith, Appl. Phys. Lett. **24**, 589 (1974).

[4] H. Carchano, R. Lacoste, and Y. Segui, Appl. Phys. Lett. **19**, 414 (1971).

[5] R. S. Potember, T. O. Poehler, and D. O.Cowan, Appl. Phys. Lett. **34**, 405 (1979).

[6] R. Kumai, Y. Okimoto, and Y. Tokura, Science. **284**, 1645 (1999).

[7] Q. D. Ling, Y. Song, S. J. Ding, C. X. Zhu, D. S. H. Chan, D. L. Kwong, E. T. Kang, and K. G. Neoh, Adv. Mat. **17**, 455 (2005).

[8] J. Chen, M. A. Reed, A. M. Rawlett, and J. M. Tour, Science. **286**, 1550 (1999).

[9] K. M. Roth, D. T. Gryko, C. Clausen, J. Li, J. S. Lindsey, W. G. Kuhr, and D. F. Bocian, J. Phys. Chem. B. **106**, 8639 (2002).

[10] L. P. Ma, J. Liu, and Y. Yang, Appl. Phys. Lett. **80**, 2997 (2002).

[11] L. D. Bolzano, B. W. Kean, M. Beinhoff, K. R. Carter, P. M. Rice, and J. C. Scott, Adv. Funct. Mater. **15**, 1933 (2005).

[12] J. Ouyang, C.-W. Chu, C. R. Szmanda, L. P. Ma, and Y. Yang, Nat. Mater. **3**, 918 (2004).

[13] S. Moller, C. Perlov, W. Jackson, C. Taussig, and S. R. Forrest, Nature. **426**, 166 (2003).

[14] H. S. Majumdar, A. Bandyopadhyay, A. Bolognesi, and A. J. Pal, J. Appl. Phys. **91**, 2433 (2002).

[15] T. Ouisse, and O. Stephan, Org. Electron. **5**, 251 (2004).

[16] R. J. Tseng, J. Huang, J. Ouyang, R. B. Kaner, and Y. Yang, Nano Lett. **5**, 1077 (2005).

[17] Y. Ohmori, H. Kajii, T. Sawatani, H. Ueta, and K. Yoshino, Thin Solid Films. **393**, 407 (2001).

[18] N. Miyaura, and A. Suzuki. Chem, Rev. **95**, 2457 (1995).

[19] K. Kaeriyama, M. A. Mehta, V. Chaturvedi, and H. Masuda, Polymer. **36(15)**, 3027 (1995).

[20] R. P. N. Sinha, Science & Culture. **25**, 494 (1960).

[21] D. R. Coulson, *Inorganic Syntheses*, Vol. XIII, McGraw-Hill, New York (1972).

[22] X. W. Zhan, Y. Q. Liu, D. B. Zhu, W. T. Huang, and Q. H. Gong, Chem. Mater. **13**, 1540 (2001).

[23] L. M. Li, G. B. Zeng, and W. D. Zhuang, Acta Chimica Sinica. **46(1)**, 9 (1988).

[24] T. Moeller, Gmelin *Handbook of Inorganic Chemistry*, Vol. 39(D3), Springer-Verlag, New York (1981).

[25] G. E. Muilenberg, *Handbook of X-ray Photoelectron Spectroscopy*, Perkinelmer, Eden Prairie, MN, (1978).

[26] D. L. Tao, Y. Z. Xu, Z. Xu, J. J. Wang, X. Q. Zhang, F. X. Guo, X. X. Liu, D. F. Xu, J. G. Wu and S. R. Xu, Thin Solid Films, **436**, 281 (2003).

[27] G. L. Zhong, K. Kim and J. I. Jin, Synth. Met. **129**, 193 (2002).

[28] Y. Z. Lee, X. W. Chen, S. A. Chen, P. K. Wei and W. S. Fann, J. Am. Chem. Soc. **123**, 2296 (2001).

[29] Y. Liu, M. S. Liu, A. K.-Y. Jen, Acta Polym. **50**, 105 (1999).

[30] J. L. Bredas, and G. B. Street, Acc. Chem. Res. **18**, 309 (1985).

[31] E. Zojer, J. Cornil, G. Leising, and J. L. Bredas, Phys. Rev. B. **59**, 7957 (1999).

[32] J. L. Bredas, R. Silbey, D. S. Boudreus, and R. R. Chance, J. Am. Chem. Soc. **105**, 6555 (1983).

[33] V. Khodorkovsky, and J. Y. Becker, in *Organic Conductors: Fundamentals and Applications*, Vol. 4 (Eds: J. P. Farges), Marcel Dekker, Inc., New York (1994).

[34] C. Y Chi, and G. Wegner, Macromol. Rapid Commun. **26**, 1532 (2005).

[35] S. M. Sze, *Physics of Semiconductor Devices,* 2nd ED, Wiley, New York (1981).

[36] M. Pope, and C. Swenberg, *Electronic Processes in Organic Crystals and Polymers,* 2nd ED, Oxford, New York (1999).

Chapter 3

Non-Volatile Flash Memory Devices based on Copolymer Containing Carbazole Units and Europium Complex Moieties

3.1 Introduction

In the previous chapter, the synthesis and characterization of a conjugated copolymer of PF8Eu has been described and a write-once-read-many-times (WORM) memory device based on this material has been developed. As we know, WORM memory device can be written only once physically and the written status can not be easily erased. But for flash type memory device, the written status can be easily erased under certain voltage condition. Recently, flash type memory devices based on polymeric materials have been demonstrated and have received a great deal of attention due to their simplicity in structure, good scalability, low-cost potential, and large capacity for data-storage [1, 2]. A number of polymeric materials, including poly(allylamine hydrochloride) [3], polythiophene [4], polyaniline [5] and polypyrrole [6] have been explored for polymer memory effects and applications. Most of the polymers in these pioneering works were used as the polyelectrolyte, matrix of a dye, or component of a charge transfer (CT) complex in a doped or mixed system. Doping or mixing, however, may not always give rise to uniformly dispersed and compatible

components, and, thus, may result in phase separation and ion aggregation, which are unfavorable to the performance of a device [7]. The design and synthesis of a processable copolymer, that can provide the required electronic properties within a single macromolecule and still possesses good chemical, mechanical and morphological characteristics, are thus a desirable alternative for memory device applications. The technique of layer-by-layer electrostatic self-assembly (ESA) of polyelectrolytes can also bring about donor and acceptor groups in a macromolecule without phase separation and aggregation [3, 8].

In single-layer molecular switching devices, the ON/OFF ratio is generally in the range of 50–80, and memory effect lasts only for a short duration (for example, about 15 min in the nitro-amine-based systems) [9]. In order to improve the performance of a single-layer memory device, we have designed and synthesized a novel copolymer, poly[NVK-*co*-Eu(VBA)$(TTA)_2$phen], or PKEu, which has both electron–donor and electron-acceptor groups in the macromolecule. In this chapter, we will describe on the flash type memory characteristics of a metal/insulator/metal (MIM) sandwich structure using this novel copolymer as the active memory material.

3.2 Experiment

3.2.1 Preparation and Characterization of the PKEu Copolymer

The Eu-containing monomer, Eu$(TTA)_2$(VBA)phen, was synthesized by the reaction of europium triisopropoxide with thenoyltrifluoroacetone (TTA), 4-vinylbenzoic acid (VBA) and 1,10-phenanthroline (phen) in anhydrous organic solvents [10]. A mixture of NVK (0.58 g, 3.0 mmol), Eu$(TTA)_2$(VBA)phen (46.1 mg,

0.05 mmol) and 4 mg of the AIBN initiator (0.5 mol% of the total monomer concentration) was dissolved in 3 mL of dry THF in a glass polymerization tube and purged with argon. The copolymerization was carried out with continuous stirring at 60°C for 72 h. The viscous solution was diluted with 5 mL of THF and precipitated into 70 mL of methanol under vigorous stirring. The resulting solid material was further purified by Soxhlet extraction with boiling acetone for 48 h, and finally dried in a vacuum oven at 40°C for 24 h [11]. Yield: 0.32 g (51.9%). M_n=1.06×10^4, M_w=1.72×10^4, PDI (polydispersity index) =1.63. Anal. Found: C, 84.94; H, 5.71; N, 6.90; Eu, 0.95 (measured by ICP). ^{13}C NMR ($CDCl_3$, 75 MHz), δ (ppm): 160.7 (C=O of TTA), 139.9 -137.6 (d, C-N of NVK), 124.9-118.7 (m, aromatic C-C of NVK, TTA and phen), 110.5-107.4 (d, aromatic C-C of NVK), 63.1 (CH of TTA), 35.8-50.1 (aliphatic carbon in the main chain). FT-IR (KBr pellet, cm^{-1}): 3051, 3025, 2966, 2928, 1624 (C=O, chelated to Eu^{3+}), 1597, 1484, 1452, 1407, 1326, 1222, 1157, 1125, 1025, 1024, 923, 841, 745+719 (carbazole ring), 616, 527, 419 (O-Eu-O).

3.2.2 Device Fabrication and Characterization

The indium-tin-oxide (ITO)/glass substrate was pre-cleaned with deionized water, acetone and isopropanol, in that order, in an ultrasonic bath for 15 min. A toluene solution of PKEu (15 mg/ml) was spin-coated onto ITO, followed by solvent removal in a vacuum chamber at 10^{-5} Torr at room temperature. The thickness of the polymer layer was about 50 nm. Finally, the 100-nm-thick square Al electrodes for needle contacts were thermally evaporated at a pressure around 10^{-7} Torr. Cyclic

voltammetry (CyV) was performed using an Autolab potentiostat/galvanostat under an argon atmosphere. TEM measurements were carried out on a JEOL JEM-2010F field emission electron microscope equipped with a GATAN Multiscan camera. Electrical measurements were carried out on a HP 4156A semiconductor parameter analyzer, HP 54600A oscilloscope and Agilent 33250A 80MHz function/arbitrary waveform generator under ambient conditions.

3.3 Results and Discussions

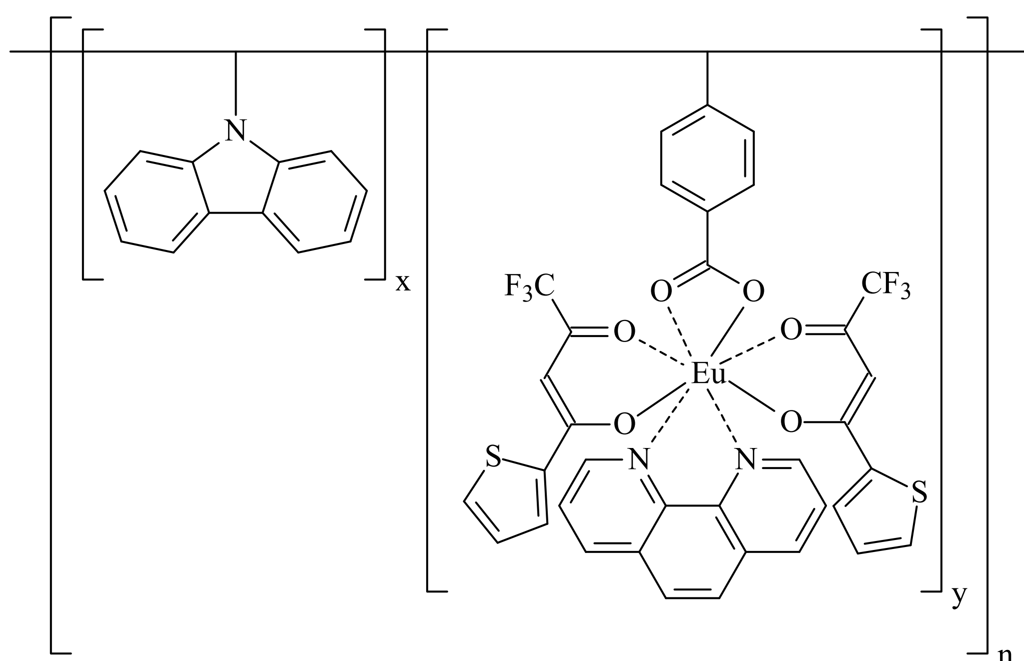

Figure 3.1 Molecular structure of the copolymer PKEu with the composition of x:y=0.987:0.013.

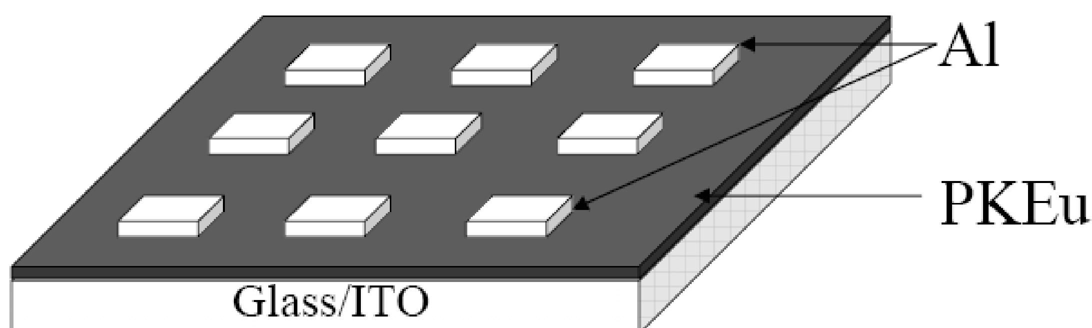

Figure 3.2 Schematic diagram of the memory device consisting of a thin film (~50 nm) of PKEu sandwiched between an ITO substrate and an aluminium top electrode.

The molecular structure of PKEu and the configuration of the memory device are shown in Fig. 3.1 and Fig. 3.2, respectively. PKEu was prepared by the free radical copolymerization of *N*-vinylcarbazole, or NVK, with a Eu-chelated (via thenoyltrifluoroacetone (TTA) and 1,10-phenanthroline (phen)) vinylbenzoate monomer, or $Eu(TTA)_2(VBA)phen$ [21]. The carbazole group, which is widely used as an electron donor and hole-transporting group [12], and the Eu complex, which acts as an electron acceptor [13, 14] and is known to exhibit memory effects [15], are thus combined into one component by copolymerization. GPC measurement indicated that the weight-average molecular weight of the resulting copolymer was around 17 000, with a polydispersity index of about 1.6 and a Eu molar content of 1.3 % (determined by ion chromatography (ICP)). Thus, the degree of polymerization was about 52. The molar content of the bulky Eu-complex units at 1.3 % allowed the casting of homogeneous films from the copolymer and ensured an adequate “doping” level for the charge carriers. PKEu exhibited good thermal stability, with an onset

decomposition temperature of about 420°C, and a glass transition temperature of about 220°C, as determined by thermogravimetric analysis and differential scanning calorimetry, respectively. PKEu is soluble in common organic solvents, such as THF, toluene and chloroform, and can be cast into transparent and uniform thin films by spin-coating. As revealed by transmission electron microscopy (TEM, Fig. 3.3), the phenomena of ionic aggregation and phase separation, which can occur in films containing rare earth complex dopants [7, 16], are absent in the present copolymer film since the Eu complexes are covalently bonded to the polymer chains.

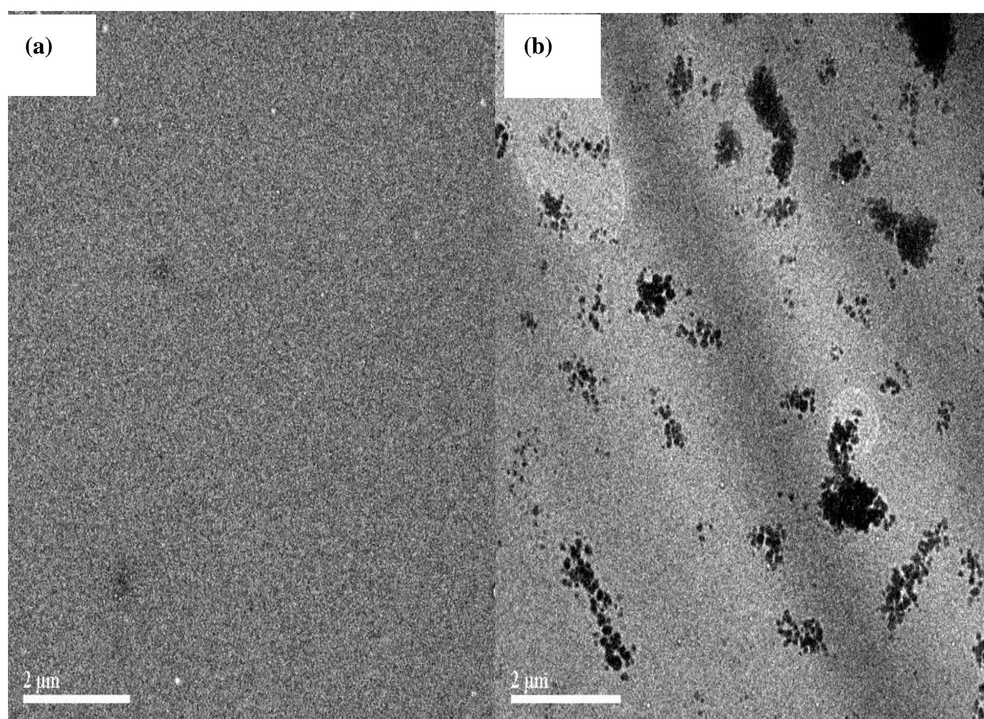

Figure 3.3 TEM image of **(a)** the PKEu film spin coated from the toluene solution; and **(b)** the PVK film doped with europium complex to a comparable Eu content of 1% (w/w) to PKEu.

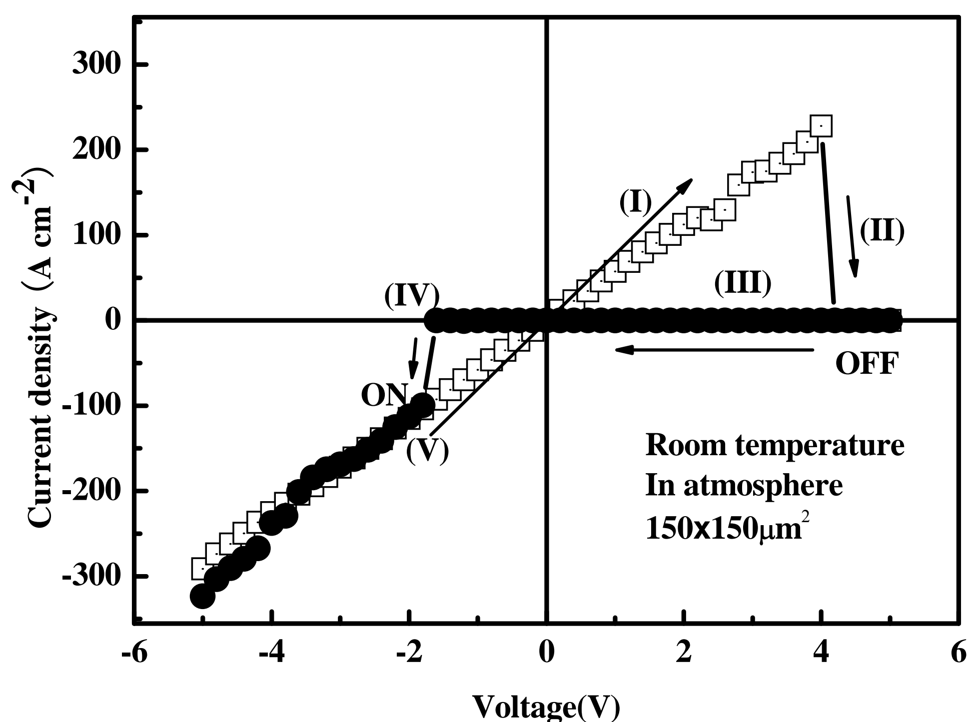

Figure 3.4 *J-V* characteristics of the Al/PKEu/ITO device based on a spin-cast film of PKEu (~50 nm) for two sweep directions. Arrows indicate the sweep directions of the applied voltage.

The memory effect of PKEu was observed in the current density (*J*)-voltage (*V*) characteristics of the Al/PKEu/ITO sandwich device, as shown in Fig. 3.4. *J* increases progressively with the applied bias (stage I). A sharp decrease in injection current occurs at about 4 V (stage II), indicating the transition of the device from the high conductivity state (ON state) to a low conductivity state (OFF state). This transition from the ON state to the OFF state is equivalent to the "writing" process in a digital memory cell. After this transition, the device remains in this state even after turning off the power. This phenomenon can be seen in the third scan (stage III) in Fig. 3.4. The *J-V* characteristics define the electrical bistability of the PKEu and also reveal the

non-volatile nature of the memory effect. One of the most important features of the present copolymer is that the ON state can be recovered by the simple application of a reverse voltage pulse (at about -2 V, stage IV). This is equivalent to the "erasing" process of a digital memory cell. The difference in transition voltages between the ON and OFF states is likely to be due to the difference in barrier heights of ITO/PKEu and Al/PKEu. Stage V of Fig. 3.4 shows the *J-V* characteristics of the device after application of a -2 V bias. The behavior is nearly identical to that of stage I. This feature allows the application of PKEu in a re-writable memory.

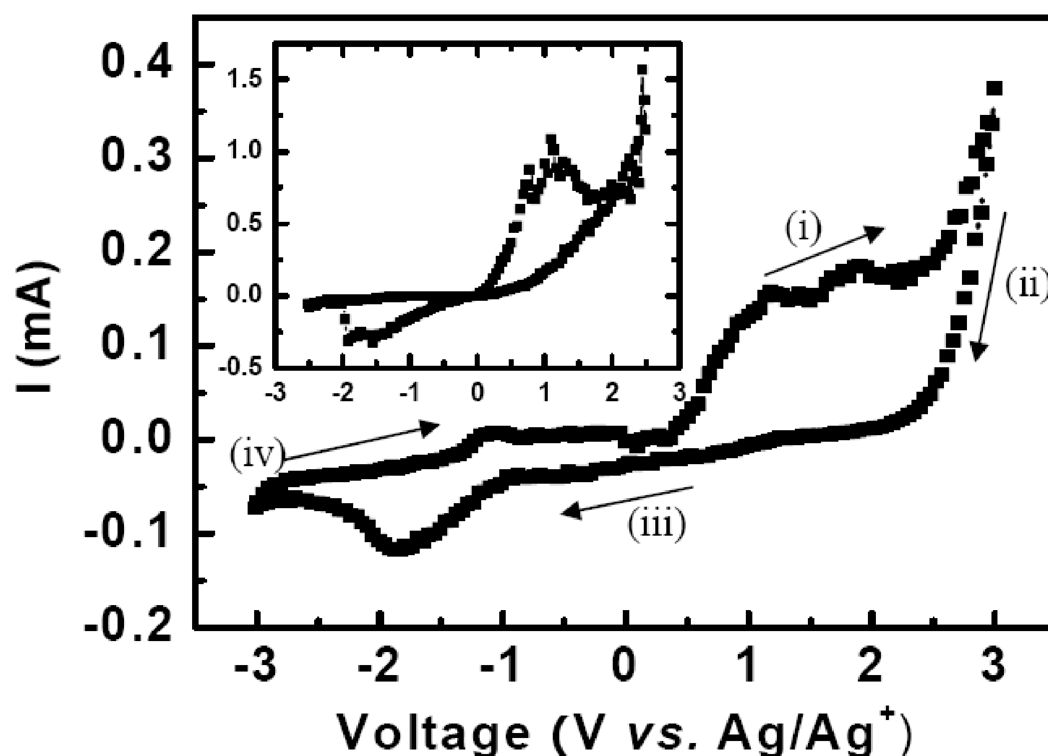

Figure 3.5 CyV sweep (from (i) to (iv)) of a thin film of PKEu on a platinum disk electrode in acetonitrile with 0.1 M of n-Bu_4NPF_6 as the supporting electrolyte. The inset is the CyV, sweep in the same electrolyte, of a PKEu film sandwiched between ITO and Al electrodes, with ITO as the working cathode.

Cyclic voltammetry (CyV) was carried out to evaluate the reduction and oxidation (redox) behavior of PKEu. The PKEu film on a Pt disk electrode was scanned anodically and cathodically in a 0.1 M acetonitrile solution of tetrabutylammoniumhexafluorophosphate (n-Bu_4NPF_6) with Ag/Ag^+ and a platinum wire as the reference and counter electrodes, respectively. Fig. 3.5 depicts the CyV curve of both the p-doping and n-doping processes of the copolymer. During the anodical scan, PKEu exhibits irreversible p-doping behavior. The oxidation peak appears at about 1.0 V *vs*. Ag/Ag^+. When scanned cathodically, PKEu film shows the irreversible n-doping behavior with a reduction peak at around -1.8 V *vs*. Ag/Ag^+. PKEu thus shows irreversible redox behavior since the oxidation and reduction peaks fall in opposite potential regions. The electrochemical behavior of PKEu was further investigated in a memory cell immersed in the same electrolyte system [17, 18]. The inset of Fig. 3.5 shows the CyV scan of a thin film of PKEu sandwiched between an ITO cathode and an Al anode. Similar redox behavior of PKEu was observed in the cell structure. The redox behavior of PKEu is distinguishable from that of the Eu-free model polymer, poly(N-vinylcarbazole) or PVK [19, 20], by the presence of a large redox potential difference (ΔE_{redox}) of about 2.8 V.

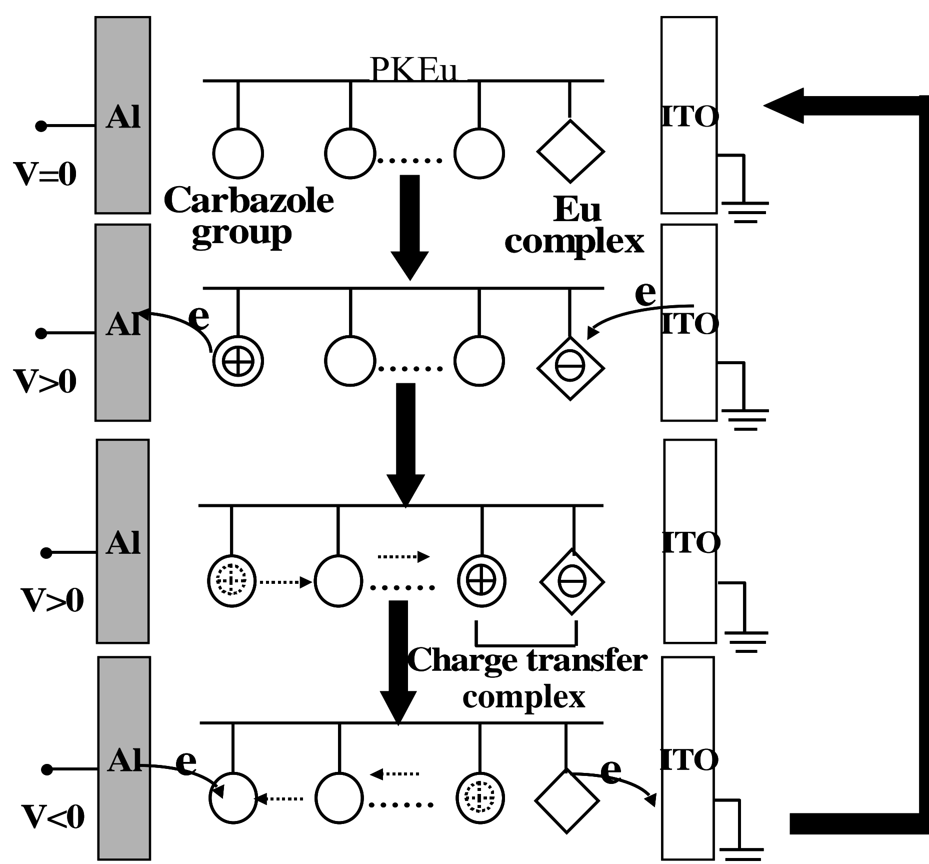

Figure 3.6 The oxidation, reduction and charge migration processes in the copolymer during memory device operation (write/erase).

The dominant carriers in PVK are holes and their mobility is strongly dependent on the applied electric field [21, 22]. The currents are dominated by space charge, ohmic, and Poole-Frenkel effects, respectively, in the low, medium and high field regions [23]. The high conductivity state (ON) of PKEu is probably similar to that of PVK since the carbazole groups are the dominant moieties in the copolymer and the Eu-complexes only act as the “dopant”. As revealed by the *J-V* and CyV results, CyV potentials are relative and differ from the switching voltages. When a forward voltage is applied, the carbazole groups near the surface are oxidized and holes are generated (ON state). With the increase in forward bias, the holes are transported from the surface near the anode to the bulk through the neighboring carbazole groups. Since

the PKEu chains are saturated, carriers probably do not move along the polymer chain. Instead, they hop between neighboring carbazole groups (either on the same or neighboring polymer chains) [23]. The carbazole group has a tendency to form a partial or full face-to-face conformation with the neighboring carbazole groups. As a result, the region of electron delocalization is extended [24]. A number of mechanisms have been proposed to explain the existence of the two conducting states in some conjugated polymers [4, 25, 26]. Taking into account of the nature of the present donor-accetor copolymer system, the redox mechanism [27, 28] may play an important role in the process. However, it differs from the normal redox process [28] by the fact that the holes must be transported to the acceptor sites by an applied voltage before charge trapping. When the voltage reaches the threshold voltage of +4 V, the reduced Eu-complex can form a charge transfer (CT) complex with the surrounding (intrachain and/or interchain) oxidized carbazole species. Because of the high ΔE_{redox} of PKEu, the CT complex is insulating (to achieve a highly conductive CT complex, the ΔE_{redox} between the donor and the acceptor must be in the range of -0.25 V ~ 0.25 V) [29, 30]. Now the material is in its low conductivity state (OFF state). The formed CT complex is not very stable because of the steric hindrance of the Eu-complex. A reversal of voltage can attract the holes (untrapping) from the bulk back to the surface to recombine with the electrons, resulting in the return of the carbazole groups and Eu complexes to their original states (erase). The above mechanism is depicted in Fig. 4.6 and the redox processes are shown in Figs. 3.7 (a) and (b).

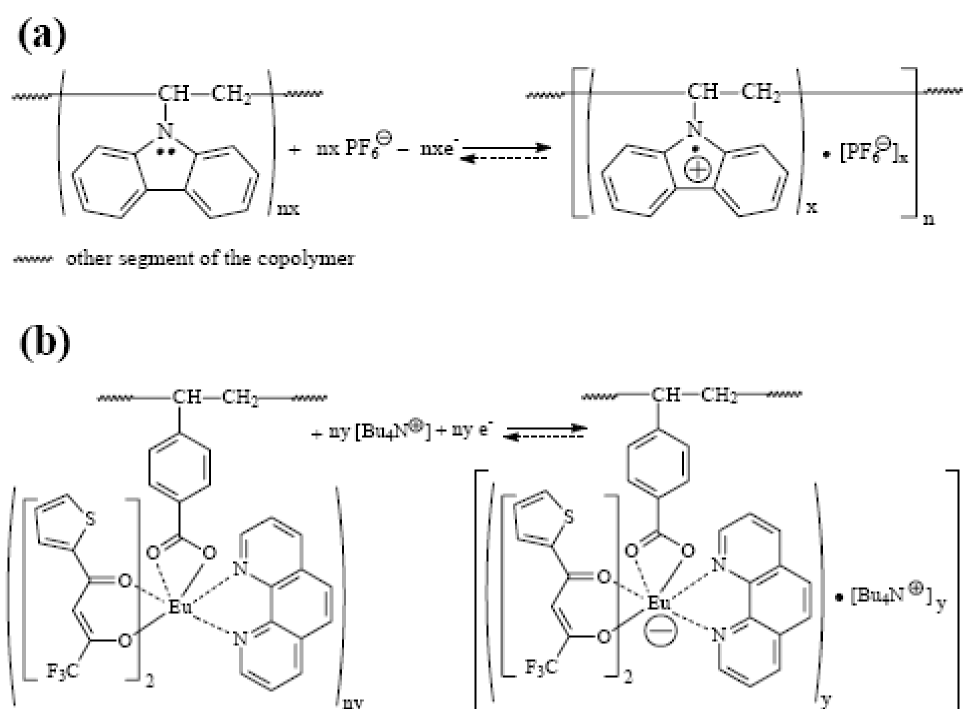

Figure 3.7 Electrode processes: **(a)** the oxidation (p-doping) and **(b)** reduction (n-doping) processes of the carbazole groups and Eu complex moieties in copolymer PKEu.

In addition to the rewriting capability, other parameters of importance to the performance of a memory device include read cycles, ON/OFF ratio, switching time and retention ability. These parameters were evaluated under ambient conditions. First of all, the effect of continuous read pulse on the ON- and OFF-states was investigated. More than one million (10^6) read cycles were conducted on PKEu. As shown in Fig. 3.8, no resistance degradation is observed for both ON- and OFF-state during the testing. Fig. 3.9 shows the ratio of the ON- to OFF-state current as a function of applied voltage for the same sweeps. An ON/OFF current ratio as high as 10^4 has been

achieved from the memory device based on PKEu. This feature promises a low misreading rate by precise control over the ON and OFF states. Another crucial performance indicator for a memory device is the switching time. Fig. 3.10(a) shows the transient response of current density versus time. Fig. 3.10(b) shows the circuit layout. The use of double-wire cable connection to the device ensured that the voltage source and the oscilloscope shared the same ground. The Al/PKEu/ITO device has a switching time shorter than 20 μs from the ON state to the OFF state. In its yet to be optimized single-layer architecture, it is slower than the writing time (~1 μs) of a NAND (NOT/AND) flash memory based on traditional semiconductor materials. Nevertheless, it is still fast enough for most consumer products applications. The retention ability of the two states was tested under ambient conditions. It was found that the devices remained in the ON state for several months without any degradation. For the OFF-state, it persisted for about 3 h. However, it is believed that the retention of the OFF-state can be significantly improved when the device is properly encapsulated [31]. The performance of the present polymer memory device compares favorably with that of the known single-layer molecular (non-polymeric) memory devices [19].

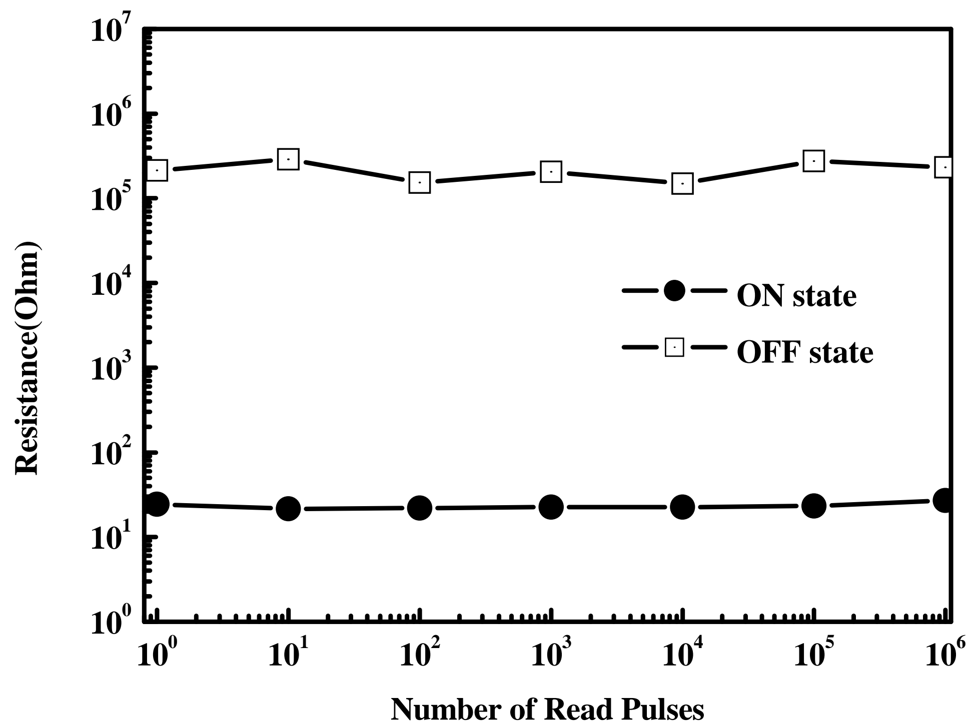

Figure 3.8 Effect of read cycles on the ON state and OFF state.

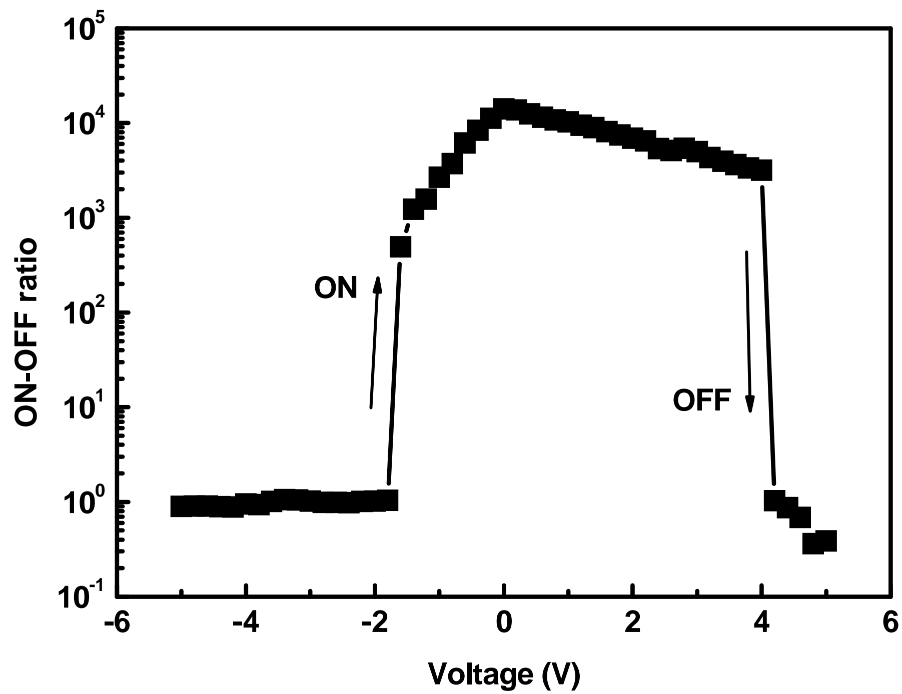

Figure 3.9 Ratio of the ON- to OFF-state current as a function of applied voltage.

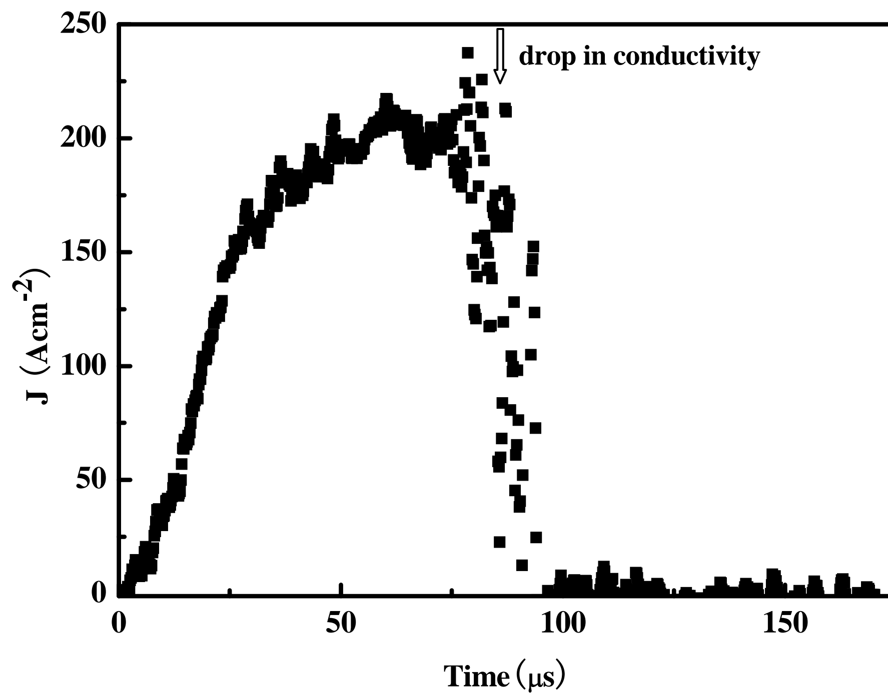

(a)

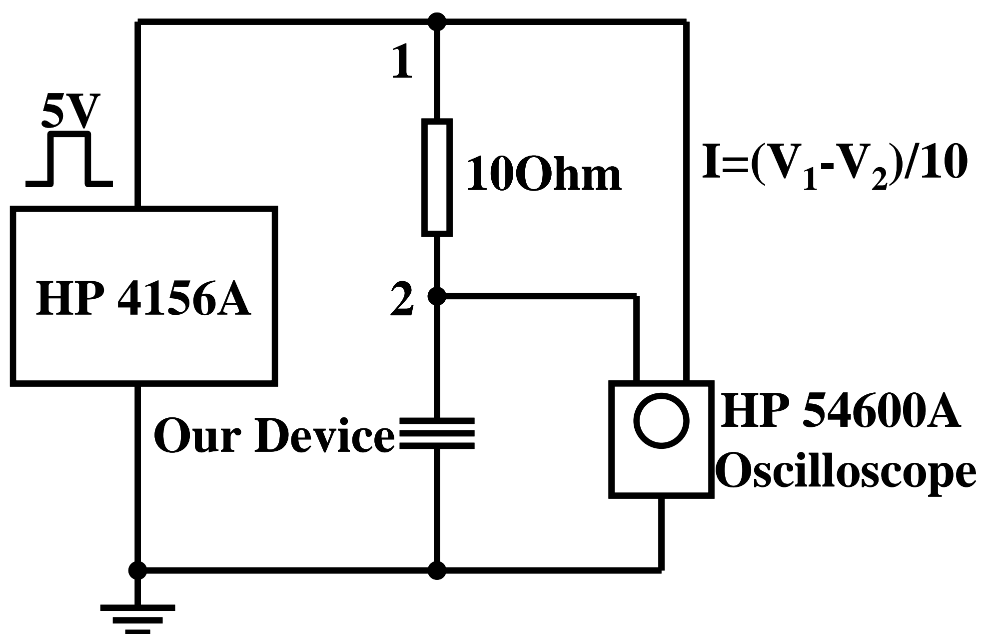

(b)

Figure 3.10 **(a)** Transient response of current density *vs*. time, showing a short switching time from ON to OFF state; **(b)** the corresponding circuit for measurement.

3.4 Conclusion

In summary, a non-volatile polymer memory device, based on a copolymer containing the carbazole (donor) and Eu-complex (acceptor) groups in a simple MIM architecture, was demonstrated. The device exhibited two distinctive bistable states of conductivity that could be achieved by applying voltage pulses of different polarities. The device remained in either state even after the power has been turned off. The device also exhibited a high ON/OFF current ratio, fast response time and acceptable retention ability under ambient conditions. More than a million read cycles were performed on the device under ambient conditions without any device encapsulation. A redox mechanism, governed by the donor-acceptor nature of the PKEu copolymer, was proposed to explain the memory effect of the device. It should be emphasized the copolymer could be readily cast into homogeneous thin films with good mechanical properties from solutions.

Reference

[1] A. Stikeman, Technol. Rev. **105**, 31 (2002).

[2] S. Moller, C. Perlov, W. Jackson, C. Taussig, S. R. Forrest, Nature. **426**, 166 (2003).

[3] A. Bandyopadhyay, A. J. Pal, Adv. Mater. **15**, 1949 (2003).

[4] D. M. Taylor, C. A. Mills, J. Appl. Phys. **90**, 306 (2001).

[5] H. Guo, V. Egan, R. Bernstein, C. M. Knobler, R. B. Kaner, Abst. Am. Chem. Soc. **219**, 510 (2000).

[6] M. A. Vorotyntsev, M. Skompska, E. Pousson, J. Goux, C. Moise, J. Electroanal. Chem. **552**, 307 (2003).

[7] G. L. Zhong, K. Kim, J. I. Jin, Synth. Met. **129**, 193 (2002).

[8] G. Decher. Science, **277**, 1232 (1997).

[9] A. Bandyopadhyay, A. J. Pal, Appl. Phys. Lett. **82**, 1215 (2003) and references therein.

[10] L. H. Wang, W. Wang, W. G. Zhang, E. T. Kang, W. Huang, Chem. Mater. **12**, 2212 (2000).

[11] Q. D. Ling, Q. J. Cai, E. T. Kang, K. G. Neoh, F. R. Zhu, Wei Huang, J. Mater. Chem. DOI : 10.1039/b405873a (2004).

[12] C. A. Walsh, D. M. Burland, Chem. Phys. Lett. **195**, 309 [1992].

[13] C. J. Liang, Z. R. Hong, X. Y. Liu, D. Zhao, W. L. Li, J. B. Peng, J. Q. Yu, C. S. Lee, S. T. Lee, Thin Solid Films. **359**, 14 (2000).

[14] H. Xin, M. Guang, F. Y. Li, Z. Q. Bian, C. H. Huang, K. Ibrahim, F. Q. Liu, Phys.

Chem. Chem. Phys. **4**, 5895 (2002).

[15] Z. M. Liu, A. A. Yasseri, J. S. Lindsey, D. F. Bocian, Science. **302**, 1543 (2003).

[16] D. L. Tao, Y. Z. Xu, F. S. Zhou, B. G. Huang, N. Duan, T. Zhang, H. Shen, Z. H. Xu, Z. Xu, J. J. Wang, X. Q. Zhang, F. X. Guo, X. X. Liu, D. F. Xu, J. G. Wu, S. R. Xu, Thin Solid Films. **436**, 281 (2003).

[17] J. N. Murray, Prog. Org. Coat. **30**, 255 (1997).

[18] A. Siove, D. Ades, E. Ngbilo, C. Chevrot, Synth. Met. **38**, 331 (1990).

[19] U. Geissler, M. L. Hallensleben, A. Rienecker, N. Rohde, Synth. Met. **84**, 375 (1997).

[20] M. Skompska, L. M. Peter, J. Electroanal. Chem. **383**, 43 (1995).

[21] A. Szymanski, M. M. Labes, J. Chem. Phys. **50**, 3568 (1969).

[22] M. Ikeda, J. Phys. Soc. Jpn. **60**, 2031 (1991).

[23] G. Safoula, K. Napo, J. C. Bernede, S. Touihri, K. Alimi, Eur. Polym. J. **37**, 843 (2001).

[24] J. Vandendriessche, P. Palmans, S. Toppet, N. Boens, F.C. De Schryver, H. Masuhara, J. Am. Chem. Soc. **106**, 8057 (1984).

[25] H. S. Majumdar, A. Bolognesi, A. J. Pal, Synth. Met. **140**, 203 (2004).

[26] T. Lee, W. Y. Wang, M. A. Reed, Ann. N. Y. Acad. Sci. **1006**, 21 (2003).

[27] D. Ofer, M. S. Wrighton, J. Am. Chem. Soc. **110**, 4467 (1988).

[28] P. Denisevich, K. W. Willman, R. W. Murray, J. Am. Chem. Soc. **103**, 4727 (1981).

[29] J. J. Mayerle, Bull. Chem. Soc. Jpn. **54**, 3170 (1981).

[30] D. B. Zhu, F. S. Wang, Organic Solid, Shanghai Science and Technology Press, Shanghai, Ch. 2 (1999).

[31] S. R. Forrest, Nature. **428**, 911 (2004).

Chapter 4

Material Properties and Electrical Performance of Mixed Polymer and Gold Nanoparticle based Flash Memory Device

4.1 Introduction

In previous two chapters, we described two kinds of polymer memory devices. One is write-once-read-many-times (WORM) memory device, which uses PF8Eu as the active layer material. Another one is flash type memory device, which uses PKEu as the active layer material. For these two devices, the memory effect comes from the materials themselves, similar as some materials from the literature [1-8]. There is another kind of nanoparticle based organic memory devices [9-13], where the organic material itself has no memory effect and the memory effect is a result of the nanoparticle incorporated. An organic bistable memory device by embedding aluminum nanoparticles in an organic layer through thermal evaporation has been demonstrated [9]. However, an accurate control of aluminum deposition process is needed. Later, a polymer memory device has been reported by using mixture of gold nanoparticles (GNPs), 8-hydroxyquinoline (8HQ) and polystyrene (PS) [11]. The 8HQ serves as the electron donors, the GNPs serve as the electron acceptors, and the PS only serves as matrix and plays no role in the memory effect. Nanofiber/nanotube and GNPs hybrid system has also been developed to memory application by using the

charge transfer mechanism. Examples of this kind of system include the polyaniline nanofiber and GNPs memory device, which uses polyaniline nanofiber as electron donor and GNPs as electron acceptor [12], and the tobacco mosaic virus nanotube and GNPs system, which uses virus nanotube as electron donor and GNPs as electron acceptor [13].

In this chapter, we will introduce the fabrication and operation of a MIM structured non-volatile memory device using poly(N-vinylcarbazole) (PVK) containing GNPs with weight ratio of 12:1 as the active layer between two electrodes [14]. In our device, the PVK serves as both the matrix and electron donor [15], and the GNPs serve as electron acceptors. The as-fabricated device exhibits a low conductivity property and can be programmed to high conductivity state, with a high ON/OFF current ratio up to 5 orders of magnitude. The high conductivity state can also be erased to the low conductivity state by only using a reverse bias. It has the strong potential on flash-type memory device applications.

As we know, the material property of the active layer will greatly affect the device property. In this chapter, we also probe the morphological, and charge-carrier transport properties of the mixed films through microscopy and space-charged limited current (SCLC) measurement. And we provide a detailed analysis of the different active layer material mixing weight ratio, different active layer film thickness and different top metal electrode to the performance in PVK and GNPs based memory cells.

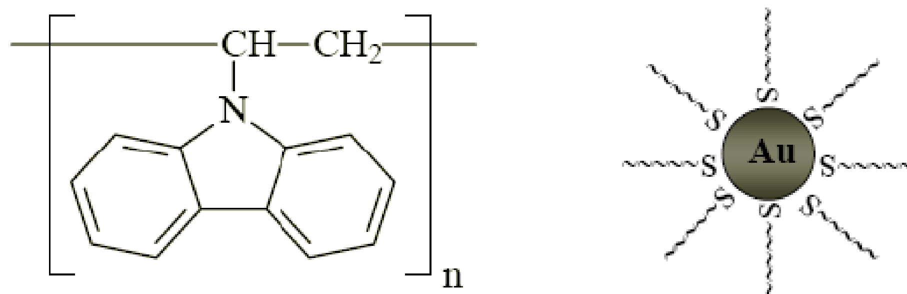

Figure 4.1 Molecular structure of PVK (left) and schematic structure of gold nanoparticle (right)**.**

4.2Experiment

The chemical structure of the PVK and GNP, are shown in Fig. 4.1. The PVK was obtained from Aldrich Chemical Co. and the GNPs were prepared by the two-phase growth method [16]. From the transmission electron microscopy picture (Fig. 4.2) of the GNPs we can know the GNPs have a size distribution of 1.5-6.5 nm. The PVK:GNPs solution was prepared by mixing the PVK and GNPs with weight ratios of 100:0, 99:1, 20:1, 12:1, 6:1 and 3:1 into the toluene solvent. The AFM polymer samples were prepared by spin coating the PVK:GNPs solution onto the TaN coated silicon wafer. The devices used for the study of hole mobility were grown on indium tin oxide (ITO) coated glass substrates followed by a 70 nm thick Au top electrode. All the ITO coated glass was cleaned with deionized water, acetone and isopropanol, in that order, in an ultrasonic bath for 20 min before use. Surface morphologies of the organic film samples were studied using a Digital Instruments atomic force microscope operated in the non-contact (tapping) mode.

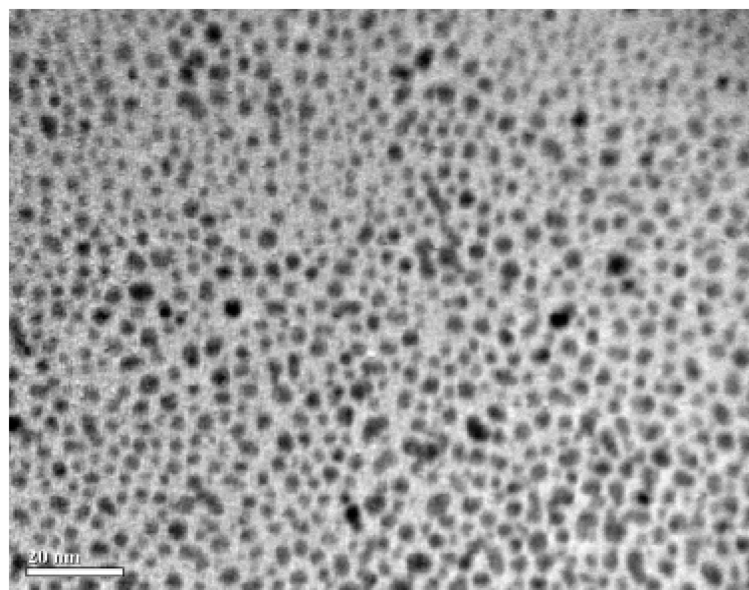

(a)

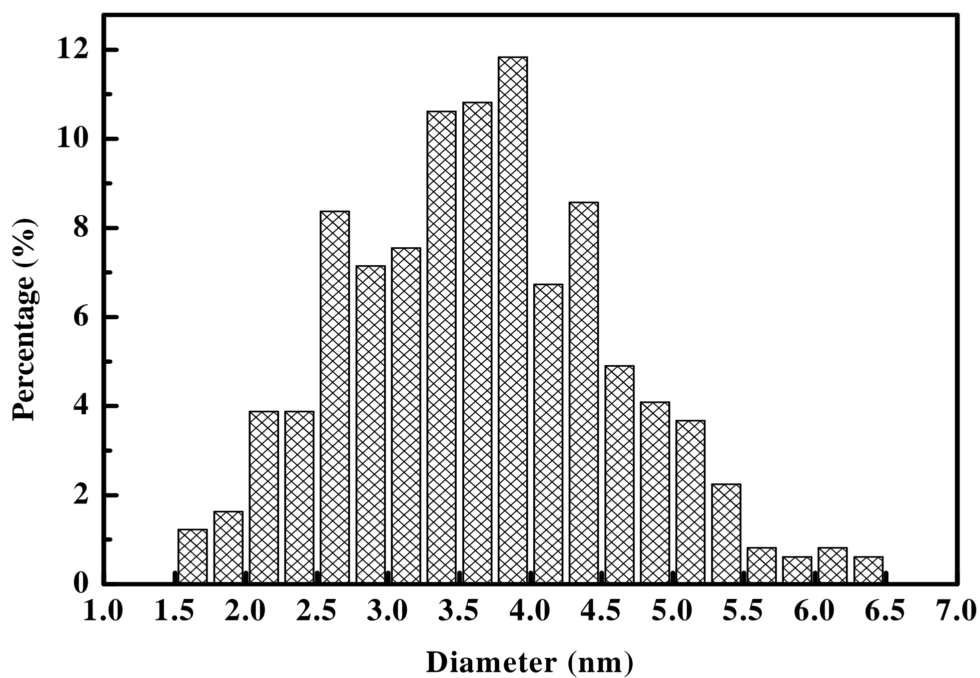

(b)

Figure 4.2 (a) Transmission electron micrograph picture of gold nanoparticles and **(b)** histogram of GNPs.

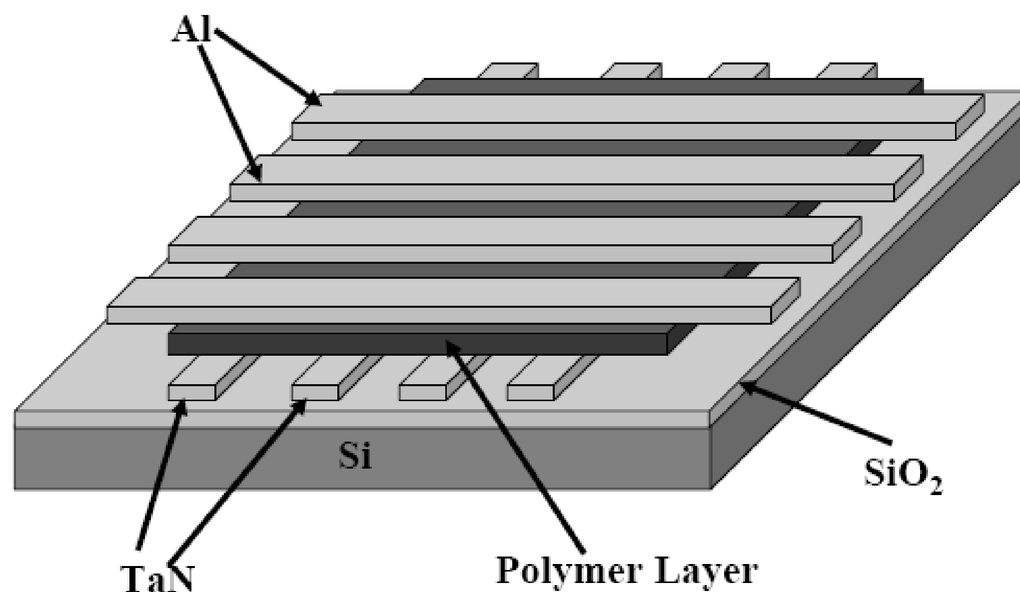

Figure 4.3 Schematic diagram of the sandwich structure device.

Fig. 4.3 shows the basic device structure consisting of the PVK:GNPs film sandwiched between a TaN bottom electrode and an Al top electrode. The TaN was sputtered onto the SiO_2 covered Si substrate through a shadow mask with 200 μm wide lines. The shadow mask was used to pattern and define the electrode area. The toluene solution of PVK:GNPs was sequentially spin-coated on the TaN, followed by solvent removal in a vacuum chamber at 10^{-5} Torr under 60°C for 9 hours. The thickness of the polymer films were about 1.3 μm, 130 nm, 50 nm, and 25 nm prepared for different purpose, as measured by a step profiler. Finally, the top Al, Cu or Au electrode was thermally evaporated with line-width of 200 μm or 400 μm at a pressure of ~10^{-7} Torr through a shadow mask. The top and bottom electrodes were aligned perpendicular to each other, so as to define an active cross area of 200 μm× 200 μm or 200 μm×400 μm. A control sample based on PVK-only solution was also

been prepared. Electrical measurements were carried out using a HP 4156A semiconductor parameter analyzer in a dark chamber with the TaN electrode grounded. All electrical measurements were conducted under ambient condition without any encapsulation.

4.3Results and Discussions

4.3.1 Film Morphology

We first investigate the relationship between mixing ratio and morphology of PVK:GNPs thin films by using AFM data. Fig. 4.4 shows AFM images for TaN and five representative PVK:GNPs mixed films. The root-mean-square (RMS) surface roughness data RMS of TaN and five PVK:GNPs mixed films is shown in Table 4.1. Since TaN has been used as bottom electrode, we firstly measured the TaN surface and RMS_{TaN}=0.45 nm. The surface of pure PVK film is smoother than that of the TaN film with RMS_{PVK}=0.29 nm. This is because that with a long chain molecular structure, PVK can be readily cast into uniform and homogeneous film. Comparing with the surface of pure PVK film, that of the 20:1 PVK:GNPs film is a litter rough with $RMS_{20:1}$=0.39 nm, which is due to the introduction of 5 wt% of GNPs. For GNPs concentration under 15 wt% in the PVK:GNPs mixed film, keeping increase the GNPs concentration has negligible affection on the film surface roughness, as we can see from Table 4.1 (RMS variable between 0.39 nm to 0.46 nm). If we keep increasing the GNPs concentration to 25 wt%, the quality of surface morphology will greatly decrease. As we can see from Table 4.1, the RMS of 3:1 PVK:GNPs film

dramatically increases to 1.76 nm.

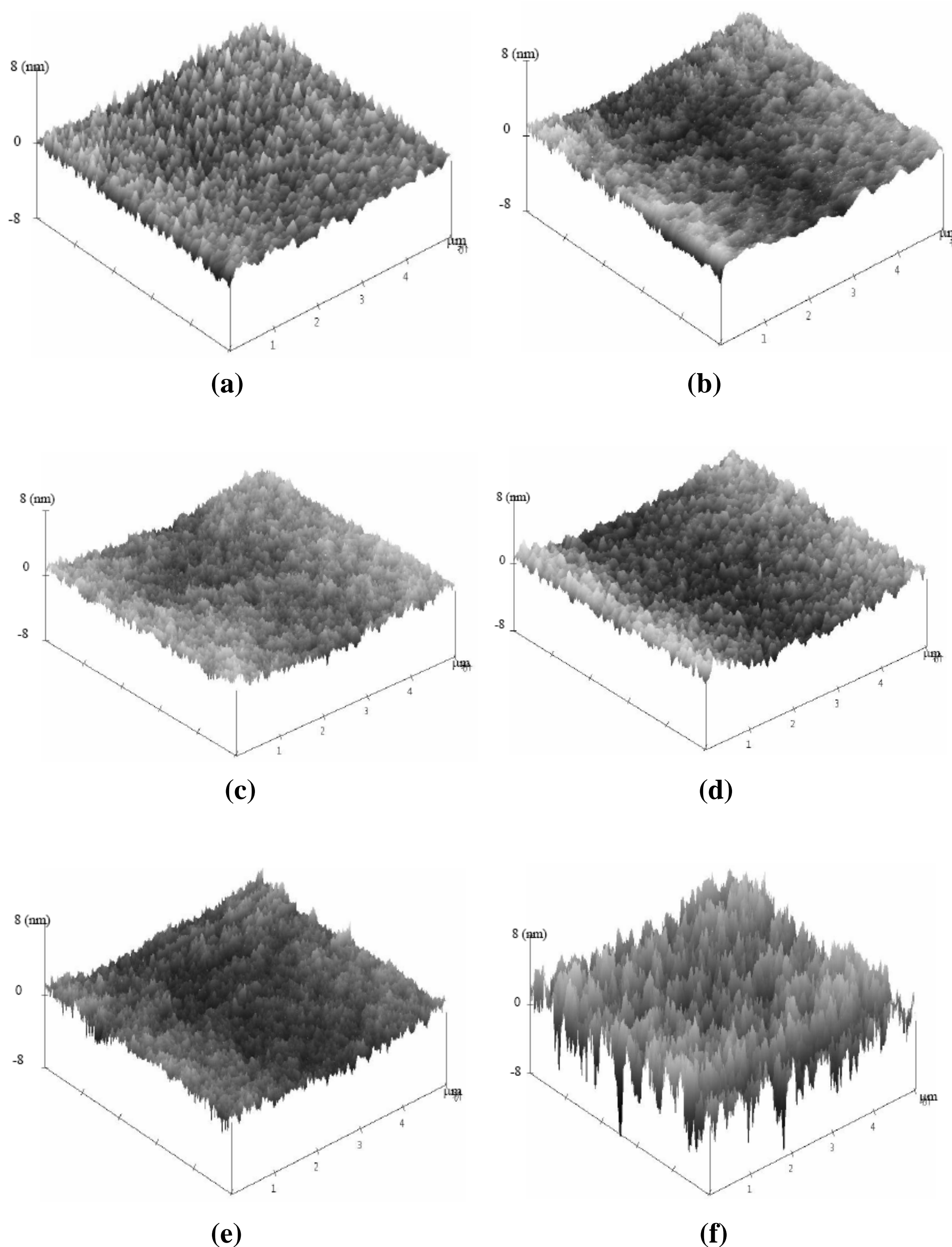

Figure 4.4 AFM images of **(a)** TaN film (150 nm); **(b)** pure PVK film (200 nm); **(c)** 20:1 PVK:GNPs (200 nm); **(d)** 12:1 PVK:GNPs film (200 nm); **(e)** 6:1PVK:GNPs film (200 nm); **(f)** 3:1 PVK:GNPs film (200 nm). The scan size in the AFM images is 5 μm x 5 μm with the height given in nanometer.

Table 4.1 Root-mean-square surface roughness of different films.

Material	**TaN**	**PVK**	**PVK:GNPs = 20:1**	**PVK:GNPs = 12:1**	**PVK:GNPs = 6:1**	**PVK:GNPs = 3:1**
RMS	**0.45 nm**	**0.29 nm**	**0.39 nm**	**0.40 nm**	**0.46 nm**	**1.76 nm**

4.3.2 UV-Visible Absorption Spectra

The UV-visible absorption spectra of GNPs, PVK and PVK:GNPs (with weight ratio of 12:1) in THF solution (1.0×10^{-5} mol/L) and as a thin film on quartz are shown in Fig. 4.5(a) and (b), respectively. The GNPs show a broad absorption band extending through the entire UV-visible spectrum. The undoped PVK solution exhibits three strong absorption bands at 295, 331 and 344 nm (correspond to the $^1A\rightarrow{}^1L_a$ and $^1A\rightarrow{}^1L_b$ transitions), with the absorption edge at about 370 nm [17]. Due to the low concentration of GNPs in solution, PVK:GNPs mainly shows the absorption peaks of the undoped PVK. However, the absorption edge of PVK:GNPs has also been extended into the long wavelength range. As shown in Fig. 4.5(b), the GNPs and undoped PVK film exhibit similar absorption behavior as they are in solution, while the absorption peaks of PVK:GNPs film are obviously broaden. This phenomenon is probably arisen from the interaction between the GNPs and PVK in solid state when excited by UV irradiation. The far distance between GNPs and PVK in dilute solution can prevent such an interaction. The charge transfer complex formed between the GNPs and PVK in the solid state can extend the delocalization of

carbazole moieties, and thus broaden the absorption peaks [18].

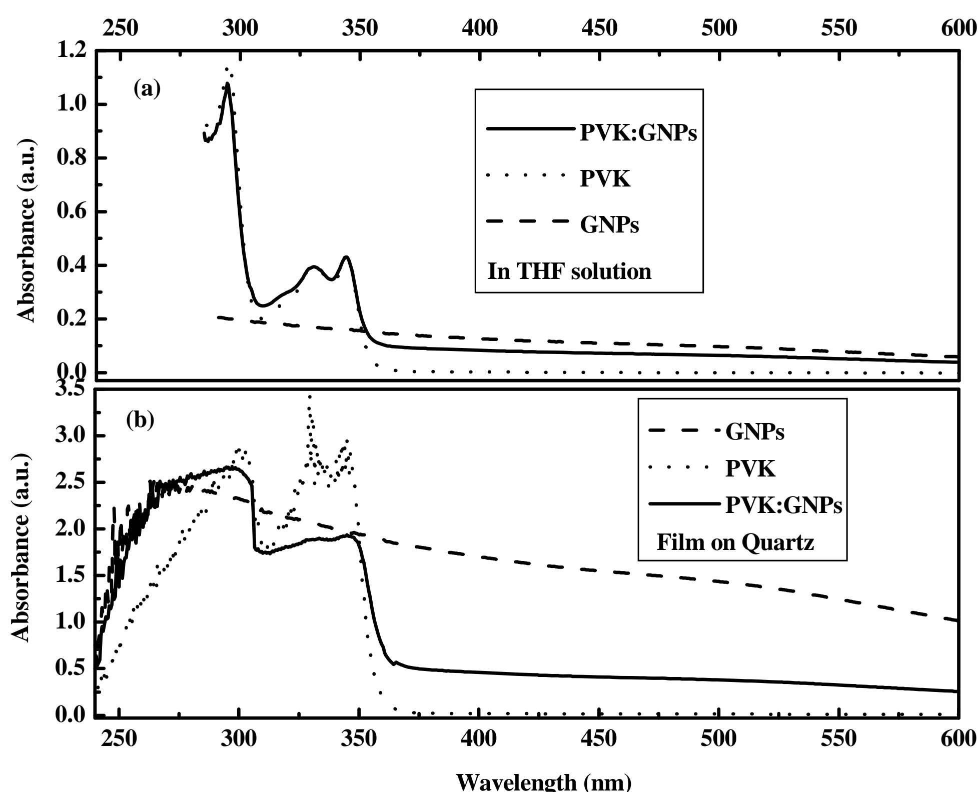

Figure 4.5 (a) UV-visible absorbance spectra of GNPs, PVK and PVK:GNPs in THF solutions ($1x10^{-5}$mol/L); **(b)** UV-visible absorbance spectra of GNPs, PVK, and PVK:GNPs films on quartz (the curves are normalized for a better view).

4.3.3 Hole Mobility in Mixed Films

Since PVK is dominant in the active layer of our device, it serves as the path for charge carrier transport. As we know, PVK is a hole conducting material. Knowing how the GNPs will affect the hole mobility in the PVK:GNPs film is an important issue. Therefore, we model the *J-V* (current density-voltage) characteristics for hole-only devices using SCLC theory, viz. [19],

$$J = \frac{9}{8}\varepsilon\varepsilon_0\mu\theta\frac{V^2}{d^3}, \tag{1}$$

where $\varepsilon \approx 3$ is used as the relative dielectric constant of the organic film, ε_0 is the vacuum dielectric constant, $\theta \leq 1$ is the shallow trapping factor (where $\theta = 1$) in the trap-free limit), d is the film thickness, and μ is the charge-carrier mobility.

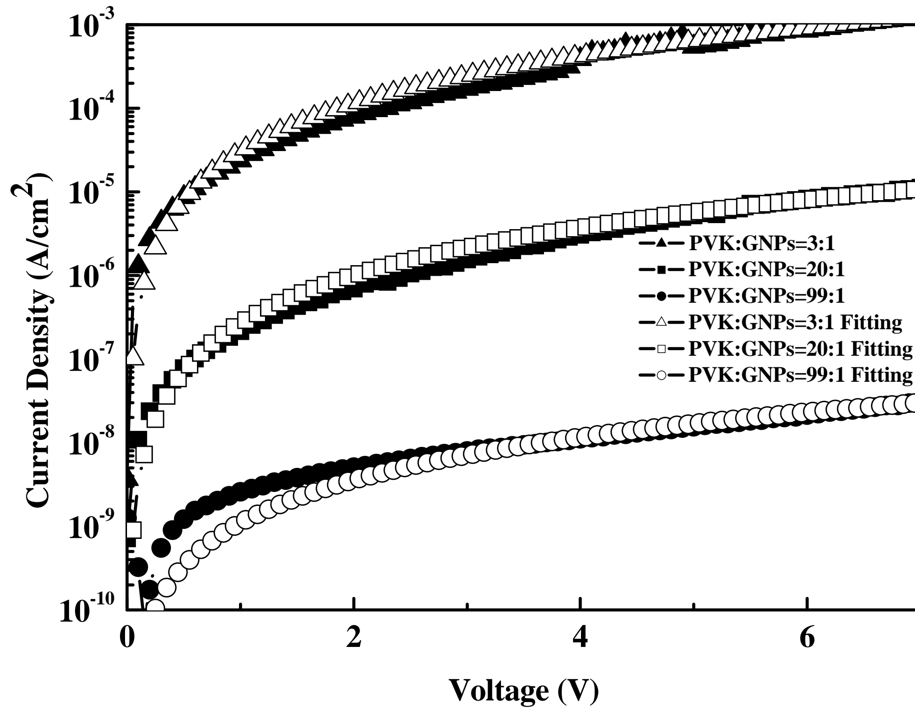

Figure 4.6 Current density vs. voltage characteristics of 3:1 PVK:GNPs (triangles), 20:1 PVK:GNPs (squares), and 99:1 PVK:GNPs (circles) films sandwiched between ITO and Au electrodes. The filled symbols are experimental data, while the open symbols are fitting data based on space charge limited current theory.

Fig. 4.6 shows the *J-V* characteristics of 1 μm-thick PVK:GNPs films of various compositions sandwiched between ITO and Au. In this configuration, holes are injected from ITO into the organic film, whereas electron injection from Au is discouraged due to its high work function (5.1 eV). The open sign lines show fits to the data using the field dependent SCLC of Eqs. (1). The zero-field mobilitys of holes

μ_0 in the mixing PVK:GNPs films can be extracted from the fitting curves and are shown in Table 4.2. From Table 4.2 we can see, the μ_0 of PVK:GNPs films increase as the weight percent of GNPs is increased. It can increase from 8.3x10^{-9}cm^2/Vs for 99:1 PVK:GNPs (circles in Figure 4.6) to 1.0x10^{-4}cm^2/Vs for 3:1 PVK:GNPs (triangles in Figure 4.6).

Table 4.2 Zero-field hole mobility μ_0 in different PVK:GNPs films sandwiched between ITO and Au.

sample	μ_0 (cm^2/Vs)
PVK:GNPs=3:1	**1.0x10^{-4}**
PVK:GNPs=20:1	**9.0x10^{-7}**
PVK:GNPs=99:1	**8.3x10^{-9}**

4.3.4 Device Performance of Device based on 12:1 Mixing Ratio

The typical *J-V* characteristics for our 12:1 PVK:GNPs based device are shown in Fig. 4.7. The memory effect of the device is observed in the *J-V* curves of the Al/PVK:GNPs/TaN sandwich device. The *J-V* characteristics are recorded by scanning applied voltage from 0 V to 4 V and then going back to 0 V. It distinctively displays two conducting states. With an applied voltage on the as-fabricated device, though the current increases slowly with the voltage, the current remains low. The current density is in the range of 10^{-8} A/cm^2 at 1 V. This is the low conductivity state

(OFF-state). When the applied voltage is increased further to ~3 V, a sharp increase in the current is observed, indicating the device transition from the OFF-state to a high conductivity state (ON-state). This transition from the OFF-state to the ON-state serves as the "writing" process for the memory device. For the programmed device, the device shows a high current for the voltage applied. The current density at 1 V is about 10^{-3} A/cm^2. This current is 5 orders of magnitude higher than that in the OFF-state. Fig. 4.8 shows the ratio of the ON- to the OFF-state current as a function of applied voltage. The distinct bi-electrical states in the voltage ranging from 0 to 2 V allows a low voltage (e.g., 1.0 V) to read the "0" or "OFF" signal (before writing) and "1" or "ON" (after writing) signal of the device. Curve II in Fig. 4.6 shows a sweep from 0 V to 4 V after the first sweep. It can be seen that the device, after reaching its high conductivity state, remains in this ON-state even turning off the power. The ON-state can be returned to the OFF-state by applying a reverse bias as indicated in curve III, where the current density suddenly drops to 10^{-8} A/cm^2 at -1.7 V, corresponding to the "erasing" process for the memory device. The erased state ("0") could be further written to the high conducting state ("1") when a switching threshold voltage is applied, indicating that the memory device is rewritable, as indicated in curve IV. The write and erase processes can be repeated for about 50 times. To show the memory effect is come out of inserting GNPs into the PVK, we also measured the J-V curve of pure PVK based device. No memory effect was observed from Al/PVK/TaN device, as shown in Fig. 4.9.

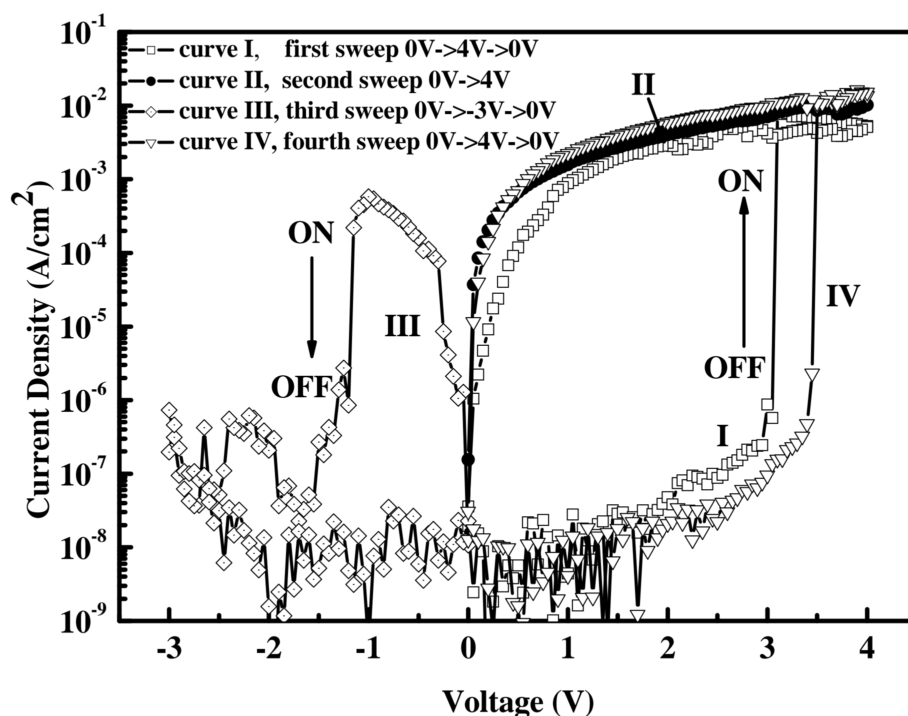

Figure 4.7 Typical *J-V* characteristics of the Al/12:1 PVK:GNPs (130 nm)/TaN device.

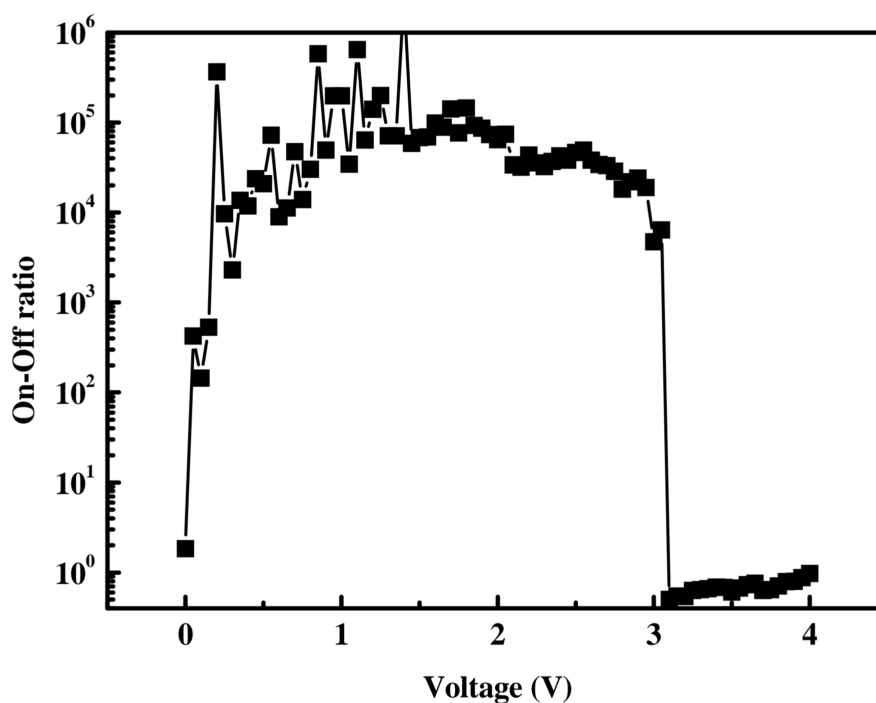

Figure 4.8 The ON- to OFF-current ratio as a function of applied voltage.

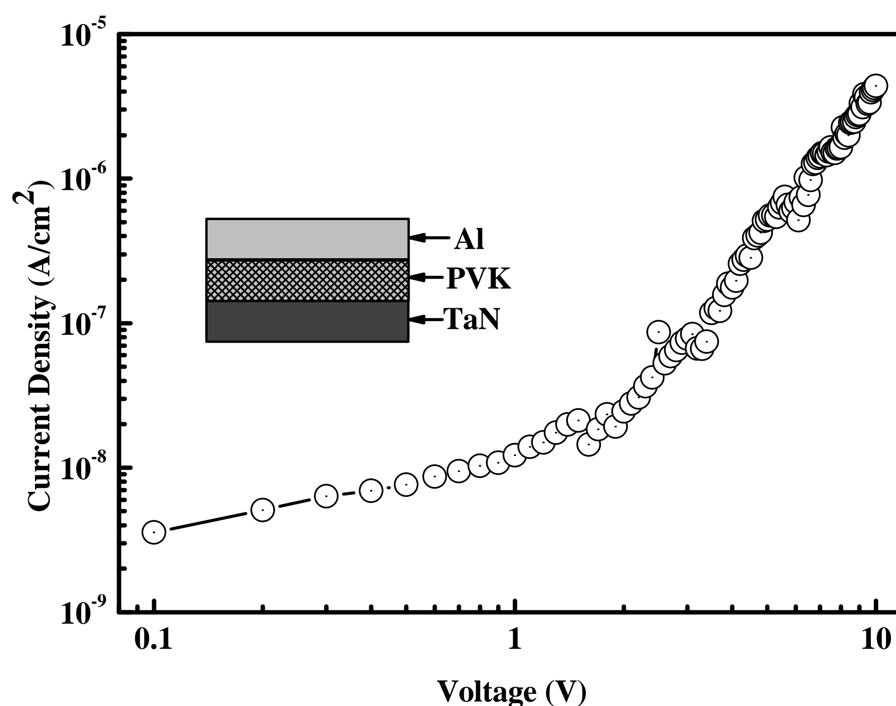

Figure 4.9 *J-V* characteristics of the Al/PVK/TaN device. Inset: Schematic diagram of the Al/PVK/TaN device.

The electrical bistability suggests that the Al/PVK:GNPs/TaN devices can be used as nonvolatile flash-type memory. Since stability is a very important characteristic to memory device, the stability of the device was characterized under a constant voltage stress of 1.0 V, as shown in Fig. 4.10. Little degradation in current density for both the ON- and OFF-states was observed during the test. The thermal stability of the device in both the ON- and OFF-states was also measured. The device was found to be stable in both its ON- and OFF-states from room temperature to around 70°C (Fig. 4.11).

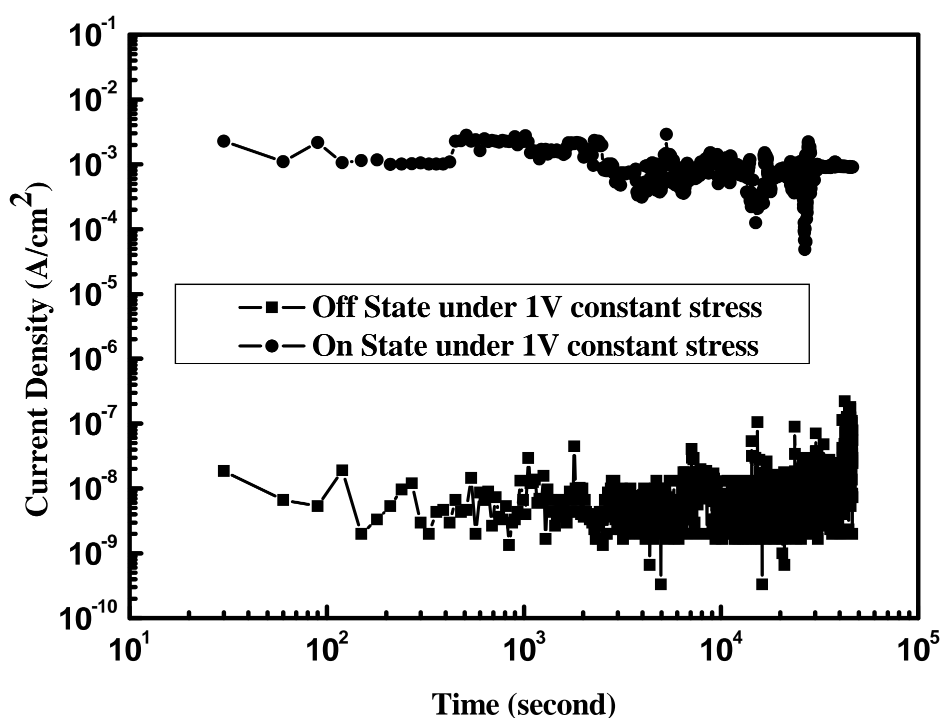

Figure 4.10 The stability characteristics of the Al/PVK:GNPs/TaN devices in either ON or OFF state under a 1 V constant voltage stress.

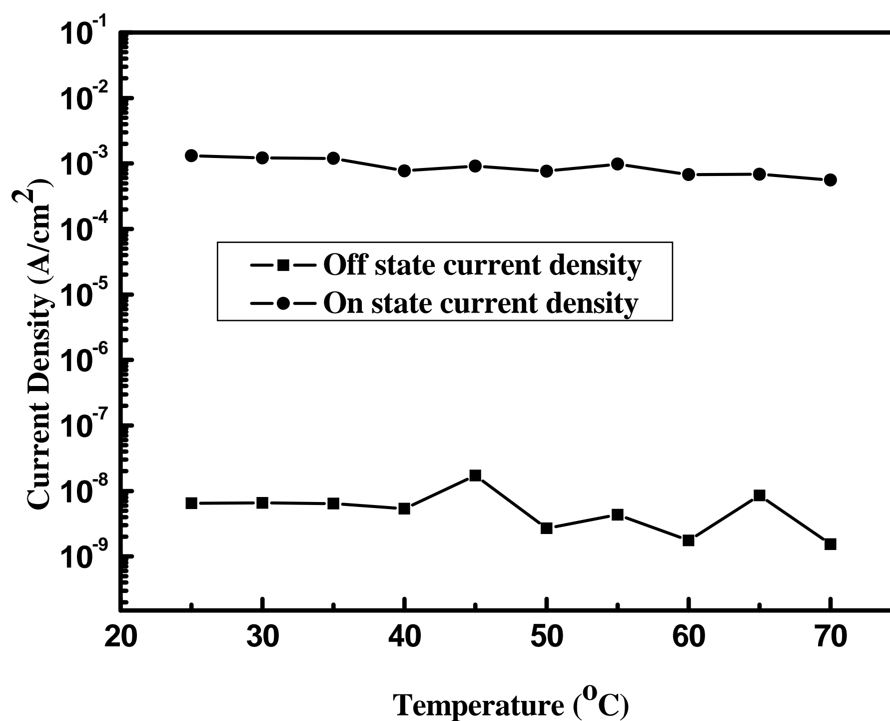

Figure 4.11 The *J-T* characteristics of the Al/PVK:GNPs/TaN device in either ON or OFF state under a 1 V read voltage.

The response time for both write and erase process has also been measured. The device in the OFF-state can be switched to the ON-state by a pulse of 6 V with a width of 1 μs. The device in the ON-state can be switched back to the OFF-state by a pulse of -10 V with a width of 1 μs.

Electrical bistability and memory effect in the Al/PVK:GNPs/TaN devices are due to the incorporation of GNPs in the PVK. By mixing the GNPs into the PVK polymer, the PVK serves both as the matrix for GNPs and electron donor since it has a strong capability to provide electrons [20], while the GNPs act as electron acceptors. Since PVK is dominant in the middle active layer of our device, it serves as the path for charge carrier transport. When a high electric field is applied to the device, the electric-field-induced charge transfer complex between the PVK and GNPs will be formed with the PVK positively charged and the GNPs negatively charged. The distortion due to the presence of a charge tends to change the electronic states in the vicinity of the charge such that the HOMO energy level shifts upward and the LUMO energy level shifts downward.[21] This change will decrease the bandgap and dramatically increase the conductivity of the organic materials. It is known that charge transfer complex strongly depends on the electric field. For the devices in the ON-state, a reverse bias could cause the charge transfer complex return back to their original states and hence the device will be erased to its OFF-state.

4.3.5 Device Performance under Different Mixing Ratio

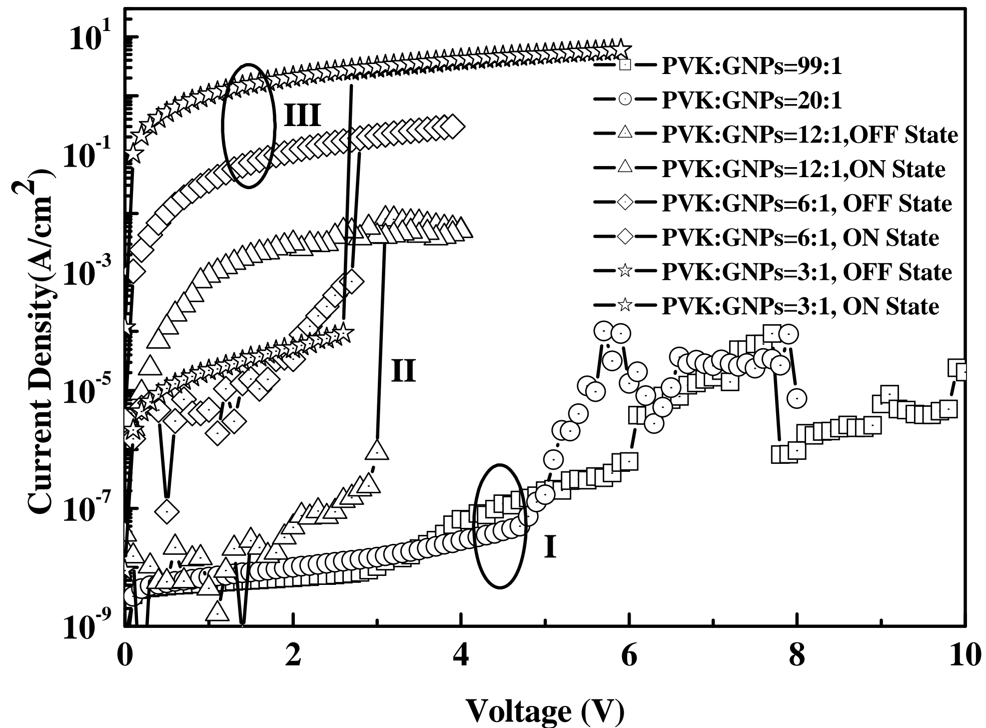

Figure 4.12 *J*-*V* characteristics of the Al/PVK:GNPs (130 nm)/TaN devices with different PVK:GNPs weight ratio. Area I: 99:1 PVK:GNPs and 20:1 PVK:GNPs based devices; area II: 12:1 PVK:GNPs based device; area III: 6:1 PVK:GNPs and 3:1 PVK:GNPs based devices.

Except using 12:1 PVK:GNPs mixture as the active material, we also fabricated devices by using 99:1 PVK:GNPs, 20:1 PVK:GNPs, 6:1 PVK:GNPs and 3:1 PVK:GNPs mixtures and tried to see the effect of mixing ratio to the memory effect. Of all the devices, the thickness of the active layer was maintained at 130 nm. Fig. 4.12 shows the device *J*-*V* curves of different weight ratios and we can separate the *J*-*V* curves into three regions based on the performance. 99:1 PVK:GNPs and 20:1 PVK:GNPs belong to region I, in which no memory effect is observed. 12:1 PVK:GNPs belongs to region II, in which flash-type memory effect is observed. 6:1 PVK:GNPs and 3:1 PVK:GNPs belong to region III in which memory effect is

observed but it might be because of film breakdown. According to the *J-V* curve of 99:1 PVK:GNPs, the current increases slowly with the voltage initially. When the applied voltage increases to 7.7 V, a sharp decrease in the current is observed. If we repeated the sweep for one more time, the current will follow the previous curve instead of staying under the low conductivity state, which means the device can not show two stable conductivity states and can not be used as the memory device. If we kept increasing the GNPs into the mixture till the weight ratio of PVK:GNPs reached 20:1, no significant difference is observed from the *J-V* curve. A similar negative differential resistance phenomenon is observed from 20:1 PVK:GNPs device. Interestingly, if we increased the PVK:GNPs weight ratio to 12:1, a different story is observed. As we described in our previous part, 12:1 PVK:GNPs device shows a flash-type memory effect. *J-V* of 6:1 PVK:GNPs and 3:1 PVK:GNPs devices show the *J-V* curves of devices based on PVK:GNPs with weight ratio 6:1 and 3:1 respectively. Two conductivity states are distinctively displayed on the curves. With an applied voltage on the as-fabricated device, though the current increases slowly with the voltage, the current remains low. When the applied voltage is increased further to ~2.7 V (for 6:1 PVK:GNPs device) or ~2.6 V (for 3:1 PVK:GNPs device), a sharp increase in the current is observed, indicating the device transition from the low conductivity state to a high conductivity state. If we did one more sweep after the first sweep, it can be seen that the device, after reaching its high conductivity state, remains in this ON-state even turning off the power. The ON-state can not be returned to the OFF-state by applying a reverse bias. Comparing with the ON-state current of

the 12:1 PVK:GNPs device, the ON-state current of the 6:1 PVK:GNPs and 3:1 PVK:GNPs are quite high. And we can not see the area dependence from these two kinds of device. (We used current density instead of current here is just for easily comparing with other devices) We considered that the high conducting state might because of film breakdown.

4.3.6 Device Performance under Different Film Thickness

Fig. 4.13 shows the *J-V* curves of devices with different active layer thickness. All these devices are based on PVK:GNPs mixture with weight ratio of 12:1. The active layers' film thickness of the four figures from Fig. 4.13(a) to Fig. 4.13(d) are 1.3μm (device A), 130nm (device B), 50 nm (device C) and 25 nm (device D) respectively. All the devices are based on same structure. Device C and device D have the same device size of 400 μm x 200 μm. All the four devices show two distinguished conductivity states. But there are still some differences among them. Device A and device B show similar *J-V* curves. Both can be turned on by using positive bias and be turned off by using negative bias and a flash-type memory effect is kept. The differences between these two devices are the switching voltages. For device A, the turn on voltage is about 7.4 V and the turn off voltage is about -5.1 V. For device B, the turn on voltage is about 3 V and the turn off voltage is about -1.7 V. The differences between the switching voltages should come out from the thickness difference. It should be noticed that the switching voltage doesn't show an absolutely linear relationship to the active layer thickness. This indicates that the switching

voltage isn't decided by the electric field only but other issues. The effect of the thickness to the device performance is also showed on the current density. We can use 1 V voltage as the reading voltage to read the current of the two different conductivity states of the two devices. For device A, the ON state current density under 1 V is about 2×10^{-7} A/cm^2. But for device B, the ON state current density under 1 V is about 10^{-3} A/cm^2. There are 4 orders of difference in magnitude. The difference between the two OFF state current is neglectable. Device C and device D also show similar *I-V* curves. Both show a low conductivity state initially and can be turned on by using positive bias but can not return to the low conductivity state by using negative bias, which means the OFF to ON transition is non-recoverable. The turn on voltage of device C is about 3 V and that of device D is about 2.3 V. Comparing with the equivalent currents of device A and device B, the ON state currents and the OFF state currents of the device C and device D are all much larger. This is also because of the active layer thickness decreasing. If we compare the *I-V* curves of device C and device D, we may find that the OFF state current of device D is much higher than that of device C, but the ON state currents of the two devices are almost the same. We further measured the ON state currents of different device sizes based on these two device structures and found there was no area dependence. (This is the reason that we use *I-V* instead of *J-V* to characterize device C and device D) Considering that the ON state can not be recovered to the OFF state for these two devices, we might say the OFF to ON transition for these two devices are breakdown phenomenon.

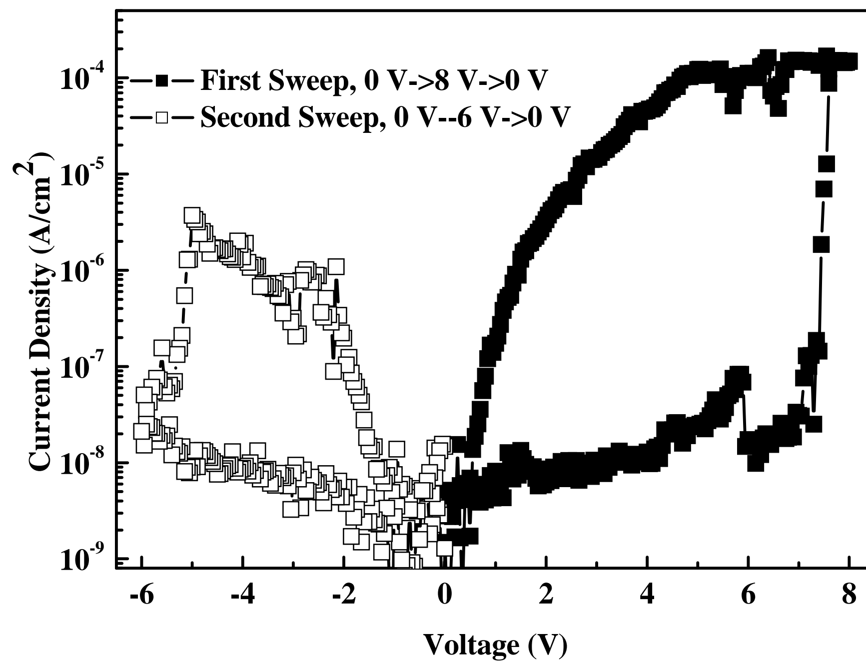

(a)

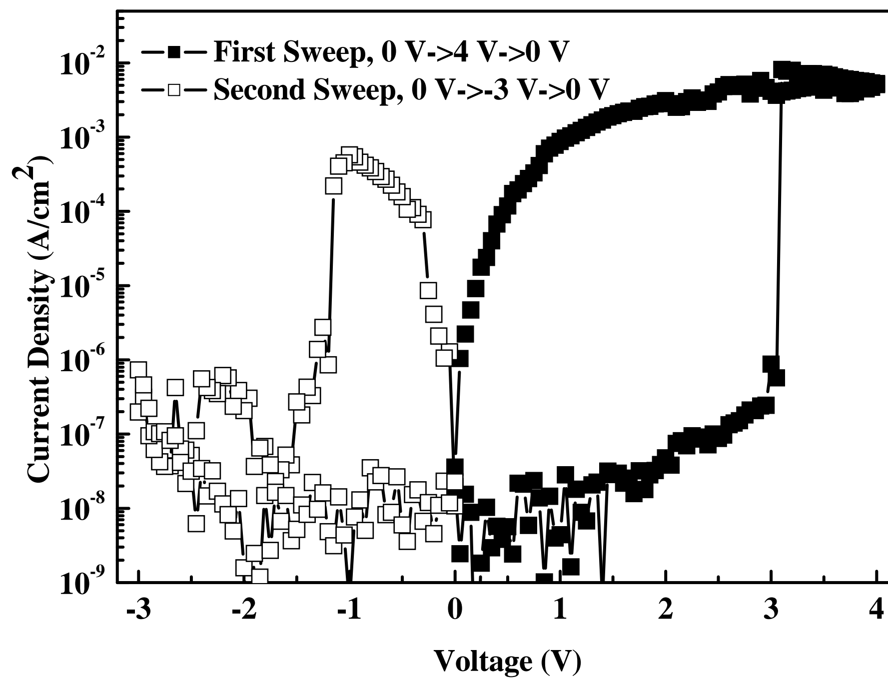

(b)

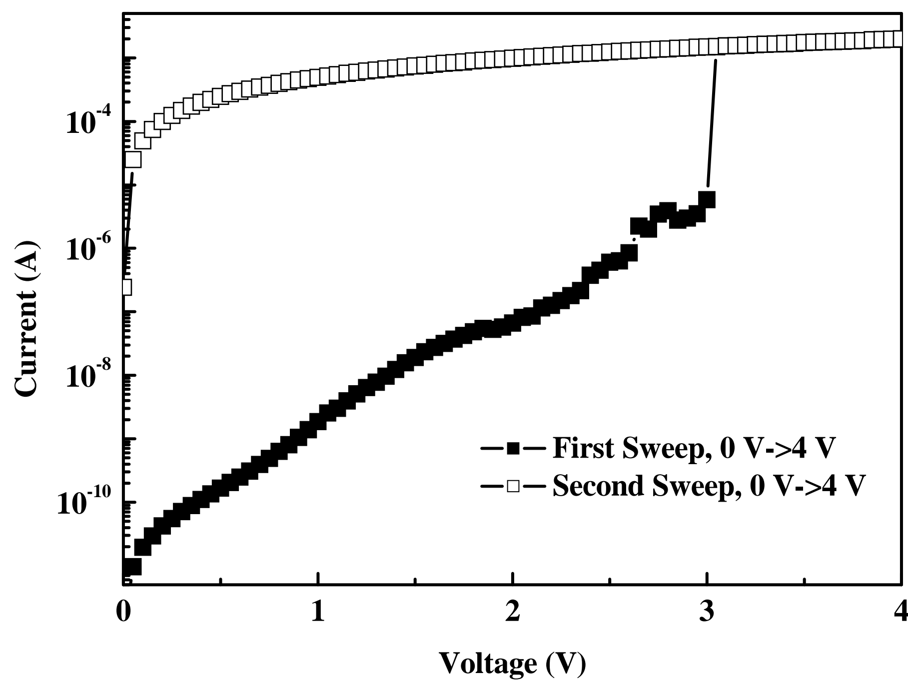

(c)

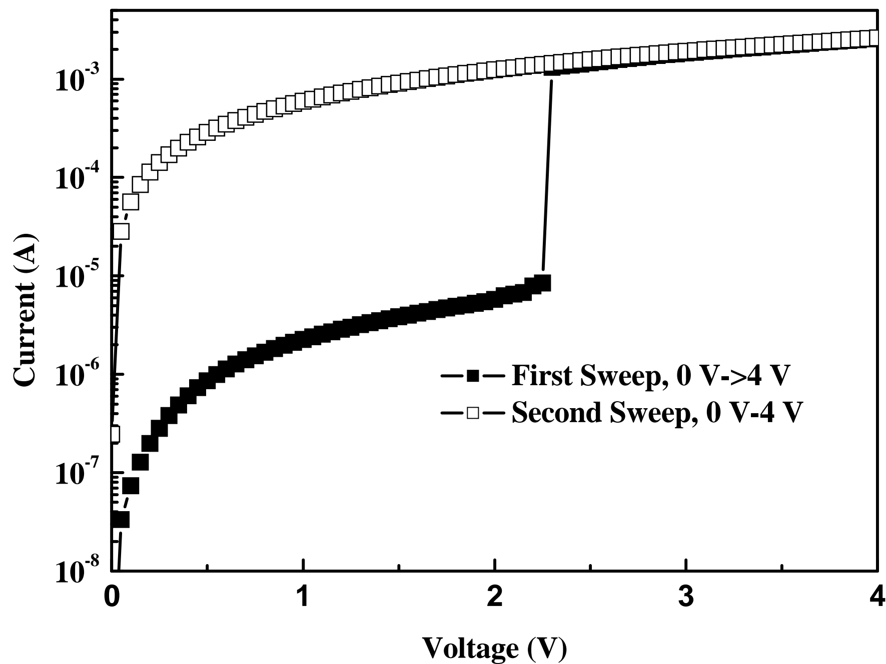

(d)

Figure 4.13 *J-V* characteristics of the Al/12:1 PVK:GNPs/TaN devices based on different polymer thickness **(a)** 1.3 μm; **(b)** 130 nm; **(c)** 50 nm; **(d)** 25 nm.

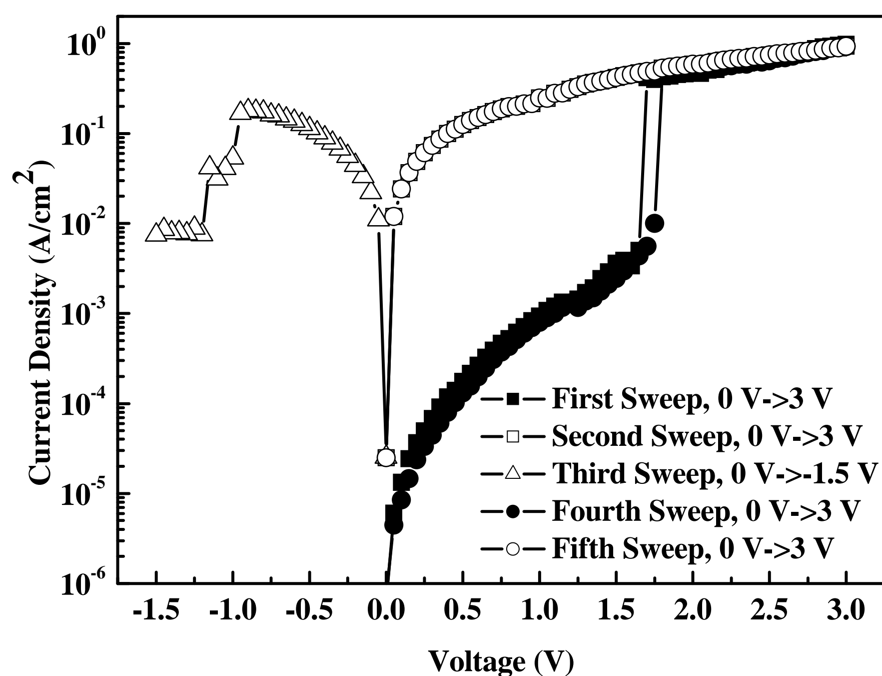

(a)

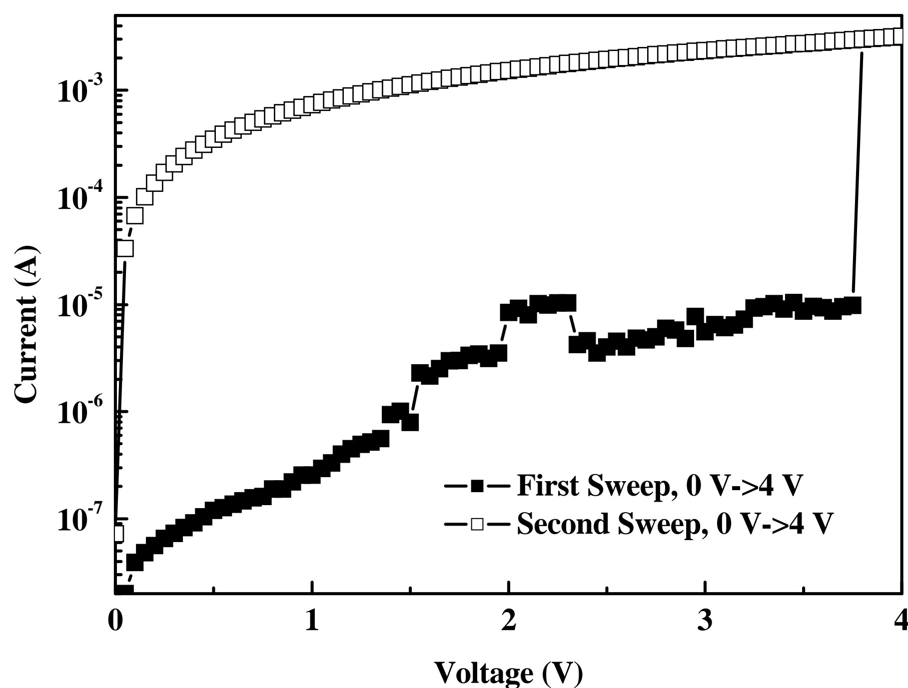

(b)

Figure 4.14 *J-V* characteristics of the 12:1 PVK:GNPs based devices with same active layer film thickness and different top metal electrodes **(a)** Cu; **(b)** Au.

4.3.7 Device Performance under Different Top Metal Electrode

It is important to understand the role of the top metal electrode in the memory device. To study this dependence, devices with different top metal electrodes were fabricated. We tried Al, Cu and Au as the top electrode and all these devices' active layers are based on 12:1 PVK:GNPs mixture and have a thickness of 130 nm. Fig. 4.14(a) shows the *J-V* curve of Cu top electrode device and Fig. 4.14(b) shows the *I-V* curve of Au top electrode device. Al top electrode device is our typical device and has already been described in Fig. 4.7 and Fig. 4.13(b). As shown in Fig. 4.14(a), the Cu top electrode device can be turned on by using a positive bias and turned off by using a negative bias. The ON-OFF transitions are repeatable and show a flash-typed memory effect. The shape of the *J-V* curves is quite similar as that of Al top electrode device. The turn on voltage of this Cu based device is about 1.65 V and the turn off voltage of it is about -0.95 V. Compare with the transition voltage of Al based device, which is 3 V for turn on and -1.7 V for turn off, that of Cu based device is quite small. The currents of the high conductivity state and low conductivity state of the Cu based device are quite high compare with those of Al based device. If we use a 1 V voltage as the read voltage, the OFF state current density is about 9×10^{-4} A/cm^2 and the ON state current density is about 0.25 A/cm^2. And the ON-OFF current ratio of the Cu based device is about 3 orders of magnitude at 0.5 V read voltage, which is smaller than that of Al based device, which has an ON-OFF current ratio of 5 orders of magnitude at 1 V read voltage. Considering that these two kinds of device have the same active material compositions and same middle layer thickness, and the

fabrication process and measurement process are all similar, the different performance between these two devices should come from the copper diffusing into the polymer layer. As we know, copper is quite easy to diffuse into polymer during the thermal evaporation process or under an external electric field. The copper ion in the polymer film might also form another conducting path and combine with the intrinsic conducting path in our polymer material. Yang et al. also reported a paper regarding copper diffusion formed memory effect [22]. Fig. 4.14(b) shows the *I-V* curve of the Au top electrode device. We can see that the I-V curve is quite similar as that in Fig. 4.13(c) and (d). The device can be turned on and can not be turned off. This might because of the gold diffusion. Comparing the *I-V* curve of the Au based device with the *J-V* curve of Cu based device, we may find that the OFF currents of these two devices are not so much different, but the ON current of the Au based device is much higher than that of Cu based device. This might be able to explain why only the Cu based device can be turned off from the ON state although both the gold and copper can diffuse into the polymer material. After gold diffuses into the polymer material, it might also assist to form a conducting path while an external electronic field is applied to the device. But the ON state current is so high which might cause the film to breakdown and can not return to the OFF state.

4.4 Conclusion

Investigating and understanding polymer thin film properties is of fundamental and technological importance. The study presented here emphasizes the properties of

mixtures of PVK and GNPs which are employed in our memory device. We have shown that the surface roughness of the mixture is increased from RMS value of 0.29-1.76 nm with the increasing of GNPs concentration. We also found that hole mobility of the PVK:GNPs mixture film can increase with the increasing of GNPs concentration. By comparing the performance of devices based on different PVK:GNPs mixing ratio, we found that 99:1 PVK:GNPs and 20:1 PVK:GNPs devices can not show memory effect. The 6:1 PVK:GNPs and 3:1 PVK:GNPs device can show two conductivity states but cannot transfer between them freely. Only the 12:1 PVK:GNPs device can perform the flash-type memory effect. If we focused on the 12:1 PVK:GNPs device and changed the active layer thickness, we will find only when the film is thick enough can the device perform the flash-type memory effect. If the film thickness is 50 nm or less, the film will be easily breakdown and no further transition can be seen. Keeping the mixing ratio and film thickness constant, we also researched how the top metal electrode affects the device performance. Same as Al top electrode device, the Cu top electrode device also shows flash-type memory effect expect that Cu top electrode device has higher ON/OFF current and lower transition voltages. From the Au top electrode device we can not see the flash-type memory effect and it might because of the gold diffusion. Overall, the device with Al top electrode and 130 nm 12:1 PVK:GNPs active layer has the best performance and have great potential on future memory application.

Reference

[1] A. Bandyopadhyay, and A. J. Pal, Appl. Phys. Lett. **82**, 1215 (2003).

[2] B. Mukherjee, and A. J. Pal, Appl. Phys. Lett. **85**, 2116 (2004).

[3] H. S. Majumdar, A. Bolognesi, and A. J. Pal, Thin Solid Films, **446**, 296 (2004).

[4] S. Moller, C. Perlov, W. Jackson, C. Taussig, and S. R. Forrest, J. Appl. Phys. **94**, 7811 (2003).

[5] Y. Song, Y. P. Tan, E. Y. H. Teo, Chunxiang. Zhu, D. S. H. Chan, Q. D. Ling, K. G. Neoh, and E. T. Kang, J.Appl. Phys. **100**, 084508 (2006).

[6] E. Y. H. Teo, Q. D. Ling, Y. Song, Y. P. Tan, W. Wang, E. T. Kang, D. S. H. Chan, and Chunxiang Zhu, Org. Electron. **7**, 173 (2006).

[7] Q. D. Ling, Y. Song, S. L. Lim, E. Y. H. Teo, Y. P. Tan, C. Zhu, D. S. H. Chan, D. –L. Kwong, E. T. Kang, and K. G. Neoh, Angew. Chem. Int. Edit. **45**, 2947 (2006).

[8] Q. D. Ling, F. C. Chang, Y. Song, C. Zhu, D. J. Liaw, D. S. H. Chan, E. T. Kang, and K. G. Neoh, J. Am. Chem. Soc. **128**, 8732 (2006).

[9] L. P. Ma, J. Liu, and Y. Yang, Appl. Phys. Lett. **80**, 2997 (2002).

[10] L. D. Bozano, B. W. Kean, V. R. Deline, J. R. Salem, and J. C. Scott, Appl. Phys. Lett. **84**, 607 (2004).

[11] J. Ouyang, C. W. Chu, C. R. Szmanda, L. P. Ma, and Y. Yang, Nat. Mater. **3**, 918 (2004).

[12].R. J. Tseng, J. Huang, J. Ouyang, r. B. Kaner, and Y. Yang, Nano Lett. **5**, 1077 (2005).

[13] R. J. Tseng, C. L. Tsai, L. P. Ma, J. Ouyang, C. S. Ozkan, and Y. Yang, Nature Nanotech. **1**, 72 (2006).

[14] Y. Song, Q. D. Ling, S. L. Lim, E. Y. H. Teo, Y. P. Tan, L. Li, E. T. Kang, D. S. H. Chan, and Chunxiang Zhu, IEEE Electron Device Lett. **28**, 107 (2007).

[15] H. Sakai, A. Itaya, and H. Masuhara, J. Phys. Chem. **93**, 5351 (1989).

[16] M. –C. Daniel, and D. Astruc, Chem. Rev. **104**, 293 (2004).

[17] K. Walter, *Introduction to Polymer Spectroscopy*; Ch.3, Springer-Verlag: Berlin, (1984).

[18] H.Khalil and K. Levon, Macromolecules. **35**, 8180 (2002).

[19] M. Pope and C. E. Swenberg, *Electronic Processes in Organic Crystals and Polymers*, 2nd ed. Oxford University Press, New York (1999).

[20] H. Sakai, A. Itaya, and H. Masuhara, J. Phys. Chem. **93**, 5351 (1989).

[21] J. L. Bredas and G. B. Street, Acc. Chem. Res. **18**, 309 (1985).

[22] L. P. Ma, Q. F. Xu, and Y. Yang, Appl. Phys. Lett. **84**, 4908 (2004).

Chapter 5

Conclusions

5.1 Conclusions

The main purpose of the study was to investigate the possible organic and polymer materials which can be used in memory devices and to develop a sandwiched metal-insulator-metal device structure for memory application. Three kinds of memory devices were developed.

A conjugated copolymer containing fluorine and chelated europium complex (named PF8Eu) was synthesized. Based on this copolymer material, we fabricated a metal-insulator-metal structured device. Under the current- voltage measurement, this device showed a write-once-read-many times (WORM) memory behavior. The memory device had a switching time of ～1 μs and an on/off current ratio as high as 10^6. No degradation in device performance was observed after 10^7 read cycles at a read voltage of 1 V under ambient conditions. The memory effect might come from the charge transfer between the fluorine moiety and europium complex. This is probable because when an electrical field was applied to the device, an electron transition would happen and thus the fluorine moiety might lose electrons and the europium complex might receive electrons. This transition can decrease the band gap of the fluorine moiety and greatly increase the conductivity of the material.

After the write-once-read-many times device, a flash-typed memory device was fabricated successfully by using poly[NVK-*co*-Eu(VBA(TTA)$_2$phen)] or PKEu, a copolymer containing carbazole units and europium complex moieties as the active layer between ITO and aluminum electrodes. Although both PF8Eu and PKEu include europium complex which serves as the electron acceptor group, there still some difference exists between these two kinds of europium complex. The europium complex in PKEu has a weaker electron affinity than that in PF8Eu, which means it can lose the electron easier than that in PF8Eu. The device could exhibit two distinctive bistable conductivity states by applying voltage pulses of different polarities. The device can remain in either state even after the power has been turned off. An on/off current ratio as high as 10^4 and a switching time of ~20 μs were achieved. More than a million read cycles were performed on the device under ambient conditions without any device encapsulation. A redox mechanism, governed by the donor-acceptor nature of the PKEu copolymer, was proposed to explain the memory effect of the device.

Beside the two kinds of europium complex contained copolymer materials, a device using polymer mixed with nanoparticle as the active layer between two metal electrodes was fabricated. The polymer we used here is poly(N-vinylcarbazole) (PVK), which is a good electron donor. The nanoparticle we used here is gold nanoparticle (GNP), which is a good electron acceptor. The first part of this experiment is based on the device with PVK:GNPs mixing weight ratio of 12:1. The device could transit between low conductivity and high conductivity easily by

applying an electrical field. Between the low conductivity state and high conductivity state, an on/off current ratio as high as 10^5 ate room temperature was achieved. The device showed a good stability under 10-hour constant stress test for both low conductivity and high conductivity state. The memory effect was attributed to electric-field-induced charge transfer complex formed between PVK and the gold nanoparticles. The second part of this experiment is focused on the influence of different PVK:GNPs mixing ratio, different active layer thickness and different top metal electrode to the device performance. By comparing the performance of devices based on different PVK:GNPs mixting ratio, we found that 99:1 PVK:GNPs and 20:1 PVK:GNPs devices can not show memory effect. The 6:1 PVK:GNPs and 3:1 PVK:GNPs device can show two conductivity states but cannot transfer between them freely. Only the 12:1 PVK:GNPs device can perform the flash-type memory effect. If we focused on the 12:1 PVK:GNPs device and changed the active layer thickness, we will find only when the film is thick enough can the device perform the flash-type memory effect. If the film thickness is 50 nm or less, the film will be easily breakdown and no further transition can be seen. Keeping the mixing ratio and film thickness constant, we investigated how the top metal electrode affects the device performance. Same as aluminum top electrode device, the copper top electrode device also shows flash-type memory effect expect that copper top electrode device has higher on/off current and lower transition voltages. From the gold top electrode device we can not see the flash-type memory effect and it might because of the gold diffusion.

Table 5.1 Comparison of electrical characteristics among 3 kinds of device.

	WORM	Flash Type	
	PF8Eu	PKEu	PVK:GNP
I_{on}/I_{off}	10^6	10^4	10^5
Read Pulse	$>10^7$	$>10^6$	
Write Time	<1μs	<20μs	<1μs
Stress Test	>10 h (under 1V)		>10 h (under 1V)
Retention Time		~ 3 h	
Temperature Test			up to 70°C

5.2 Limitations

Although we have achieved many of results from the present research, there were several limitations in the present study:

(1) Retention time of the memory devices. According to the International Technology Roadmap for Semiconductors (ITRS), for a commercial memory device to be useful, the retention time should be longer than 10 years. For our devices, the retention time was in the range of several hours to several days. It is too short to be used in commercial products. Thus, future research on improving the memory device retention time is needed.

(2) Reliability of the memory devices. In terms of memory device, the write-read-erase-read cycles is an important parameter to evaluate the stability of the device. As regards the traditional silicon based memory device, the

write-read-erase-read cycles can normally be repeated for more than 1 million times. For our device, unfortunately, this cycle could only repeat for less than 100 times. It is common knowledge that the stability of organic material cannot compete with the stability of inorganic material in the current stage of technology. This might be the reason for the poor reliability in our memory device.

(3) Mechanism of the memory effect. In our study, we proposed some mechanisms for the WORM, and flash-typed memory effects. Due to the limitation of the experimental conditions, the supporting evidences for the proposed mechanisms were not strong. Future work on the mechanism research is needed.

Nevertheless, results of the present study might enhance our understanding in the application of organic and polymer materials to the organic memory device and they might also contribute to further investigations on the material selection for organic memory device.

5.3 Suggestions for Future Work

Based on the limitations of this study, there can be several directions for further studies:

(1) Material property improvement. Since the poor reliability of our organic memory device is from the poor stability of organic material, it is a good way to improve the device reliability by improving the organic material property.

(2) Process optimization. During our study, we found that the experimental process had great effect on the device performance. For example, the deposition speed of

top electrode would affect the degree of metal diffusing into the polymer layer. By optimizing the solution preparation process, the spin coating process and the thermal evaporation process, the device performance could be greatly improved.

(3) Mechanism research. The mechanism behind the memory effect is still not clear. Many research methods could be used in the mechanism research. For example, UHV-AFM can help us understand the conformation change progress; XRD can help us understand the material crystallization; XPS can help us understand the chemical bonding between elements, etc. If the mechanism is clear, it can also help us to improve the organic memory device performance.

One should note that these three aspects may have their own difficulties and requirements. Thus, research on each individual topic should try to fulfill the requirements from each of the other aspects.

Appendix

List of Publications

Part 1: Publications related with the thesis

Journal:

- **Y. Song**, Q. D. Ling, S. L. Lim, E. Y. H. Teo, Y. P. Tan, Chunxiang Zhu, D. S. H. Chan, K. G. Neoh, and E. T. Kang, "Material Properties and Electrical Performance of Mixed Polymer and Gold Nanopartical Based Memory Device", to be submitted to *Journal of Applied Physics*.

- **Y. Song**, Q. D. Ling, S. L. Lim, E. Y. H. Teo, Y. P. Tan, L. Li, E. T. Kang, D. S. H. Chan, D. L. Kwong, and Chunxiang Zhu, "Electrically Bistable Thin-Film Device Based on PVK and GNPs Polymer Material", *IEEE Electron Device Letters,* Vol. 28, No.2, page 107-110 (2007).

- **Y. Song**, Q. D. Ling, Chunxiang Zhu, E. T. Kang, D. S. H. Chan, Y. H. Wang, and D.-L. Kwong, "Memory Performance of a Thin-Film Device Based on a Conjugated Copolymer Containing Fluorene and Chelated Europium Complex", *IEEE Electron Device Letters*, Vol. 27, No. 3, page 154-156 (2006).

- **Y. Song**, Y. P. Tan, E. Y. H. Teo, Chunxiang Zhu, D. S. H. Chan, Q. D. Ling, K. G. Neoh, and E. T. Kang, "Synthesis and Memory Properties of a Conjugated Copolymer of Fluorene and Benzoate with Chelated Europium Complex", *Journal of Applied Physics*, Vol. 100, page 084508 (2006).

- Q. D. Ling, **Y. Song**, S. J. Ding, Chunxiang Zhu, D. S. H. Chan, D.L. Kwong, E. T. Kang, and K. G. Neoh, "Non-Volatile Polymer Memory Device Based on a Novel Copolymer of N-Vinylcarbazole and Eu-Complexed Vinylbenzoate", *Advanced Materials*, Vol. 17, No. 4, page 455-459 (2005).

Conference:

- **Y. Song**, Q. D. Ling, S. L. Lim, E. Y. H. Teo, Y. P. Tan, E. T. Kang, D. S. H. Chan,

and Chunxiang Zhu, "Material Properties of Mixed Polymer and Gold Nanoparticles Structure for Memory Applications", *2007 Materials Research Society Spring Meeting*, 2007.

- **Y. Song**, Q. D. Ling, Chunxiang Zhu, E. T. Kang, D. S. H. Chan, Y. H. Wang, and D. L. Kwong, "Memory Effect of Device Based on a Novel Copolymer PF8Eu", *Extended Abstracts of the 2005 International Conference on Solid State Devices and Materials*, pp. 386-387, 2005.

Part 2: Other Publications

Journal:

- Y. P. Tan, **Y. Song**, E. Y. H. Teo, Q. D. Ling, S. L. Lim, Patrick G. Q. Lo, D. S. H. Chan, E. T. Kang, and Chunxiang Zhu, "WORM-Type Device with Rectifying Effect Based on a Conjugated Copolymer of Fluorene and Europium Complex", Journal of The Electrochemical Society, Vol 155 (1), page H17-H20 (2008)

- Q. D. Ling, S. L. Lim, **Y. Song**, Chunxiang Zhu, D. S. H. Chan, E. T. Kang, and K. G. Neoh, "Nonvolatile Polymer Memory Device Based on Bistable Electrical Switching in a Thin Film of Poly(N-vinylcarbazole) with Covalently Bonded C_{60}", *Langmuir*, Vol.23, page 312-319 (2007).

- Q. D. Ling, W. Wang, **Y. Song**, Chunxiang Zhu, D. S. H. Chan, E. T. Kang, K. G. Neoh, "Bi-stable Electrical Switching and Memory Effects in a Thin Film of Copolymer Containing Electron Donor-Acceptor Moieties and Europium Complexes", *Journal of Physical Chemistry B***.** Vol. 110(47), page: 23995-24001 (2006).

- Q. D. Ling, F. C. Chang, **Y. Song**, Chunxiang Zhu, D. J. Liaw, D. S. H. Chan, E. T. Kang, and K. G. Neoh, "Synthesis and Dynamic Random Access Memory Behavior of a Functional Polyimide", *Journal of the American Chemical Society*, Vol. 128, page: 8732-8733 (2006).

- Q. D. Ling, **Y. Song**, E. Y. H. Teo, S. L. Lim, Chunxiang Zhu, D. S. H. Chan, D. L. Kwong, E. T. Kang, and K. G. Neoh, "WORM-Type Memory Device Based on a Conjugated Copolymer Containing Europium Complex in the Main Chain", *Electrochemical and Solid-State Letters*, Vol. 9(8), pgae: G268-G271 (2006).

- E. Y. H. Teo, Q. D. Ling, **Y. Song**, Y. P. Tan, W. Wang, E. T. Kang, D. S. H. Chan, and Chunxiang Zhu, "Non-volatile WORM memory device based on an acrylate polymer with electron donating carbazole pendant groups", *Organic Electronics*, Vol. 7, page: 173-180 (2006).

- Q. D. Ling, **Y. Song**, S. L. Lim, E. Y. H. Teo, Y. P. Tan, Chunxiang Zhu, D. S. H. Chan, D. L. Kwong, E. T. Kang, and K. G. Neoh, “A Dynamic Random Access Memory Based on a Conjugated Copolymer Containing Electron-Donor and –Acceptor Moieties”, *Angewandte Chemie International Edition*, Vol. 45(18), page 2947-2951 (2006).

Conference:

- E. Y. H. Teo, Q. D. Ling, **Y. Song**, Y. P. Tan, W. Wang, E. T. Kang, D. S. H. Chan, and Chunxiang Zhu, “Bi-stable State for WORM Application Based on Carbazole-containing Polymer”, *Mater. Res. Soc. Symp. Proc.*, vol. 937 M10-14, 2006.

- Y. P. Tan, Q. D. Ling, E. Y. H. Teo, **Y. Song**, S. L. Lim, G. Q. Lo, E. T. Kang, Chunxiang Zhu, and D. S. H. Chan, “A WORM-Type Memory Device with Rectifying Effect Based on a Conjugated Copolymer of PF6Eu on Si Substrate”, *Mater. Res. Soc. Symp. Proc.*, vol. 937 M10-29, 2006

- Q. D. Ling, **Y. Song,** E. Y. H. Teo, S. L. Lim, Chunxiang. Zhu, D. S. H. Chan, D. L. Kwong, K. G. Neoh, E. T. Kang, “Rewritable and WORM-Type Molecular/Polymer Memories”, *NUS-Fudan Joint Centennial Symposium on Bioengineering, Materials & Nanotechnology*, 2005